# General Disclaimer

## One or more of the Following Statements may affect this Document

- This document has been reproduced from the best copy furnished by the organizational source. It is being released in the interest of making available as much information as possible.

- This document may contain data, which exceeds the sheet parameters. It was furnished in this condition by the organizational source and is the best copy available.

- This document may contain tone-on-tone or color graphs, charts and/or pictures, which have been reproduced in black and white.

- This document is paginated as submitted by the original source.

- Portions of this document are not fully legible due to the historical nature of some of the material. However, it is the best reproduction available from the original submission.

# TECHNICAL AND INVESTIGATIVE SUPPORT FOR HIGH DENSITY DIGITAL SATELLITE RECORDING SYSTEMS

Progress Reports #8 - 11

Covering Reporting Period April - June 1982

NASA Contract No. NAS5-264.‾

IITRI Project No. K06003

Prepared for:

Mr. C. Powell, Code 728
NASA/Goddard Space Flight Center
Greenbelt Road
Greenbelt, Maryland 20771

Prepared by:

R. A. Schultz
Associate Engineer
Magnetic Recording
IIT Research Institute
10 West 35th Street
Chicago, Illinois 60616

July 1982

## FOREWORD

This is the eighth progress report on IITRI Project K06003 (formerly E06514) entitled "Technical and Investigative Support for High Density Digital Satellite Recording Systems." The work reported herein was conducted for NASA/Goddard Space Flight Center under Contract No. NAS5-26493 during the period April - May, 1982. This report contains comprehensive results from the magnetic media investigation task of the contract, including revisions to progress reports 4 through 7 issued from November 1981 through March, 1982. C. Donald Wright acted as the project leader and Robert A. Schultz conducted the technical investigations with assistance from Theodore Shaifer and Frank Jaworski.
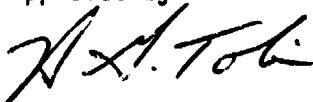
Data for this report are recorded in IITRI Logbooks C26427, C26492, C26508, C26602, C26609, C26758, and C26760.

Prepared by

Robert A. Schultz
Associate Engineer
Magnetic Recording

Approved by

Henry G. Tobin
Assistant Director
Engineering Division

# TABLE OF CONTENTS

## LIST OF TABLES

# LIST OF FIGURES

**IIT RESEARCH INSTITUTE**

# LIST OF FIGURES (cont.)

# TECHNICAL AND INVESTIGATIVE SUPPORT FOR
# HIGH DENSITY DIGITAL SATELLITE RECORDING SYSTEMS

NASA Contract No. NAS5-26493
IITRI Project No. K06003
Period Covered April - June 1982

## 1.  INTRODUCTION

The overall goal of this contract is to provide technical and investigative support to NASA Goddard Space Flight Center in the development of High Density Digital Satellite Recorders.  The general requirements for 150 megabits per second record/reproduce data transfer rates from satellites is addressed by this program and by competing satellite recorder manufacturers.

This summary report describes methods and results of examinations and tests conducted on magnetic recording tapes under consideration for a high density digital (HDDR) satellite recording system.  The examinations and tests investigate the performance of tapes with respect to their physical, magnetic and electrical characteristics.  Each test section includes introductory remarks indicating the objective of the test, the likely significance of typical results, and the importance of the characteristics under investigation to the application.  Theoretical discussions of measurement methods are provided where appropriate.  Methods and results are discussed in each section, but the results of some sections have been tabulated together to facilitate their comparison.  The conclusion of each test section relates the test results to their possible significance and attempts to correlate the results of that section with the results of other tests.  Some of the sections analyze sources of error inherent in the measurement methods or relate the value of the information obtained co the objectives of the test or the overall purpose of the project.

## 1.1 Requirements of the Tape for the HDDR Satellite Recorder System

General requirements of the magnetic media for the HDDR Satellite Recorder System include long term durability of the base film and the oxide binder system, low abrasivity to the recorder head material, stable magnetic characteristics, the ability to record and reproduce short wavelengths, and freedom from oxide binder system defects that produce loss of signal or "drop outs." More specific requirements are described in the individual test sections, but the definition of the requirements and their relative importance is expected to change during the development of the recording system as problems are identified and the limits of current state-of-the-art are approached.

## 1.2 Description of Candidate Tape Types

Five tape types currently under investigation for the HDDR Satellite recording system are intended for wideband instrumentation or video applications and have nominal thicknesses of 1 mil (0.001 inch). Fou· of the tape types, Ampex 466 and 721, Fuji H621, and 3M 5198 have cobalt doped or adsorbed iron oxide magnetic particles, while a fifth type, Ampex 797, has gamma ferric oxide ($\gamma Fe_2O_3$) particles. In addition to the oxide binder systems and the polyester (mylar) base films, each tape type has a back coating to prevent layer-to-layer adhesion, increase friction, and/or reduce the build up of static charges.

Some of the test methods and equipment employed for this project require specific tape widths in order to obtain results for comparisons of tape types. A few types have not yet been obtained in all necessary widths, and a tape slitter currently in use for another project will be available soon for the preparation of any samples not yet obtained in the required tape widths.

Tissue cleaning of these prepared samples is planned prior to testing. In addition, many early tests were conducted on Fuji Beridox tape obtained from a video cassette rather than Fuji H621 which has been obtained in 1 inch width. Fuji Beridox test results will be supplemented by Fuji H621 results as the tests are repeated.

## 2. PHYSICAL PROPERTIES

This section describes the physical characteristics of the subject tapes, especially characteristics that may affect the long term durability and reliability of the tape as well as the integrity of the head-tape interface. Physical dimensions and dimensional variability have been or will be determined for each tape type. Relative flexibility and dynamic tracking and guidance measurements, which are dependent mainly on the base film properties of the tapes, have been conducted or are planned. Bulk properties of the oxide binder systems including abrasion resistance, binder strength, and lubricant content have been investigated. The oxide surfaces have been characterized by scanning electron microscopy, coefficient of friction measurements, relative head material abrasivity tests, and elemental analysis.

## 2.1 Tape Thickness

Tape thickness is measured during sample preparation for M-H measurements. Although slight thickness differences between tape types are not expected to have a large effect on their relative performance, thickness variation within a given tape type may be an indication of poor manufacturing process controls.

The possible effects of solvents on the tape mylar were examined during the following procedure. Mylar samples were re-exposed to solvents for one hour periods after the initial short preparation exposure time and thickness measurement. The long re-exposure did not change the measured mylar thickness, indicating that the short exposures do not cause errors due to mylar dissolving, swelling, or softening.

### 2.1.1 Procedure

Ten to sixteen layers of tape were measured with a micrometer and the results were divided by the number of layers measured. The measurements were made on the total thickness of the tape, on the tape with the back coating removed with cotton swabs or Kim Wipes using acetone, tricloroethylene or methyl-ethyl-ketone (MEK) as solvents, and on the mylar base alone with both the back coating and the magnetic oxide coating removed. The back coating and oxide thickness were determined by subtracting the sequential measurements. MEK has been employed as the solvent during all except the earliest tests.

The micrometer must be accurately zeroed and must have a slip mechanism which provides a low and repeatable measurement pressure. The micrometer may have a 0.1 mil vernier scale, or 0.2 mil resolution

can be observed between 1.0 mil divisions if a vernier scale is not available. Several measurements or a single 16 layer sample should not vary by more than ±0.2 mil, and the median value of those measurements was recorded. The test method produces average measurements for tape sections less than three feet long. The precision of the average measurement technique approaches 20 microinches (0.02 mil).

### 2.1.2 Results

Table 2.1 lists maximum and minimum thickness values for each tape type and lot investigated to date. Additional oxide binder system measurements on each individual sample are presented in Table 3.1 to facilitate comparisons of thickness and magnetic induction measurement variations.

### 2.1.3 Conclusions

Thickness variations of Ampex 721, Fuji H621, and 3M 5198 do not exceed the 20 microinch (0.02 mil) limit of precision of the test method. The results for Ampex 466 and Ampex 797 include oxide and mylar thickness variations slightly greater than that limit of precision. This increased variation could be due to less dense oxide binder systems suggested by SEM (Section 2.9) combined with measurement errors produced by pressure variations of the micrometer.

Table 2.1.1: Tape Thickness and Flexibility

| Test  Tape Manufacturer and Type (Lot) | Range of Thicknesses (mils) | | | | Flexibility (degrees) |
|---|---|---|---|---|---|
| | Oxide | Mylar | Back Coating | Total | |
| Ampex 466 (5166041921) | 0.20 0.21 | 0.86 0.91 | 0.04 0.06 | 1.13 1.17 | 52° |
| (1731J) | 0.21 0.23 | 0.88 0.89 | 0.05 0.06 | 1.13 1.17 | |
| Ampex 721 (11Q024182) | 0.19 0.21 | 0.87 0.91 | 0.04 0.06 | 1.11 1.17 | 67° |
| Ampex 797 (76142, 164485221-4, Lot A-1) | 0.16 0.18 | 0.87 0.92 | 0.03 0.04 | 1.08 1.11 | 55° |
| (76142, 264485591-16, Lot No A-2)* | 0.21 | 0.86 | 0.03 | 1.11 | |
| (76142, 164485222-47, Lot A-1)* | 0.18 | 0.89 | 0.06 | 1.13 | |
| Fuji H621 (079903)* | 0.23 | 0.79 | 0.05 | 1.08 | --- |
| (079552)* | 0.23 | 0.78 | 0.08 | 1.08 | |
| 3M 5198 (41575-1-01-58) | 0.19 0.20 | 0.76 | 0.08 | 1.03 1.04 | --- |
| (41575-1-01-16) | 0:19 | 0.78 0.79 | 0.08 | 1.04 1.05 | |
| (41575-1-01-35)* | 0.19 | 0.79 | 0.05 | 1.03 | |

* Thickness measurement results based on single samples of these lots.

## 2.2 Flexibility

Measurement of tape flexibility is a simple test that may indicate the tendency of a tape to produce oxide binder debris.

### 2.2.1 Procedure

The relative flexibilities of the magnetic tapes were measured by the method specified in "Magnetic Head/Tape Interface Study for Satellite Tape Recorders, Technical Report, Volume I" prepared during IITRI Project No. E6134 and dated February, 1971. The test fixture includes a horizontal clamping surface, a coordinate grid to indicate the position of the free end of the tape, and a swing-away support which maintains the tape sample horizontally during mounting and allows the sample to bend freely for the measurement. The angle of curvature (deflection from the horizontal) was measured for the line extending between the clamping point and the free end of the tape sample. All tapes were maintained in the same environment prior to and during the testing which approximated the environmental conditions specified for the test, $70^{\circ}F \pm 3^{\circ}F$ and 30% $\pm$ 3% RH.

### 2.2.2 Results

Measured flexibilities are listed in Table 2.1.1. The Ampex type 797 sample was a 1/4 inch tape width, and the Ampex type 466 sample was a one inch tape width rather than the 1/2 inch width specified for the test. Subjective observations of 3M 5198, Fuji H621, and a new 1/2 inch sample of Ampex 797 suggest that results comparable to those in Table 2.1.1 would be obtained for all of these tape types.

### 2.2.3 Conclusions

All of the measured angles are greater than the $30^{\circ}$ minimum angle specified by the IITRI guide lines as an indicator of acceptable flexibility. Observations indicate that all of the tapes would meet the guidelines, and that other factors such as cleanliness (Section 2.11) are more important than flexibility for the short term production of debris. However, additional flexibility testing should be conducted concurrently with future long term endurance and environmental testing of the tapes.

### 2.3 Binder Strength

The strength of the oxide binder system was observed subjectively during binder removal with methyl-ethyl-ketone (MEK) for thickness measurements. The observations are listed in the second column of Table 2.3. The observations indicate a loose correlation with abrasion resistance.

### 2.4 Abrasion Resistance

This test provides a relative measure of the resistance to abrasion of magnetic tape oxide binder systems. The raw data that is presented allows ranking of tapes according to their abrasion resistance, but the correlation between the test results and the useful life of tape oxide during normal or abusive conditions has not been determined. Nonlinear effects of the test method are under study.

### 2.4.1 Procedure

Grade 25 chrome steel balls 0.125 inch in diameter are employed. The balls have a Rockwell C scale hardness specification of 62-66 and a roundness tolerance of 25 microinches.

Prior to use, shipping lubricant and contaminants are removed from the balls with benzene. Skin contact is prevented during mounting of the balls in the test fixture and during tape preparation and mounting. A new ball is employed for each test.

Prior to mounting the virgin tape samples, a small part of the back coating is removed with methyl-ethyl-ketone (MEK) and cotton swabs. Contact between the MEK and the oxide coating is avoided. Abrasion during coating removal is minimized by preparation without motion on a clean polyester sheet.

A 0.227 Newton (23.1 gram) normal force is applied to the tape through the steel ball as it is dragged back and forth across the tape along a 2.67 inch path. The ball passes are counted until a tungsten lamp behind the sample is visible through the clear polyester base material of the sample. Multiple samples of each tape type are tested and the mean value and standard deviation of the number of passes until failure is calculated. For highly abrasion resistance tape types (above 500 passes), the wear is monitored periodically, and the number of passes between the last unworn observation and the first worn observation is averaged.

## 2.4.2 Results

The first column of Table 2.3.1 presents the raw data of abrasion resistance obtained with the specified normal force applied to the ball. The results will be normalized and corrected for oxide coating thickness pending consideration of nonlinear effects caused by the test method. The most obvious nonlinear effect is the increased contact surface between the

Table 2.3.1: Bulk Physical Properties of Oxide Binder Systems

| Test Tape Type (lot) | Abrasion Resistance (Ball Wear Test) Trials | Passes Mean | σ | Min | Binder Strength Observation, Ease of Removal with MEK | Lubricant Content (% weight of oxide binder system) Benzene Extraction | Freon TF Extraction |
|---|---|---|---|---|---|---|---|
| Ampex 466 (5166041921) | 4 | 1400 | 303 | 1010 | Easy | 1.80* | 1.79 |
| Ampex 721 (110024182) | 6 | 60 | 18 | 32 | Difficult | 1.15 | 1.47 |
| Ampex 797 (76142, 164485221-4, Lot A-1) | 7 | 4 | 2 | 2 | Very Easy | 0.62 | 0.83 |
| Fuji Beridox (PFD 018) | 6 | 119 | 39 | 75 | Very Difficult | 0.81 | 0.59 |
| 3M 5198 (41575-1-01-58) | 3 | 1900 | 731 | 918 | Difficult | 0.74 | -0.68 |

ball and the oxide if the ball wears a groove into the tape before it wears through the oxide. This would decrease the pressure on the oxide and could cause the number of passes to increase as the square of the relative abrasion resistance.

The effect of the surface finish of the steel balls is under study. Optical microscope observations of new balls at 400x reveal a surface finish much smoother than the worn ball surface following a large number of passes on an abrasion resistant tape type.

### 2.4.3 Conclusions

The results for Ampex 797 with the 0.227 Newton normal force employed in the current test series indicate a lower relative abrasion resistance than the results described in the December 1981 progress report, which employed a 0.765 Newton normal force and a used Ampex 797 sample with an uncertain history.

Based on the current test results, the abrasion resistance of the subject tapes falls into three categories: highly resistant Ampex Type 466 and 3M Type 5198, moderately resistant Ampex Type 721 and Fuji Beridox, and nonresistant Ampex 797. The vast difference in test results between categories suggests the need for theoretical consideration, life testing, or some other investigation with the aim of determining the meaningfulness of a nonlinear scale rather than the linear absolute number of passes scale of Table 2.3.1.

## 2.5 Lubricant Content

This test measures the weight of lubricants and other low molecular weight compounds which are extractable by a solvent as a percentage of oxide binder system weight. Lubricant is added to the oxide binder system to reduce friction, but excessive lubricant may weaken the integrity of the binder polymer. Benzene is the usual extraction solvent for this test but the possible use of fluorocarbon lubricants suggested the use of Freon TF as the extraction solvent.

### 2.5.1 Procedure

Obtain virgin samples of each tape under consideration. The samples must not be contaminated with body oils, lint or dirt. Tweezers, petri dishes, and work surfaces covered with clean polyester sheets are required to facilitate sample handling and preparation.

All samples should be 18 square inches $\pm$1%. Two tape strips 0.248 $\pm$0.002 inches wide and 36 $\pm$0.03 inches long provide this area tolerance. Five samples were employed for the oxide binder weights and benzene extracted lubricant weights in the current experimental series. Single samples were employed for Freon TF extractions, with the exception of 3M Type 5198, where a second sample was tested following an unusual result with the first sample.

Label and weigh each tape sample prior to treatments. An analytical balance with 10 microgram resolution is suitable. Divide the preweighed samples into groups for oxide binder system removal and lubricant ex-tractions.

Remove the oxide binder system with methyl-ethyl-ketone (MEK) and cotton swabs or lint free wipers (Kim Wipes). Note that contact of the MEK and the back coating is unavoidable. However, if the tape is placed oxide up on a polyester sheet and stroked lightly with an MEK saturated wiper, the back coating will adhere firmly to the polyester sheet before it is loosened significantly. The adhesion will prevent mechanical disruption of the MEK wetted back coating and will minimize addition of dissolved oxide binder to the back coating. Note the ᴄase of oxide removal with MEK as a subjective indication of the oxide binder system strength (Section 2.3).

Extract the lubricant from the other groups of samples by soaking for at least 12 hours in selected solvents. Stand the tape on edge in petri dishes during benzene treatment to facilitate complete wetting. Freon treated samples may be soaked in loosely capped polypropylene bottles. The oxide binder system and back coating should remain intact during extraction and subsequent sample drying.

Dry thoroughly, and reweigh all samples. Calculate the mean weight losses following treatment for each group. Calculate the lubricant weight as a percent of the oxide binder system weight:

$$\frac{\text{Lubricant weight}}{\text{Binder weight}} \times 100\% = \% \begin{array}{l}\text{Lubricant} \\ \text{Content}\end{array}$$

### 2.5.2 Results

The lubricant contents of the subject tapes are listed in the last column of Table 2.3.1. Standard deviations of the oxide binder system weights were less than or equal to 0.5% of the weights, while standard

deviations of the benzene extracted lubricant weights ranged from 5% to 19% of the weights. The lubricant weight variability may be due to experimental error such as contamination of a sample by a single dust particle or incomplete wetting of the samples. One benzene treated 3M Type 5198 sample was deleted from the calculations due to a very low lubricant weight and a visible residue on the tape surface after drying which suggested incomplete wetting.

Both of the 3M 5198 samples subjected to Freon TF extractions gained identical weights during the initial extraction. The Freon TF treated samples were resoaked for an additional 72 hours following the initial post treatment weighing. The 3M Type 5198 samples continued to gain weight during this treatment while weights of other samples did not change significantly.

### 2.5.3 Conclusions

Lubricant weights of the tapes are within or close to IITRI guidelines which recommend a 1% lower limit and a 2% upper limit. That conclusion ignores the 3M Type 5198 Freon TF treatment results which are obviously due to phenomena other than extraction of lubricants. Elemental surface analysis (Section 2.6) has not provided clear cut evidence of the lubricant types or amounts in the subject tapes.

The results indicate that single samples are acceptable for oxide binder system weights but that a mean value derived from five or more lubricant sample weights is desirable.

## 2.6 Elemental Surface Analysis

Detection and measurement of elements present near the oxide coating surface of magnetic tapes provides indications of the types and relative amounts of metal oxides, binders, and lubricants on the tape surfaces. Two methods, electron microprobe analysis (EMA) and ion microprobe analysis (IMA), have been employed for elemental analysis. Both methods direct beams of high energy charged particles onto the surface of the tapes which induce the emission of small ions or x-rays from materials of the oxide surface. During these probes, the sample size and depth can be controlled by the focus, energy, and intensity of the particle beams.

The ions released from the tape surface by the IMA beams are directed to a mass spectrometer which separates, detects, and counts the individual atoms or, in some cases, small polyatomic ions released from the tape surface. The x-rays emitted by the electron probe are characteristic of the elements in the sample.

Of the two methods, the EMA is considered more repeatable and quantitative than the IMA, but the IMA is more sensitive and can detect all elements while the EMA is restricted to measurement of elements with atomic weights between 5 and 20 at trace levels by wavelength analysis. EMA can identify heavier elements only as major constituents (>10%).

The EMA wavelength dispersion analysis intensity measurements are based on several standards such as $SiO_2$ for silicon, Teflon for flourine, sodium chloride for chlorine, metallic iron for iron, and metallic cobalt for cobalt. Since the matrices of the tape samples and the standards are very different, the precision of the EMA measurements is not better than 30% relative.

Although IMA counts individual atoms or ions, matrix effects are even more pronounced on the generation of ions during IMA. Quantitative results from IMA obtained by computer analysis of the data employed relative sensitivity factors which give even poorer precision than EMA, not better than ±50% under the best of conditions. It is felt that higher precision for a surface analysis is virtually impossible.

### 2.6.1 Procedure

Virgin tape samples obtained for each tape type were placed in polyethylene bags to prevent chemical contamination and were submitted for analysis of the outer 2 microinch (500 Å) surface layer of the oxide binder coating. Each tape type was mounted on an aluminum substrate with conductive aluminum paint for analysis.

Electron excited X-ray analysis was conducted with an electron microprobe employing a 6 KV accelerating voltage, a 15 nA sample current, and a 3.2 mil (80 µm) beam diameter. These conditions were intended to produce a 2 microinch penetration depth and essentially no damage to the sample surface. Intensities of silicon, flourine, oxygen and carbon were measured during this analysis.

Ion microprobe analysis was conducted with an oxygen ion beam accelerated to 20 KV with a 1 nA beam current and a 100 µm beam diameter. These conditions were intended to sputter away the oxide binder system surface to a 2 microinch depth. Secondary ions generated by the sputtering were analyzed in a mass spectrometer. Mass spectra of positive and negative ions were obtained for each sample. Chlorine and cyanide intensities were measured from the negative ion spectra. Iron and cobalt intensities were measured from the positive ion spectra.

## 2.6.2 Results

Electron microprobe results for the light elements oxygen, silicon, flourine and carbon were obtained from wavelength dispersion analysis of the emitted X-rays. Relative intensities of these elements corresponding to the proportion of atoms in the sample volume are listed in Table 2.6.1. The intensities were evaluated with results of other analyses to obtain the estimated weight percentages in Table 2.6.2 for silicon and flourine. The high intensities of carbon and oxygen indicated in Table 2.6.1 support the expectation that those elements make up the bulk of the oxide binder system polymers in each of the tapes.

Figures 2.6.1 through 2.6.5 are mass spectra of negative ions generated during the ion microprobe of each tape oxide surface. Figures 2.6.6 through 2.6.10 are mass spectra of positive ions generated during the ion microprobe of each tape oxide surface. The vertical counts scale is logarithmic, so peaks that extend into the upper third of the spectra represent major constituents (>10%) of the detected elements and ions, while peaks that do not rise above the lower third of the spectra are constituents generated 100 to 1000 times less frequently than the major constituents. Due to matrix effects, the height of a peak is not necessarily proportional to the amount of an element on the sample surface. Table 2.6.3 lists some of the likely elements or ionic species associated with the peaks of the mass spectra. This table identifies the position of a peak on the horizontal axis of the mass spectra, which has units of atomic mass per unit charge of the electron (M/E).

The negative mass spectra indicate that the ratio of detected chlorine atoms to flourine atmos is about 10:1 for most of the samples. However, these counts were not used directly in the attempt to quantify the data. Instead, EMA and IMA data were computer analyzed by a program that employs relative sensitivity factors for the IMA counts. The results of this analysis for chlorine and cyanide are shown on Table 2.6.1. A similar analysis was employed for iron and cobalt, and the results were combined with Table 2.6.1 to generate Table 2.6.2, which indicates the approximate weight percentages of selected elements on the tape sample oxide surfaces. These elements were considered due to their possible applications in lubricants (Si, F), cross linking agents (Cl) and oxide (Fe, Co). The balance of each tape surface is composed of carbon, oxygen, nitrogen and hydrogen which are presumed major constituents of the binder polymers, and elements such as sodium, magnesium, aluminum, sulfur, potassium, calcium and titanium which appear to be present at trace levels. The trace elements are listed in Table 2.6.3. The generation of cyanide ions during IMA is associated with popular urethane polymers.
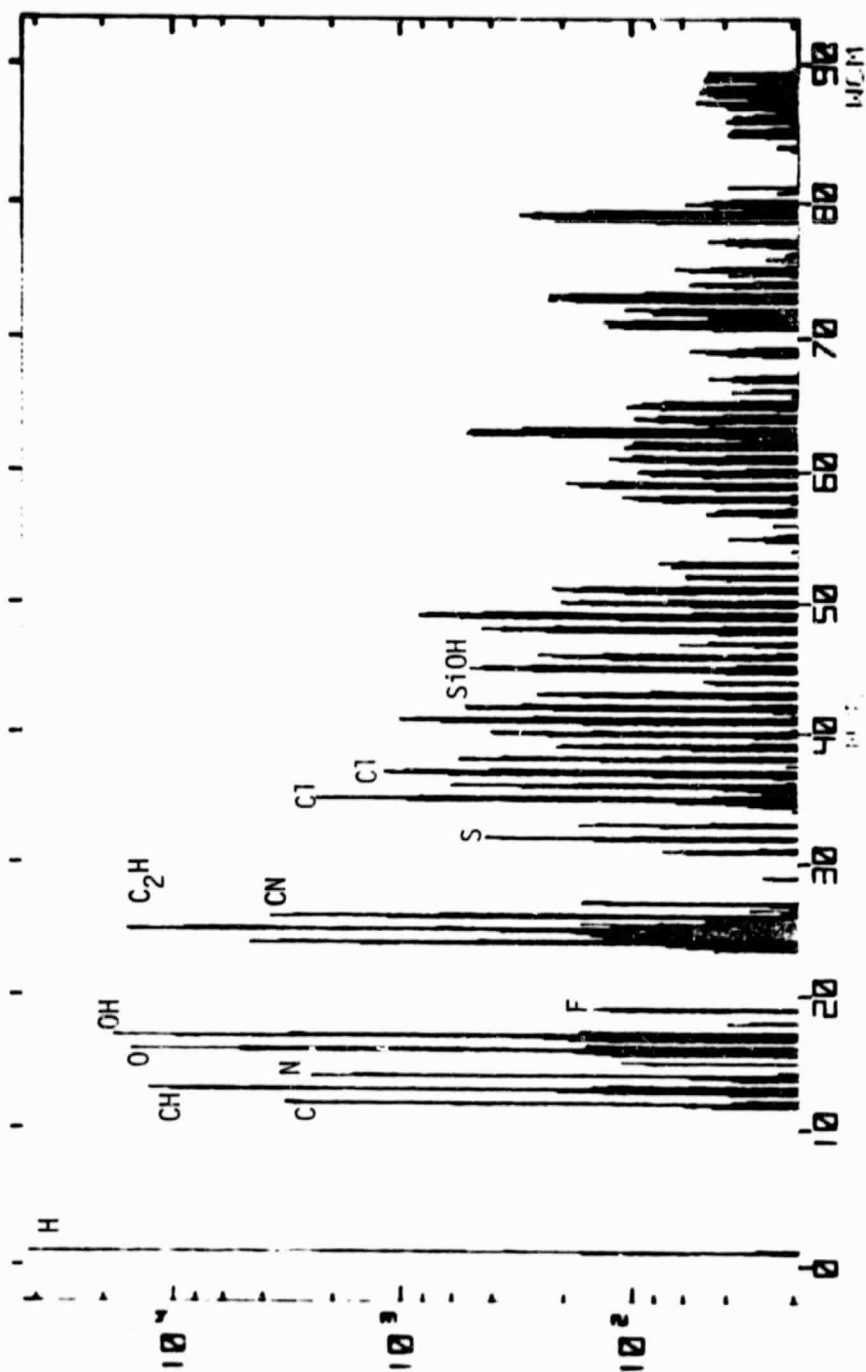
Figure 2.6.1: IMA negative ion spectrum of Ampex 466 oxide surface
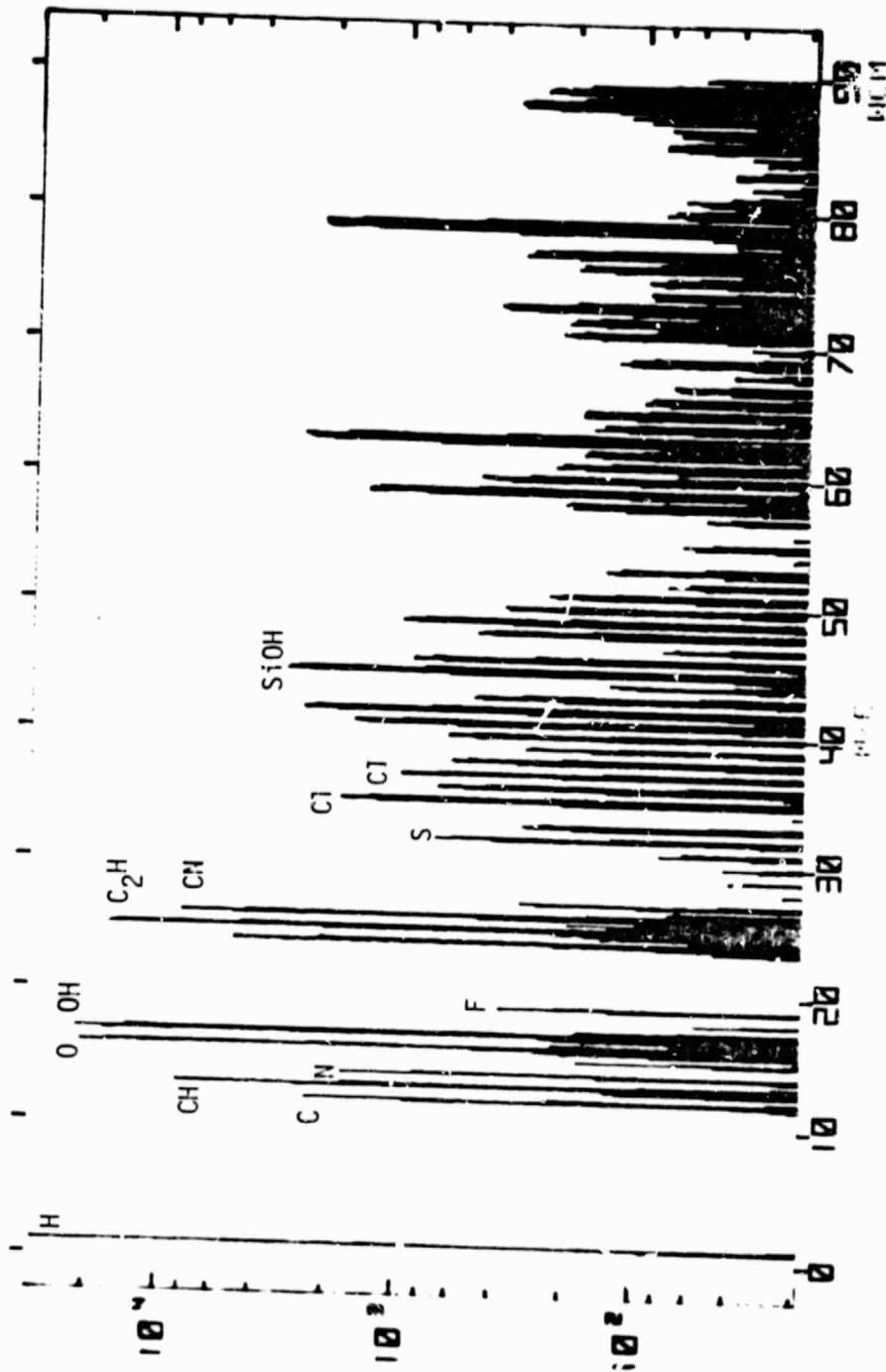
Figure 2.6.2: IMA negative ion spectrum of Ampex 721 oxide surface

21
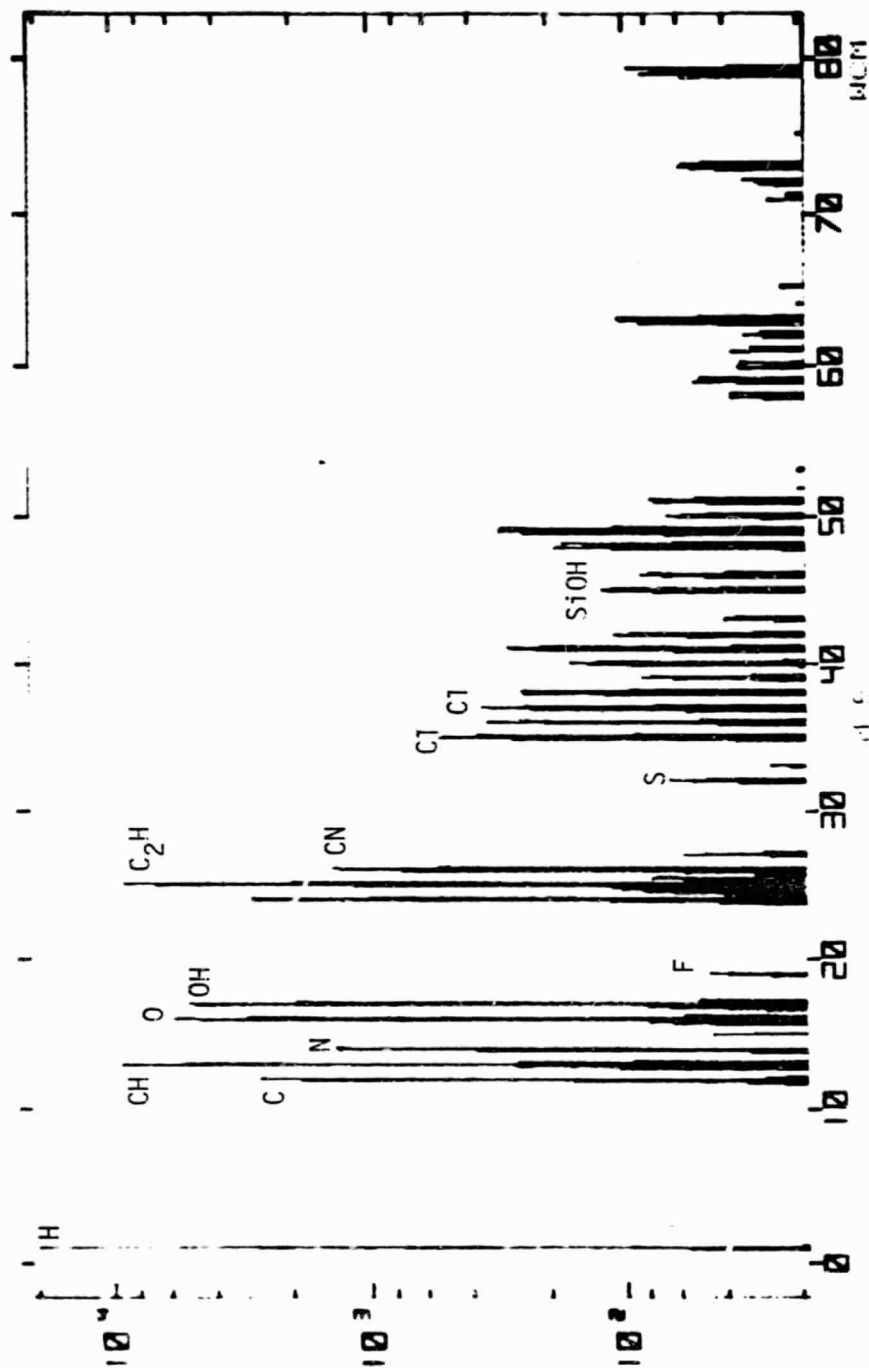
Figure 2.6.3: IMA negative ion spectrum of Ampex 797 oxide surface

22
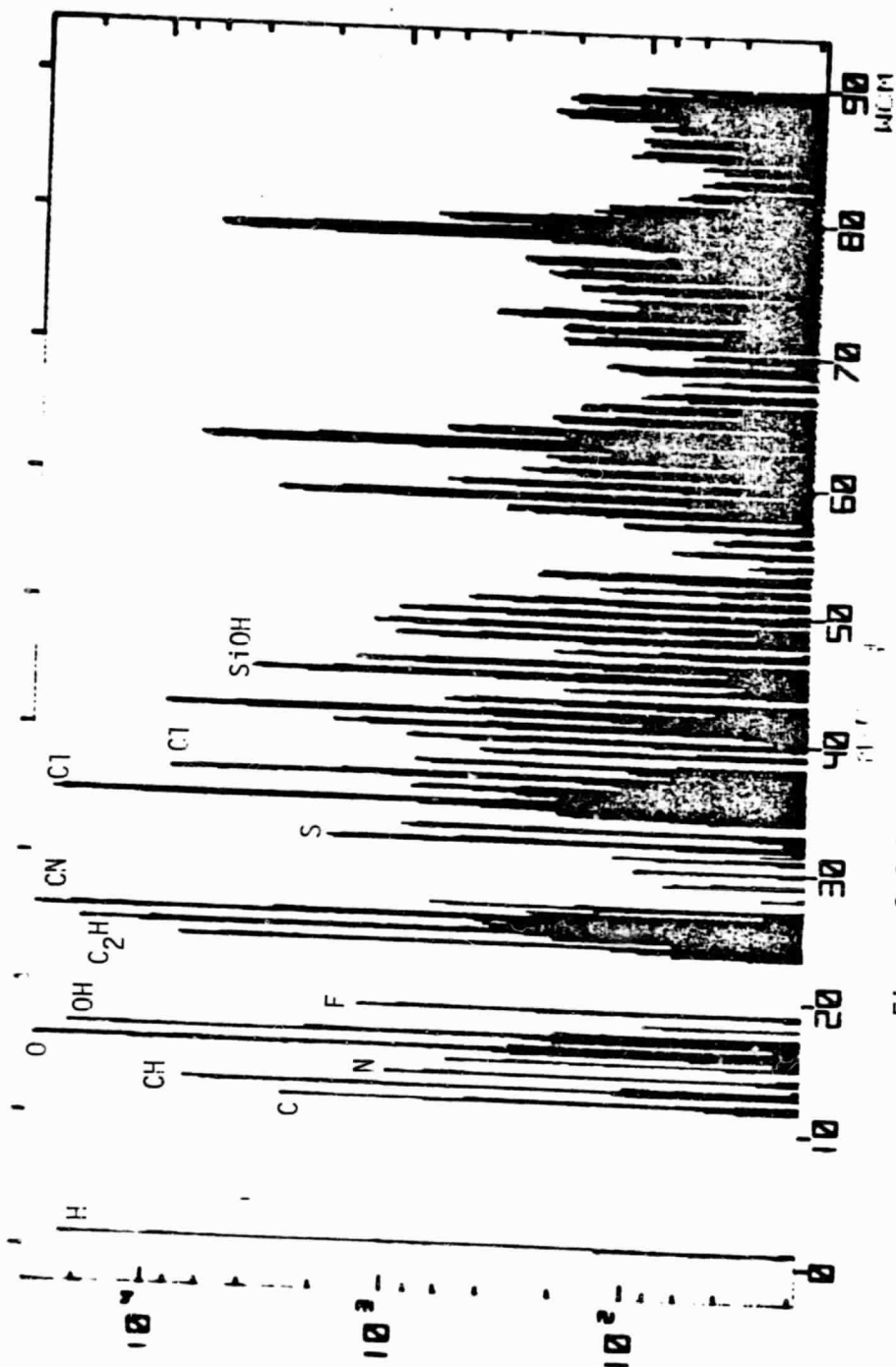
Figure 2.6.4: IMA negative ion spectrum of Fuji Beridox oxide surface
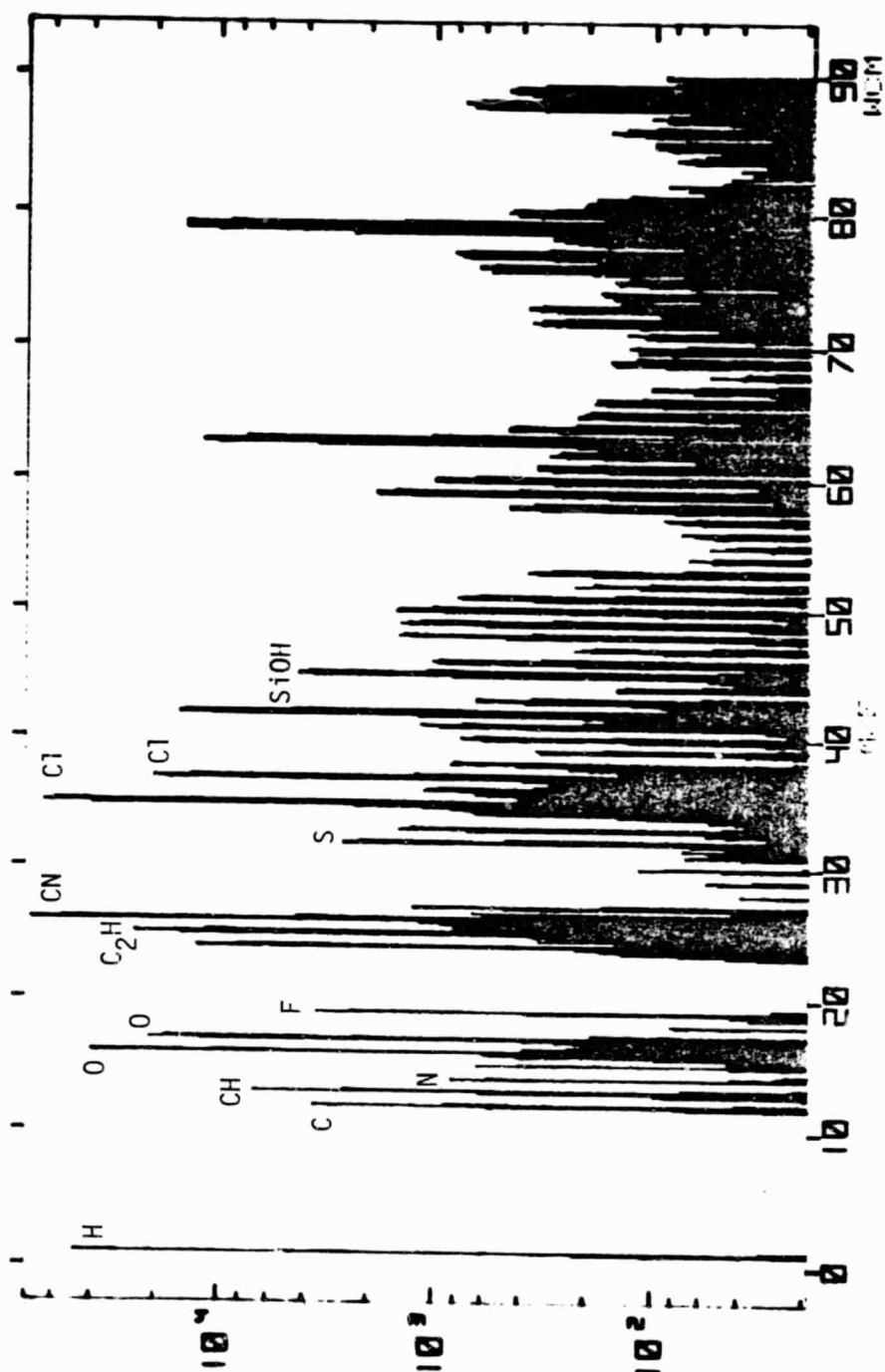
Figure 2.6.5: IMA negative ion mass spectrum
of 3M 5198 oxide surface

24
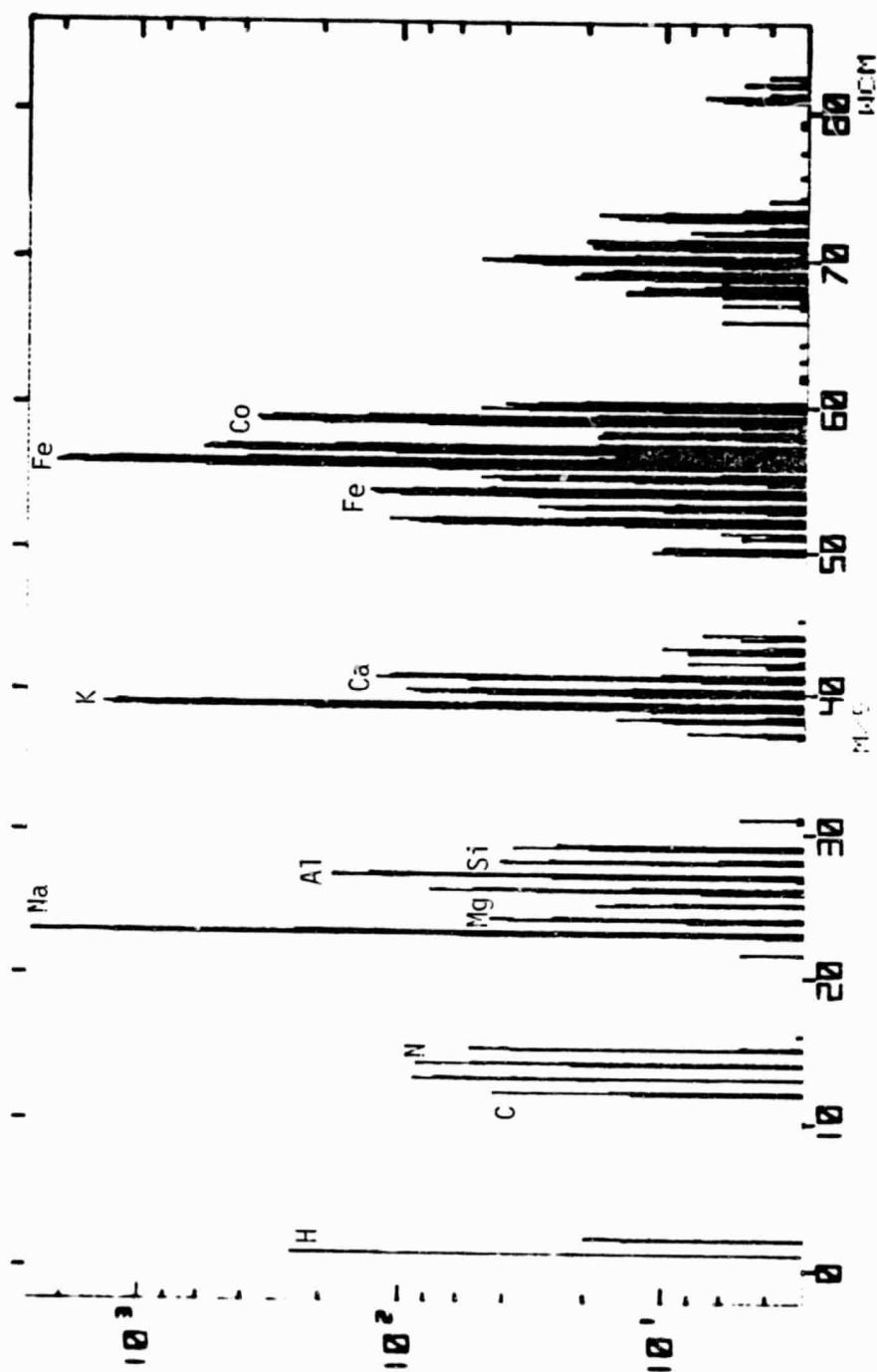
Figure 2.6.6: IMA positive ion mass spectrum of Ampex 466 oxide surface

25
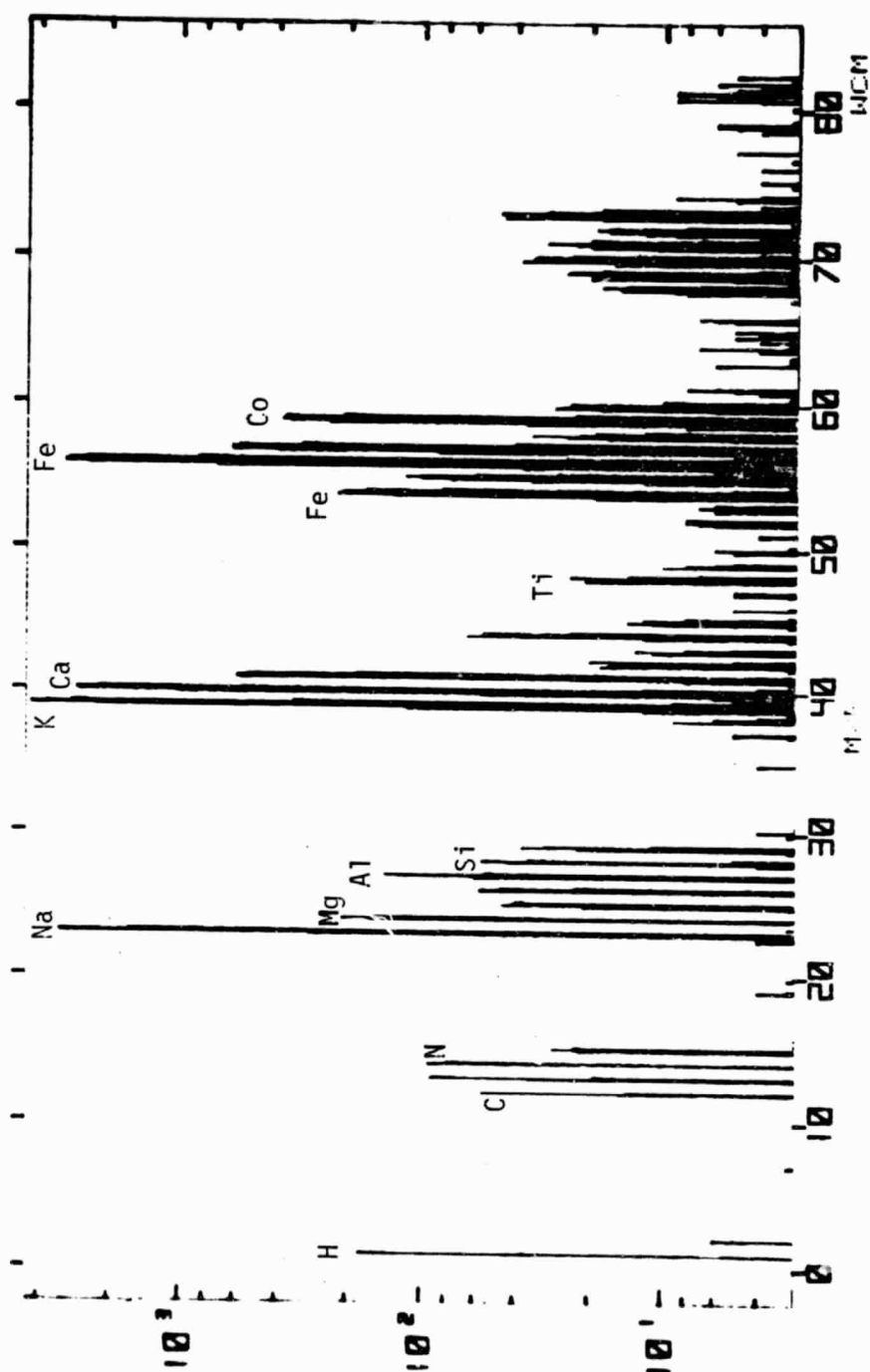
Figure 2.6.7:   IMA positive ion spectrum
of Ampex 721 oxide surface

26
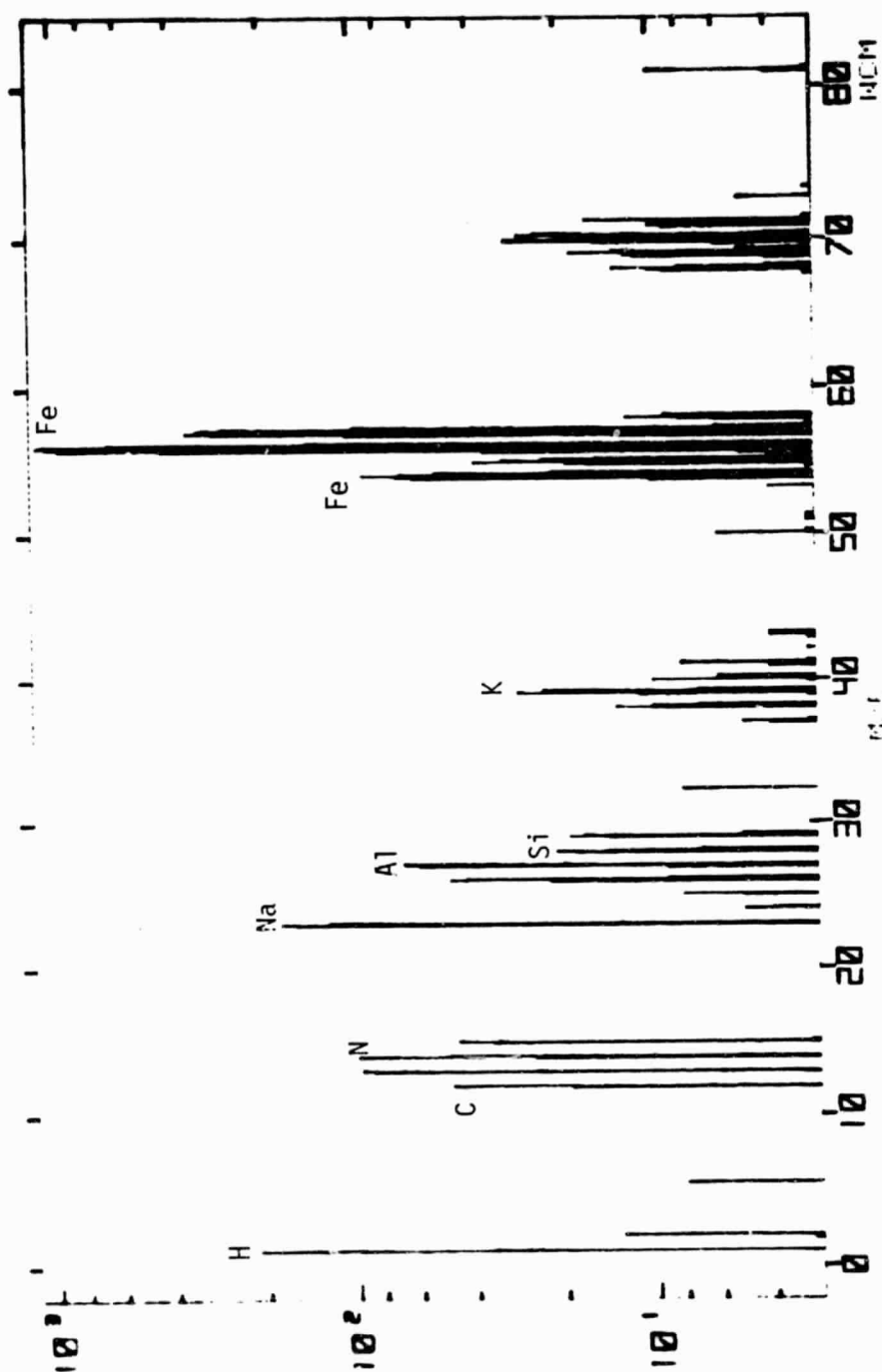
Figure 2.6.8: IMA positive ion spectrum
of Ampex 797 oxide surface
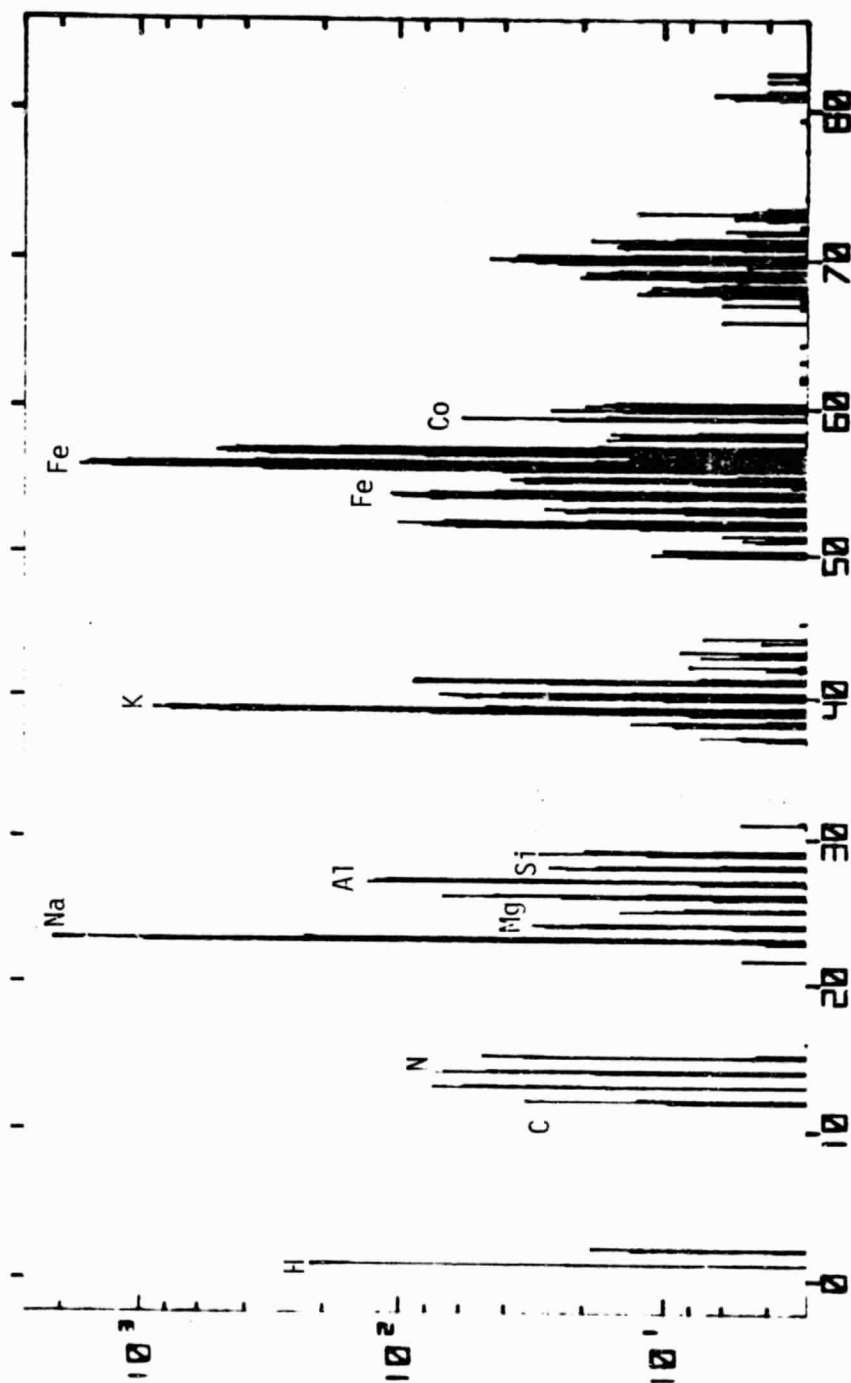
Figure 2.6.9: IMA positive in spectrum of Fuji Beridox oxide surface
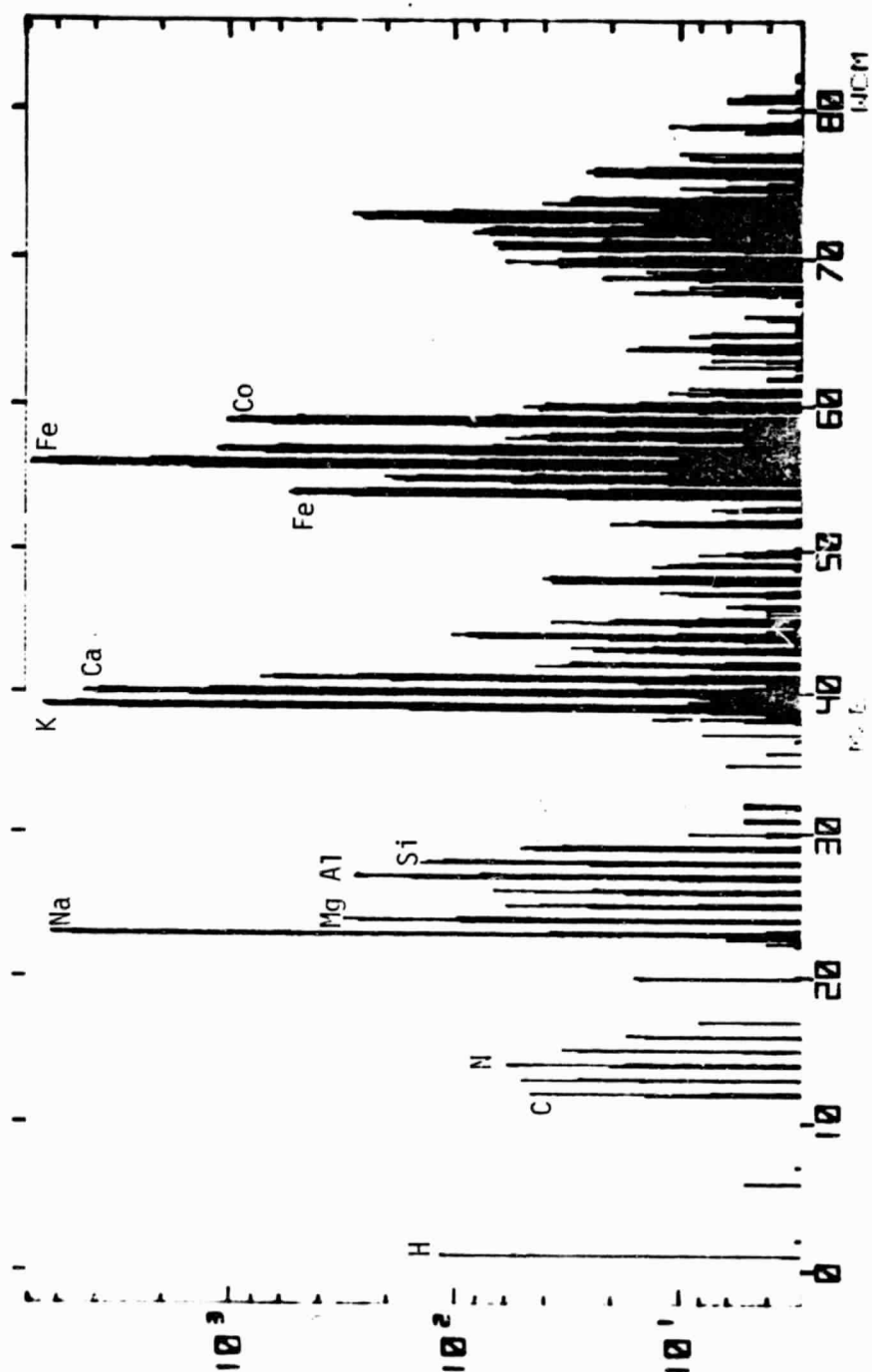
Figure 2.6.10: IMA positive ion spectrum of 3M 5198 oxide surfuce

29

Table 2.6.1: Relative Intensities of Elements and Cyanide Ions

| Tape Type | Electron Microprobe X-ray Wavelength Dispersion Analysis | | | | Ion Microprobe Negative Ion Analysis | |
|---|---|---|---|---|---|---|
| | Silicon | Flourine | Oxygen | Carbon | Chlorine | Cyanide |
| Ampex 466 | 366 | 109 | 12234 | 23125 | 50 | 2719 |
| Ampex 721 | 414 | 117 | 14342 | 15826 | 27 | 2997 |
| Ampex 797 | 260 | 87 | 11391 | 31655 | 14 | 1465 |
| Fuji Beridox | 181 | 108 | 10901 | 24474 | 35 | 2105 |
| 3M 5198 | 555 | 160 | 13348 | 16727 | 286 | 13393 |

Table 2.6.2: Elemental Composition of Magnetic Tape
Oxide Surface by Weight Percentages

| Tape Type (Lot) | Silicon | Flourine | Chlorine | Iron | Cobalt |
|---|---|---|---|---|---|
| Ampex 466 (5166041921) | 0.30 | 0.20 | 2.6 | 40 | 0.05 |
| Ampex 721 (110024182) | 0.35 | 0.20 | 0.10 | 40 | 0.05 |
| Ampex 797 76142, 16 4485221-4, Lot A-1) | 0.05 | 0.05 | 0.05 | 40 | 0.00 |
| Fuji Beridox (PFD 018) | 0.04 | 0.15 | 2.5 | 40 | 0.05 |
| 3M 5198 (41575 1 01 58) | 0.40 | 0.40 | 3.0 | 40 | 2.5 |

## Table 2.6.3: Identification of
## Peaks on Ion Microprobe Mass Spectra

| Negative Spectra | | Positive Spectra | |
|------|----------------|------|----------------|
| M/E | Element or Ion | M/E | Element or Ion |
| 1  | Hydrogen | 1  | Hydrogen |
| 12 | Carbon   | 12 | Carbon |
| 13 | CH       | 13 | CH |
| 14 | Nitrogen | 14 | Nitrogen |
| 16 | Oxygen   | 23 | Sodium |
| 17 | OH       | 24 | Magnesium |
| 19 | Flourine | 27 | Aluminum |
| 25 | $C_2H$   | 28 | Silicon |
| 26 | CN       | 39 | Potassium |
| 32 | Sulfur   | 40 | Calcium |
| 35 | Chlorine | 48 | $T_i$ |
| 37 | Chlorine | 54 | Iron |
| 45 | $S_iOH$  | 56 | Iron |
|    |          | 59 | Cobalt |

32

### 2.6.3 Conclusions

The question of IMA repeatability may hinder its usefulness for tape type identification. However, IMA shows the presence of trace elements and measures the levels of major constituents with a degree of precision that may suffice to detect gross variations in formulation or production of tape oxide binder systems. IMA would be useful for analyzing small contaminant inclusions on a tape surface. Bulk analysis of oxide binder systems should be considered if more quantifiable and repeatable data are desired.

Silicon and flourine levels measured in the tapes do not correlate well with lubricant content test results and do not provide clear cut evidence of single lubricants based on one of those elements in any of the tape types.

Chlorine levels measured in the tapes may be correlated with abrasion resistance test results and suggest that the high abrasion resistance of Ampex 466 and 3M 5198, and the moderately high abrasion resistance of Fuji Beridox may result from vinyl chloride cross linking agents of the binder polymers. Ampex 721 and Ampex 797 have low and very low abrasion resistances respectively and also have much lower chlorine levels than the three abrasion resistant types.

The cobalt level on the Ampex 797 oxide surface is very low as expected. Although cobalt was detected in the other four types, the level for 3M 5198 reported in Table 2.6.2 is much higher than the levels reported for the other cobalt types. However, the iron:cobalt counts ratios indicated in Figures 2.6.6 through 2.6.10 suggest a much smaller variation in cobalt levels if each tape is assumed to have the same iron level as suggested by

Table 2.6.2. It appears likely that unspecified differences in test conditions between IMA spectra and quantitative analysis data collection occurred. The cobalt variation suggested by the table could also be caused by different depths of cobalt adsorption leading to matrix effects rather than vastly different weight percentages of cobalt in the tape types.

## 2.7 Coefficient of Friction

This test measures the coefficient of friction between the tape oxide binder system and the tape head. The symbol $\mu_s$ represents the coefficient for the static case when there is no relative motion between the tape and the head, while $\mu_d$ represents the dynamic case when the tape moves across the head. The coefficients are dimensionless ratios which increase as the friction between the tape and the head increases. Low values of $\mu$ are desireable for overall performance, and critical stick slip speed generally increases as the difference between $\mu_s$ and $\mu_d$ decreases.

The standard equation for "belt friction" is:

$$\mu = \frac{1}{\beta} \ln \left(\frac{T_1}{T_2}\right)$$

where $\mu$ is the coefficient of friction, $\beta$ is the total wrap angle in radians, $T_1$ is the take up tension, and $T_2$ is the supply tension. For small total wrap angles and equilibrium conditions, the friction force F of the tape across the head is approximately the difference between the take up and supply tensions:

$$F_d = T_1 - T_2$$

$$\text{or}$$

$$T_2 = T_1 - F \tag{2.7.1}$$

Therefore: $\quad \mu = \frac{1}{\beta} \ln \left(\frac{T_1}{T_1 - F}\right) \tag{2.7.2}$

When the tape changes direction, there is no relative motion or acceleration between the tape and the head for a brief instant, and a peak static friction force $F_s$ occurs just before the tape begins to slip across the head. Once forward tape motion across the head begins, the dynamic friction force $F_d$ occurs between

the tape and the head. Although the tape accelerates with respect to the head after slippage begins, very little force is required to accelerate the low mass of the tape, and the test conditions may be assumed to have a nominal effect on the force tension relation of equation 2.7.1, which assumes equilibrium conditions.

### 2.7.1 Procedure

A Video Research Corporation Model 9209 Tape Tester with a recorder head mounted on a strain gauge and a Minnetech Labs Model MTM 106 Tension Meter were employed for the current test series. The head position was adjusted for a $15^{o}$ total wrap angle, and the tape tester tension control was adjusted for a tape tension near 8 ounces. The tape tester speed control was set as low as possible to allow acceptable and repeatable operation of the tester while minimizing tape acceleration with respect to the head. The speed and tension controls were not readjusted during the test series.

The strain gauge measures the frictional drag force F associated with the tape movement across the head, while the tension meter measures the take up tension $T_1$ in the tape following reverse to forward changes of tape motion. The transducers were calibrated under static conditions by orienting the tester so that weights could be hung from the free end of a tape secured across the face of the head and threaded through the tension sensor. The drag force strain gauge amplifier gain was adjusted for a 10 gram/division deflection on a Tektronix Model 7623A storage oscilloscope with a Model 7A18 Dual Trace Amplifier set at 50 mv/div, and the 4 gram/div scale was obtained by changing the calibrated sensitivity control 20 mV/div. The second oscilloscope

channel was connected to the tension meter output, and the oscilloscope sensitivity was adjusted for a 50 gram/div deflection. The channels were rezeroed after reorienting the tape tester in its normal operating position, and the zero levels were checked frequently to reduce errors in the absolute value of force and tension which would result from zero level drift.

Samples of virgin 1/2 inch tape maintained at 70°F and 30% RH prior to and during testing were placed on the tester, the frictional forces were monitored while reversing the tester direction, and five cscillo-scope traces of each tape type with reverse to forward direction changes were stored and photographed. A new section of tape was positioned near the head for each photograph in order to maintain the virgin condition of the tape. The tape head was cleaned with ethanol and cotton swabs between each change of tape types.

Static and dynamic friction forces along with simultaneous take up tensions were calculated from measurements of the photographs, and the coefficients of friction were calculated from equation 2.7.2. Mean values and standard deviations were obtained for each coefficient and each tape type from the photographic data of each tape type.

2.7.2 Results

Figures 2 7.1 through 2.7.4 are photographic records of friction test results. The horizontal scale on each photograph represents 0.1 second/division. Each photograph has two traces which represent the take up tension and the head friction force during a forward to reverse change of the tape motion across the head. Since coefficients of
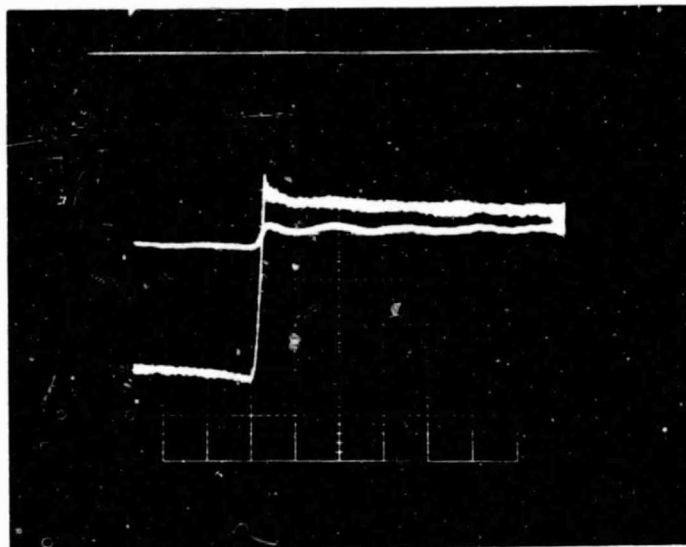
Figure 2.7.1: Friction force and take up tension for Ampex 721.

Horizontal: 0.1 s/div

Vertical: -40 g to 40 g friction force (wide trace)
0 g to 400 g take up tension
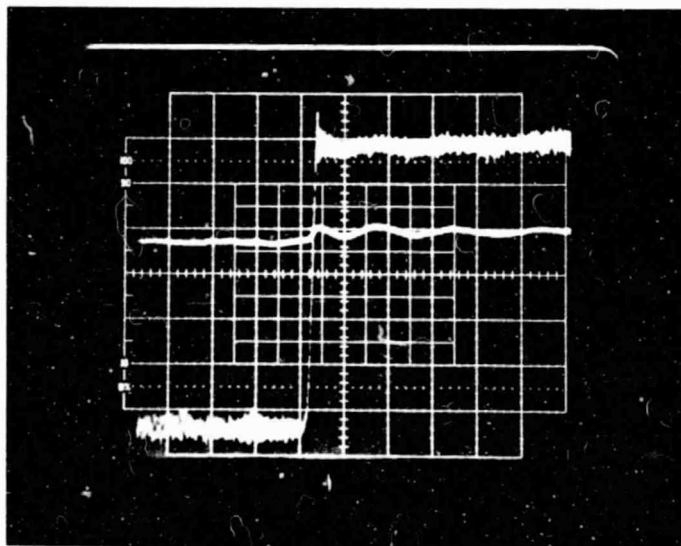


Figure 2.7.2: Friction force and take up tension for Ampex 797.

Horizontal: 0.1 s/div

Vertical: -16 g to 16 g friction force (wide trace)
0 to 400 g take up tension

IIT RESEARCH INSTITUTE

38
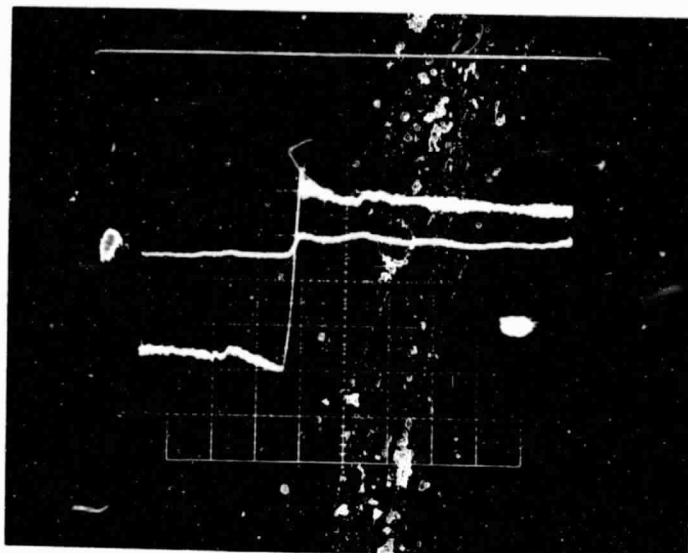
Figure 2.7.3:  Friction force and take up tension for Fuji Beridox.

Horizontal:  0.1 s/div

Vertical:  -40g to 40g friction force (wide trace)
0 to 400g take up tension
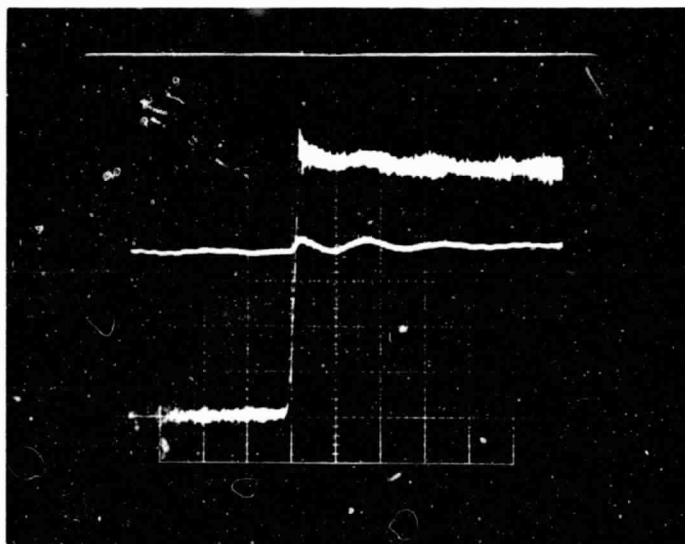
Figure 2.7.4:  Friction force and take up tension for 3M 5198.

Horizontal:  0.1 s/div

Vertical:  -16g to 16g friction force (wide trace)
0 to 400g take up tension

IIT RESEARCH INSTITUTE

39

friction are a function of the ratio of two forces and the equipment was calibrated with gram weights, the vertical scales are expressed in units of grams/division (one gram = 0.035 ounce). The vertical center of each photograph corresponds to a drag force of zero, and the lower edge of each photograph four divisions below the center corresponds to a take up tension of zero. The tension scale is 50 grams/division on each photograph. The drag force scale is 10 grams/division on the Ampex 721 and Fuji Beridox photographs, and 4 grams/division on the Ampex 797 and 3M5198 photographs.

The drag force of the tape against the head makes a sharp transition from a negative value to a positive value at the instant of the tape direction change. The peak drag force immediately after this direction change is caused by the static force when the tape is not moving with respect to the head. Negative peaks just before the direction change on the Ampex 721 and Fuji Beridox photographs are probably caused by stick slip as the tape motion across the head slows to less than the critical stick slip speed. Two "sawteeth" which would be expected for two stick slip cycles are apparent on the Fuji Beridox photograph (Figure 2.7.3) and one Ampex 721 photograph before the direction change. The absence of discernable stick slip before the direction change on the Ampex 797 and 3M 5198 photographs is probably due to the low relative difference between $\mu_s$ and $\mu_d$ of these tape types which is likely to reduce the critical stick slip speed.

Low frequency friction force oscillations which follow the direction change and the reinitiation of tape slipping do not have

the characteristic sawtooth shape expected for stick slip, but they do follow oscillations in take up tension and appear to be caused by tension instability following the change of tape tester motor rotation. Alternatively, stick slip and the transducers could interact to dampen the stick slip waveform and give the appearance of tension oscillations on the photographs, but this is not indicated by the much greater amplitude of the tension oscillations as compared to the friction force oscillations.

The take up tensions, represented by the nearly horizontal trace on each photograph, are very stable or decrease slowly before the direction changes, increase by about 20 grams at the instant of the direction changes, and exhibit the low frequency damped oscillations associated with the friction force oscillations mentioned above following the direction changes. The tension increase at the instant of the direction changes and the following damped oscillations may be caused by the tape tester motors and drive electronics or elasti properties of the tape.

Standard deviations of 1% to 4% of the take up tension were calculated from tension measurements at the instant of the direction changes and 0.1 second after the direction changes which would cause errors of similar magnitude if tension were assumed constant for each measurement. The mean values of tension at the instantaneous points employed for tension measurements did not vary significantly from one tape type to another.

The width of the drag force traces is caused by transport vib-

rations which cannot be filtered electronically without affecting the static peaks. Increases in drag force trace width immediately after the direction change are caused by "ringing" of the head and its mount in response to the step function imposed by the tape direction changes. Trace width increases about 0.3s and 0.5s after the direction change result when transport vibration frequencies match the natural vibration frequency of the head mount. All photographic measurements were taken at the centers of the traces in order to reduce errors due to vibrational and ringing effects.

Static friction measurements were taken at the instant of peak positive friction force immediately after the direction change represented by the vertical portion of the friction force traces. The calculated mean values and standard deviations of the static coefficient of friction are presented in the first column of Table 2.7.1. Initially, the time 0.1 sec. after the direction change was selected for measurements of dynamic friction force. This point corresponds to a positive slope and intermediate amplitude level of the damped oscillations following the direction changes of each tape type. The mean values and standard deviations resulting from the 0.1 sec. dynamic coefficient of friction calculations are presented in the second column of Table 2.7.1. Analysis of the possibility of stick slip phenomena or interaction between the transducers and elastic properties of the tape suggested the possibility of erroneous dynamic data at the 0.1 sec. time. Therefore, dynamic coefficients of friction were recalculated from the available photographic data at times 0.5 seconds after the direction change when the oscillations

Table 2.7.1:  Coefficient of Friction

| Tape Manufacturer and Type (Lot) | Static Coefficient of Friction $\mu_s$ | | Dynamic Coefficient of Friction $\mu_d$ (at 0.1s after direction change) | | Dynamic Coefficient of Friction $\mu_d$ (at 0.5s after direction change) | |
|---|---|---|---|---|---|---|
| | Mean Value | Standard Deviation | Mean Value | Standard Deviation | Mean Value | Standard Deviation |
| Ampex 466 (½ inch sample not yet available) | | | | | | |
| Ampex 721 (7 593 27GJ11, 21x014061-13 | 0.296 | 0.009 | 0.255 | 0.011 | 0.237 | 0.004 |
| Ampex 797 (76142, 264485291-16, Lot A-2) | 0.203 | 0.018 | 0.194 | 0.016 | 0.181 | 0.000 |
| Fuji Beridox (PFD 018) | 0.352 | 0.010 | 0.301 | 0.014 | 0.260 | 0.005 |
| 3M 5198 (41752 090 10 42) | 0.185 | 0.015 | 0.174 | 0.014 | 0.167 | 0.009 |

have been well dampened. Two Ampex 721 and 797 photographs, three Fuji Beridox photographs, and four 3M 5198 photographs had data at 0.5 sec. The mean values and standard deviations of $\mu_d$ calculated from the 0.5 second data are presented in the third column of Table 2.7.1. The 0.5 sec. values are lower and seem to be more repeatable than the 0.1 second data.

One additional feature was noted during analysis of the force-tension photographs. The magnitude of the friction force before the direction change is consistently greater than or equal to the magnitude of the force after the direction change. The tension increase during the direction change would be expected to produce the opposite effect. A one or two gram change in the zero level was detected and corrected between some of the measurements, but the procedure prevented zero drift of the force instrumentation as a source of this consistent effect. The photographs and $\mu$ calculations suggested that this zero drift was a major source of error for individual calculations of $\mu$, but that the sample size was great enough to eliminate significant error from all tape types except 3M 5198 where the data obtained from one photograph may have reduced the mean values by about 3% (0.005 units).

### 2.7.3 Conclusions

The Ampex 797 and 3M 5198 oxide surfaces exhibit low coefficients of friction and small differences between the static and dynamic coefficients. The friction properties of Ampex 721 and Fuji Beridox samples rank third and fourth respectively, and those tape types have much greater differences between $\mu_s$ and $\mu_d$ than the low friction tape

types. No likely correlations were noted between the coefficients of friction and the results of other physical property tests such as lubricant content, abrasion resistance, and abrasivity. Scanning electron micrographs suggest that the friction properties of Ampex 797 could result from a high degree of oxide particle orientation in the longitudinal direction, while the 3M 5198 frictional properties could result from a smooth oxide surface. The smooth surface of Fuji Beridox did not result in low coefficients of friction.

The test method has several potential sources of error, and it is difficult to assess the absolute accuracy of the method. A low degree of absolute accuracy is typical of friction measurements in general, and many operating conditions including temperature, relative humidity, tape speed, tape tension, and tape wear can affect frictional properties of oxide surfaces against recorder heads. However, the repeatability of the results from the current test series indicates that the current procedure including careful control of operating conditions and photograph measurements is adequate for ranking the virgin performance of the subject tapes at typical laboratory environmental conditions. Facilities are available for additional measurements with tape wear and environmental variations. Tests with higher tape tension are also possible.

Comparison of the current results with results in the March, 1982 progress report shows wide variations in coefficients of friction and no correlation between tape type and frictional properties. These differences are probably related to the lack of adequate measurements and control over

tape tension and width suggested in previous reports which gave impetus for the tension measurements and more careful control of test conditions employed in the current test series. For this reason previous results were not included in this report, and Ampex 466 which has not been obtained in the 1/2 inch width was not included in the current test series. The differences between the previous results for a 1/2 inch Ampex 721 tape at about 9.5 ounces of tension are within 15% of the current results at 8.5 ounces of tension, and the current procedure refinements are expected to increase test repeatability to an acceptable level. The differences between the previous results with 1/4 inch tape and higher tension/tape width ratios demonstrates the need to control test conditions carefully.

## 2.8 Abrasivity

Oxide surface abrasivity or the rates of head wear produced by different tape types can be affected by many variables of the heads, the transport, the tape surface, and the environment. Some abrasion is desireable to prevent buildup of varnish on the surface of the head, but excessive head wear would be disastrous to a satellite recorder. Considerable controversy exists in the field of abrasivity testing. Although several test methods have been developed, little has been done to correlate results of various methods with actual rates of head wear or varnish buildup.

The alfesil bar test was selected for tape abrasivity measurements because the method is simple, is in wide spread use, and offers a relatively high degree of precision. The test is also under consideration as an American National Standard and is the subject of active research. Current studies by several laboratories to assess repeatability and correlation between results and actual head wear will be monitored and reviewed prior to further testing recommended below.

The most obvious factor which would affect the test results is the force of the tape against the alfesil bar, which in turn is related to the tape tension at the bar. Tape tension is usually measured at the take up reel, but the friction of the tape (usually the back coating) or transport bearings as the tape passes over guides, rollers and capstans along with the force of a vacuum column against the tape can change the tape tension between the take up reel and the location of the abrasivity test bar. Bearing friction and vacuum column force may produce relatively constant tension changes for different tape types, but pre-

liminary measurements of tension at the abrasivity test fixtu.e with three different 1/2 inch tape types and 7.5 ounce take up tension resulted in tension at the test bar from 5.5 ounces to 6.5 ounces, which suggests that tape friction and transport configuration are important variables in this test.

On the alfesil test bar, the width of the worn surface is approximately twice the depth of the worn surface, so the contact area between the tape and the test bar increases with the wear depth, in contrast to an actual head where the contact surface would not change as much as the wear depth increases. Assuming the pressure of the tape against the worn surface of the test bar decreases in inverse proportion to the area of the worn surface, the rate of wear probably decreases as the wear dep and the area of the worn surface increase. If the wear rate is directly proportional to the area of the worn surface, the amount of wear will be proportional to the square of the wear width that is measured in this test. This relationship could be tested with different lengths of a single tape type.

If tape tension and width are varied in direct proportion, the pressure (force/unit area) of the tape against the alfesil test bar should be constant at any given wear width. If the wear rate is assumed proportional to the wear width and the pressure for a given tape, this relationship and the constant tension per unit tape width specified in the procedure permits comparison of test results with different tape widths. However, a test series with a constant width for all tape types is recommended if results of current research indicate that the test results are a valid indicator of head wear.

## 2.8.1 Procedure

This currently reported test series was conducted with multiple samples on each available 1/4 inch wide tape type and a single 1 inch wide Ampex 466 sample at ambient temperatures of 75 ±5° and relative humidities of 14% to 21%. Samples were obtained from different tape reels. The following procedure was employed for each tape type, and the means and standard deviations derived from wear width measurements were calculated for each type.

Wind 1700 feet of virgin tape onto a supply reel. Mount a clean alfesil test bar with an unworn edge on the test fixture. Install the test fixture on the tape transport. The test fixture provides a 16° total wrap angle with 8° of wrap on each side of the bar. Set the transport tape speed to 3-3/4 ips and the tape tension to 16 ounces/inch of tape width. Run the test tape end-to-end for one pass only. Define the reference end of the wear pattern as the end toward lower track numbers of a tape recorder head. For recorders with supply reels that turn counterclockwise for the forward tape direction, the reference end of the wear pattern is the end closest to the tape recorder. Remove the test bar and mount on a microscope with a calibrated scale and 400 x optics. Measure the width of the wear at three points by sharply focusing the edges of the wear pattern, observing the width against the microscope scale, and multiplying the divisions by the microscope scale calibration factor. The measurement points are one-fourth, one-half, and three-fourths of the distance from the reference end to the opposite end of the wear pattern. During microscopic observation, unusual wear patterns such as scalloping of the work surface or flaking of the worn bar edge should be noted and recorded. Figure 2.8.1 illustrates a typical wear pattern and the points of wear width measurements.

49
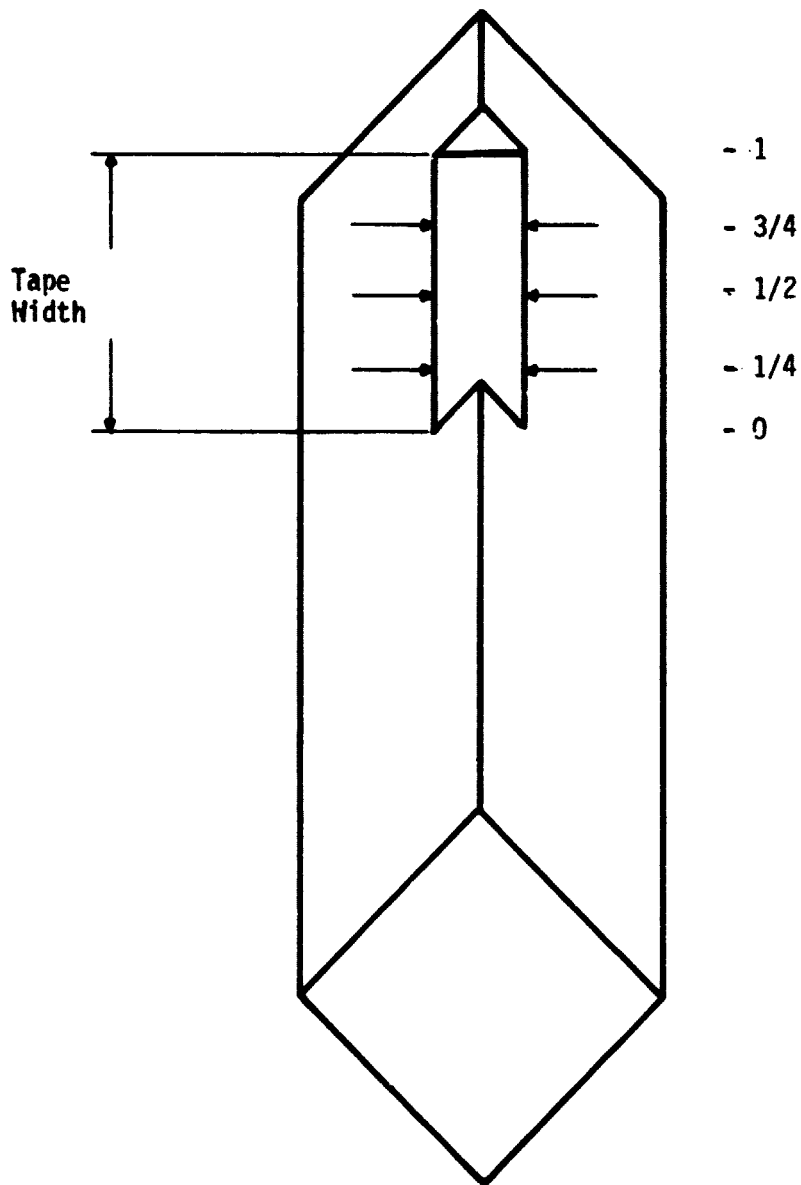
Fig. 2.8.1: Alfesil bar following abrasivity test illustrating three locations for measuring wear width (horizontal arrows). Amount of wear has been greatly exaggerated for clarity.

### 2.8.2 Results

The first column of Table 2.8 lists the results of the test series conducted at the environmental conditions specified above and with standardized tape tension/unit width. The results were obtained from a single 1 inch sample of Ampex 466, two samples each of Ampex 721 and 797, and three samples of 3M 5198

### 2.8.3 Conclusions

The current test results suggest that abrasivity increases with abrasion resistance and binder strength results in Table 2. No other likely correlations were obvious from the data obtained up to this point.

If we assume that abrasivity or wear rate is proportional to the square of the wear width, the normalized results of Table 2.2 are misleading. Ampex 721 and 3M 5198 would be 5 to 8 times more abrasive than Ampex 466 and 797 rather than 2 or 3 times more abrasive as suggested by the tabulated results. This relation could be checked by testing with different sample lengths of the same tape type.

### 2.9 Scanning Electron Microscopy

The appearance of a magnetic tape oxide surface on a scanning electron micrograph (SEM) may provide evidence regarding oxide particle size, distribution and orientation, surface roughness, and the presence of dirt or debris. The appearance can then be correlated with other surface properties such as abrasivity and coefficient of friction. The surface appearance may also indicate features responsible for bulk performance properties including abrasion resistance, orientation ratio of the particles, and surface DC noise. Production variations that affect tape performance may be analyzed by comparing SEM's from different tape lots.

Table 2.8.1: Oxide Surface Abrasivity

| Tape Manufacturer and Type (Lots) | Abrasivity (Head Wear) | | |
|---|---|---|---|
| | Width (mils) | | Width (normalized) |
| | Mean | S.D. | |
| Ampex 466 (5166041921) | 0.86 | 0.08 | 0.36 |
| Ampex 721 (11Q24182) (11Q024171) | 2.21 | 0.24 | 0.92 |
| Ampex 797 (76142,164485221-4, Lot A-1) (76142, 164485222-23, Lot A-1) | 0.93 | 0.12 | 0.39 |
| Fuji Beridox (PFD 018) | -- | -- | -- |
| 3M £198 (41575-1-01-58) (41575-1-01-15) (41575-1-01-16) | 2.39 | 0.48 | 1.00 |

IIT RESEARCH INSTITUTE

## 2.9.1 Procedure

Scanning electron micrographs of oxide surfaces have been obtained from virgin samples of each tape. Each sample was micrographed at approximately 2400 x and 12000 x with viewing angles perpendicular to the tape surface and 45° from the long axis of the tape. The long dimension of each SEM photograph corresponds to the transverse direction across the tape, and the short dimension of the photographs correspond to the long axis of the tape.

Each view was selected to represent a typical portion of tape surface. The procedure did not include a search for defects or surface variations over large areas or between tape lots.

## 2.9.2 Results

The following ten pages are the SEM's of oxide surfaces for each tape type. The viewing angles indicated on these photographs are between the line-of-sight and a line perpendicular to the tape surface.

The micrographs indicate that 3M 5198 has the smallest and most closely packed particles. Tne Ampex and Fuji tapes have roughly equivalent particle sizes. Ampex 466 and 721, and Fuji Berisox have moderately close particle packing while Ampex 797 has loose packing. The high orientation of Ampex 797 particles can be seen by comparing 0 degree 12000X views. The mottled appearance of the Fuji Beridox 0 degree 2400X view is due to uneven particle distribution which does not show clearly in the limited field of view of the 12000X image. The 45 degree 2400X Ampex 797 SEM shows a large scale surface roughness which is not apparent on any of the other tape types.
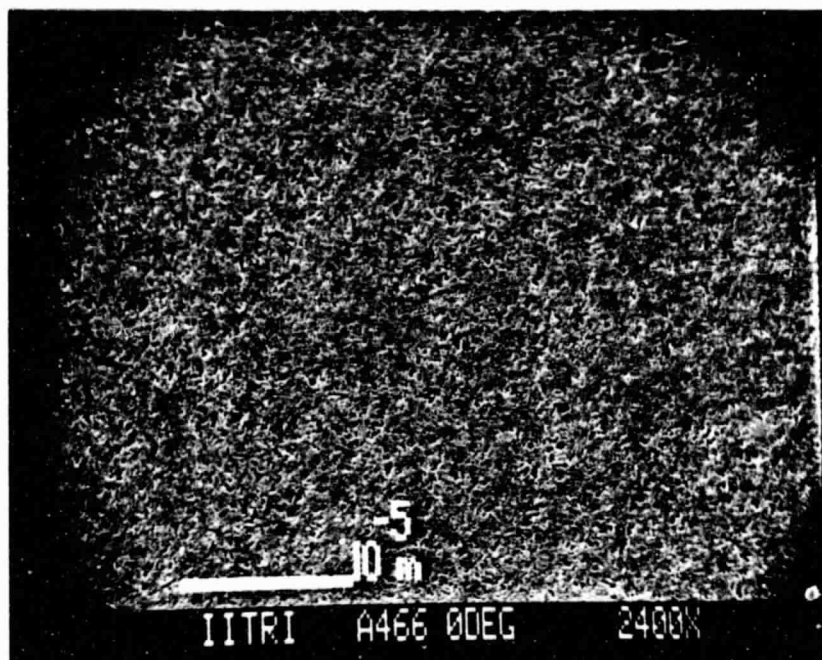
Figure 2.9.1a:   Ampex 466 Oxide Surface, 0 Degrees, 2400x
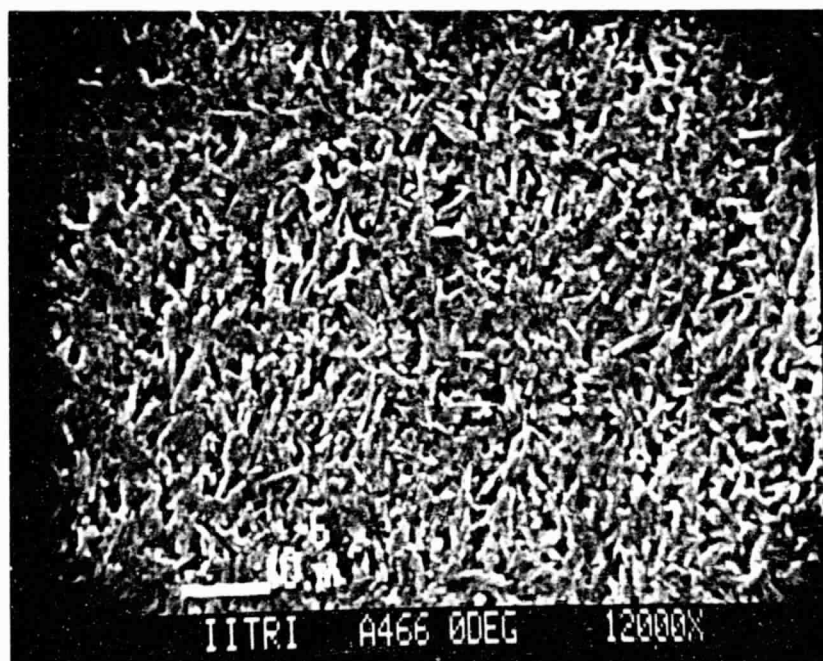


Figure 2.9.1b:   Ampex 466 Oxide Surface, 0 Degrees, 12000x

54

Figure 2.9.1c:   Ampex 465 Oxide Surface, 45 Degrees, 2250x
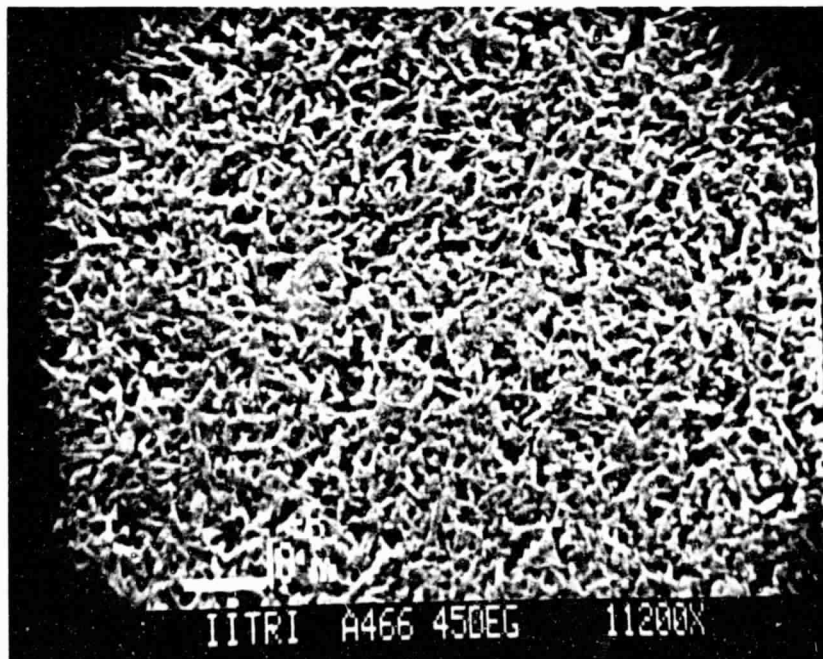


Figure 2.9.1d:   Ampex 466 Oxide Surface, 45 Degrees, 11200x

55

Figure 2.9.2a:  Ampex 721 Oxide Surface, 0 Degrees, 2400x
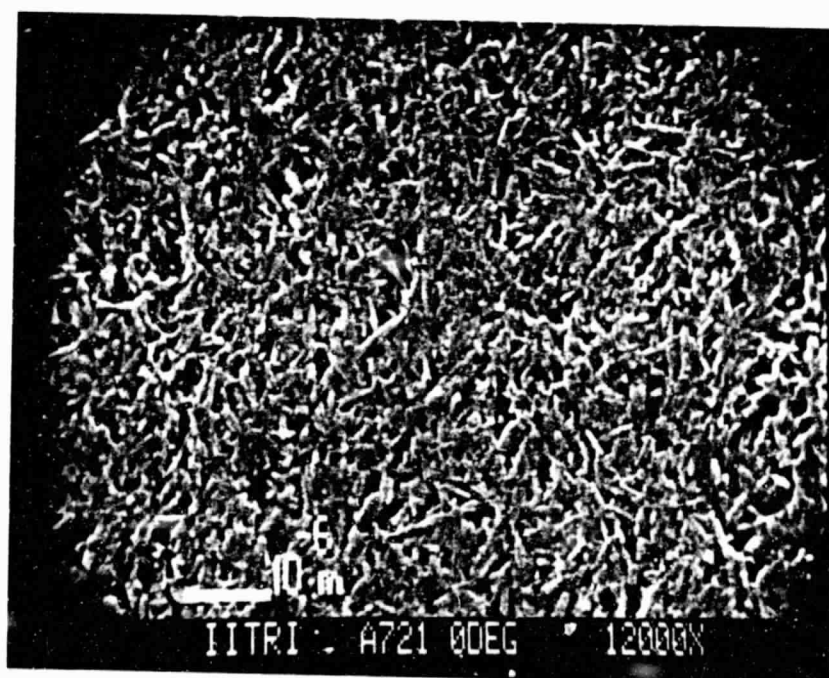


Figure 2.9.2b:  Ampex 721 Oxide Surface, 0 Degrees, 12000x
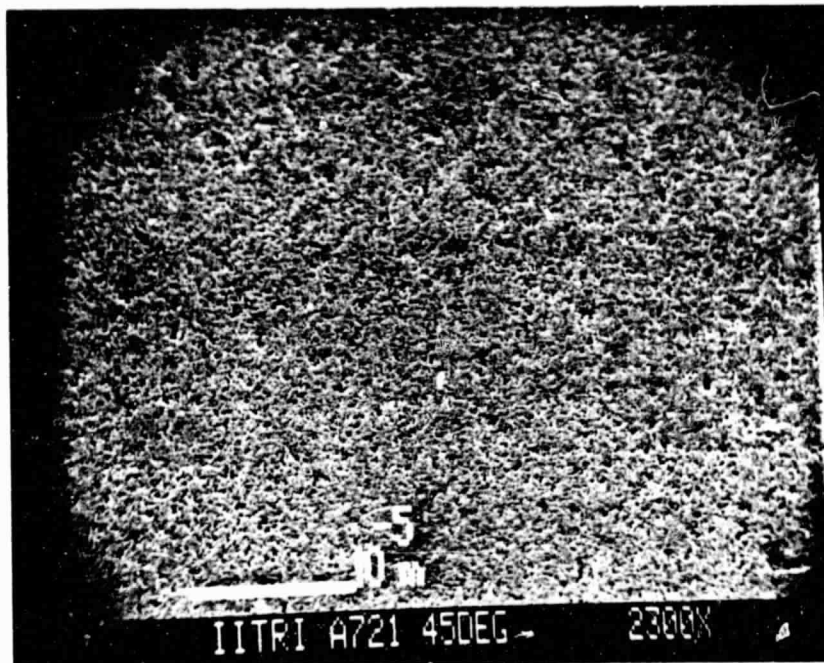
Figure 2.9.2c:  Ampex 721 Oxide Surface, 45 Degrees, 2300x
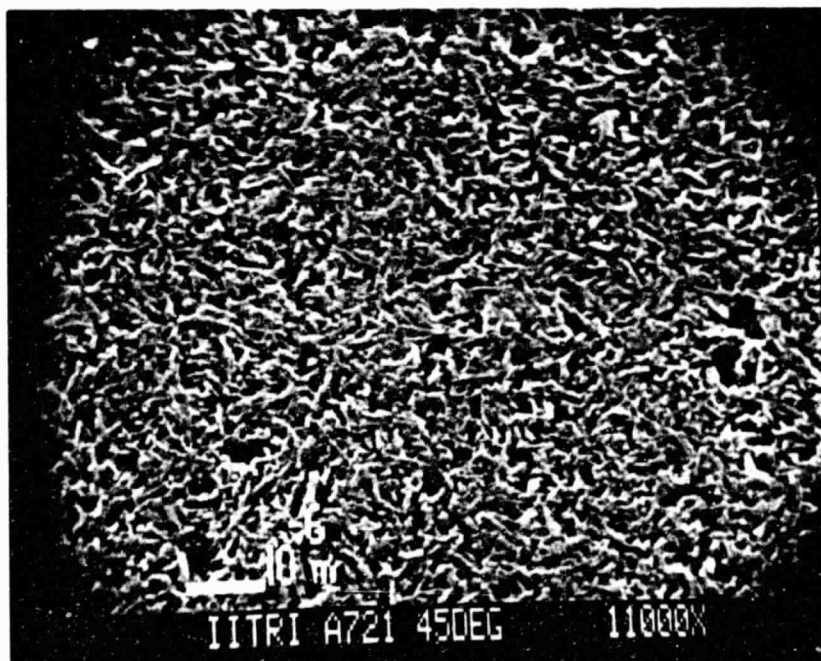


Figure 2.9.2d:  Ampex 721 Oxide Surface, 45 Degrees, 11000x

57
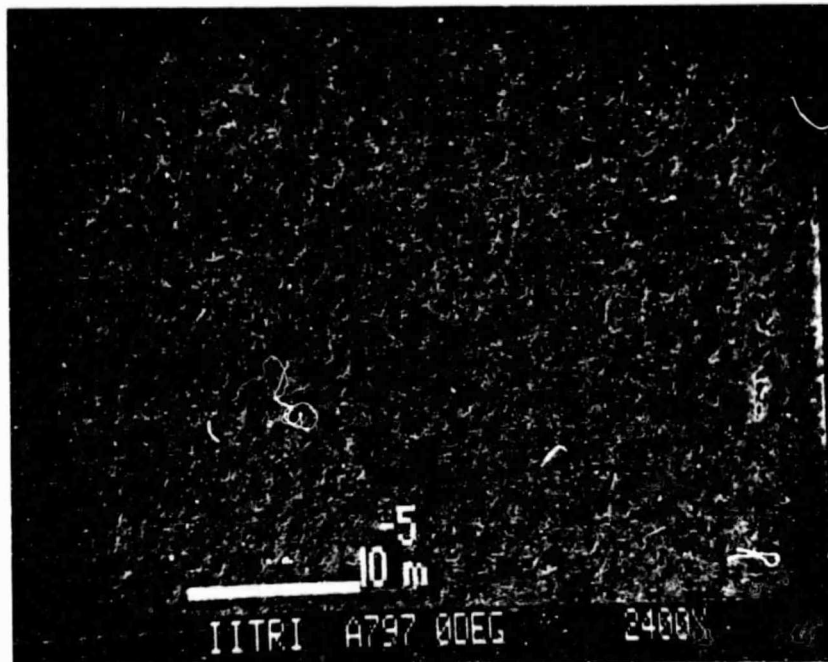
Figure 2.9.3a: Ampex 797 Oxide Surface, 0 Degrees, 2400x
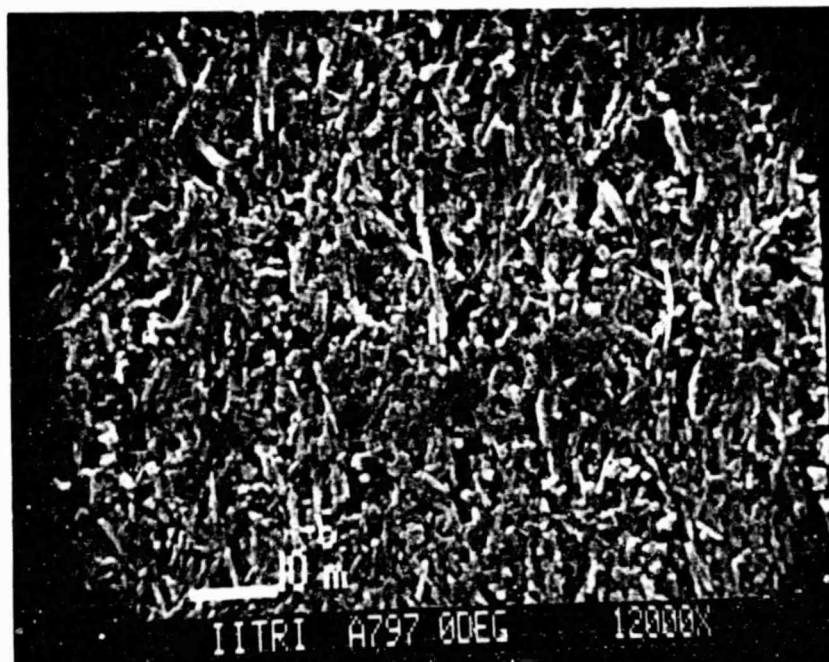


Figure 2.9.3b: Ampex 797 Oxide Surface, 0 Degrees, 12000x

58
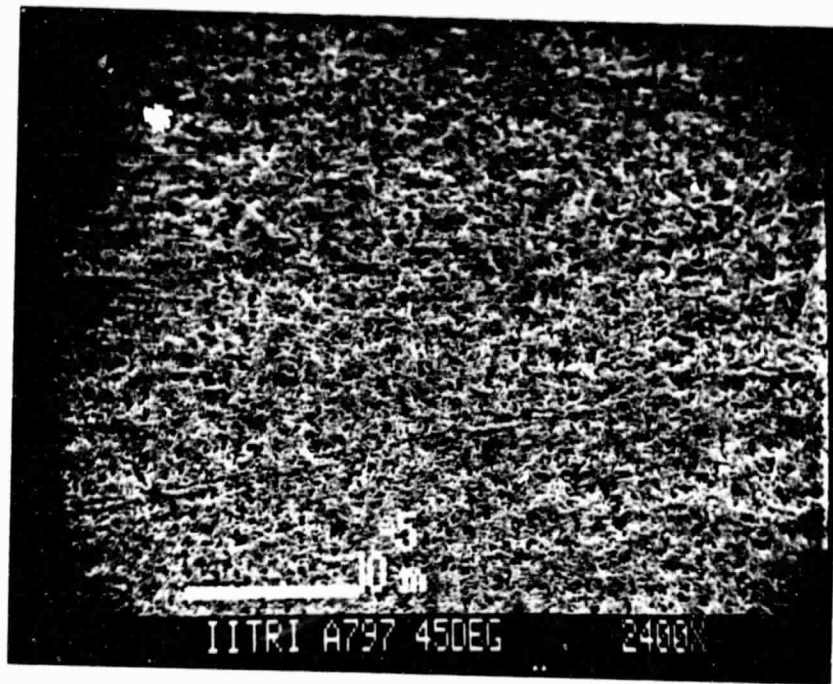
Figure 2.9.3c: Ampex 797 Oxide Surface, 45 Degrees, 2400x
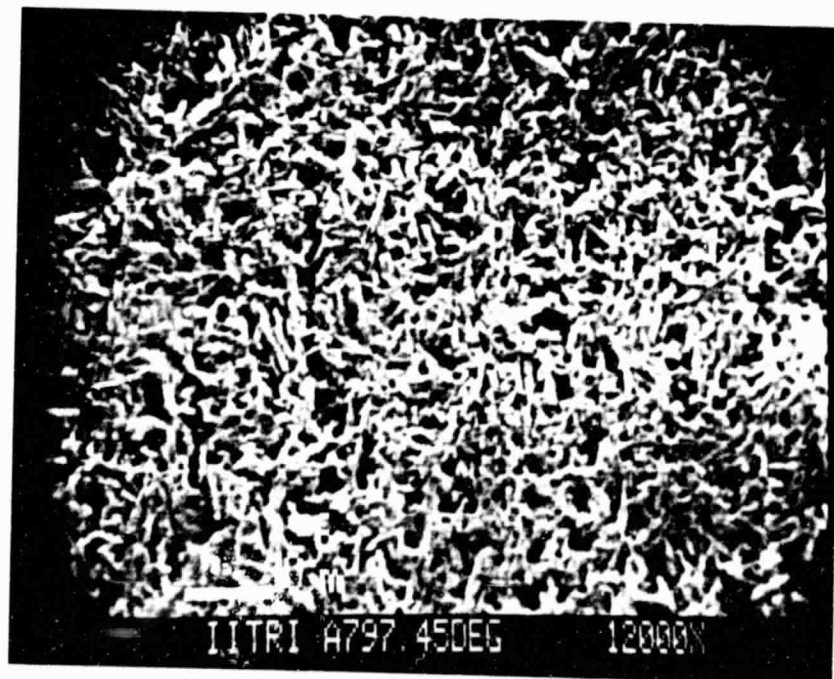


Figure 2.9.3d: Ampex 797 Oxide Surface, 45 Degrees, 12000x

59
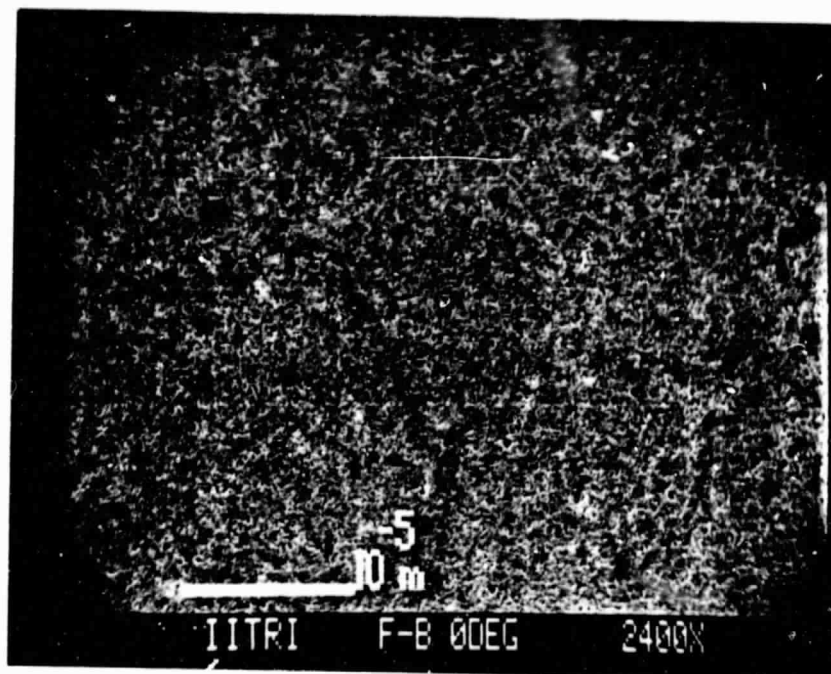
Figure 2.9.4a:  Fuji Beridox Oxide Surface, 0 Degrees, 2400x
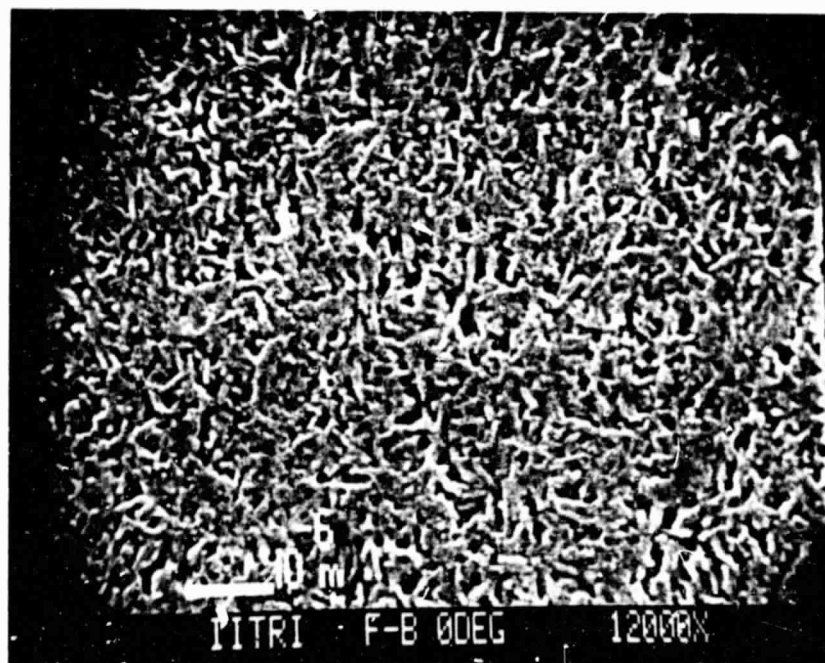


Figure 2.9.4b:  Fuji Beridox Oxide Surface, 0 Degrees, 12000x

Figure 2.9.4c:   Fuji Beridox Oxide Surface, 45 Degrees, 2200x
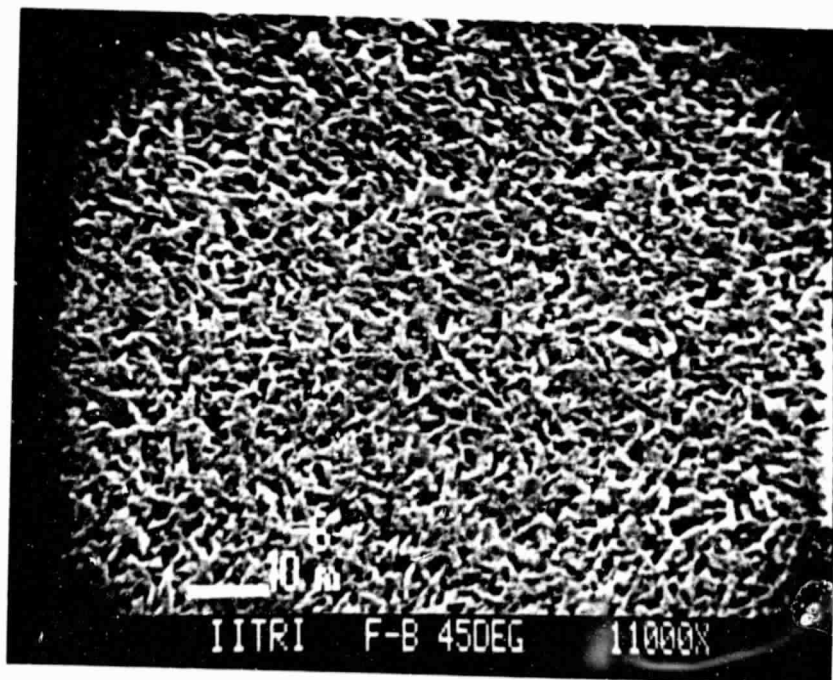


Figure 2.9.4d:   Fuji Beridox Oxide Surface, 45 Degrees, 11000x
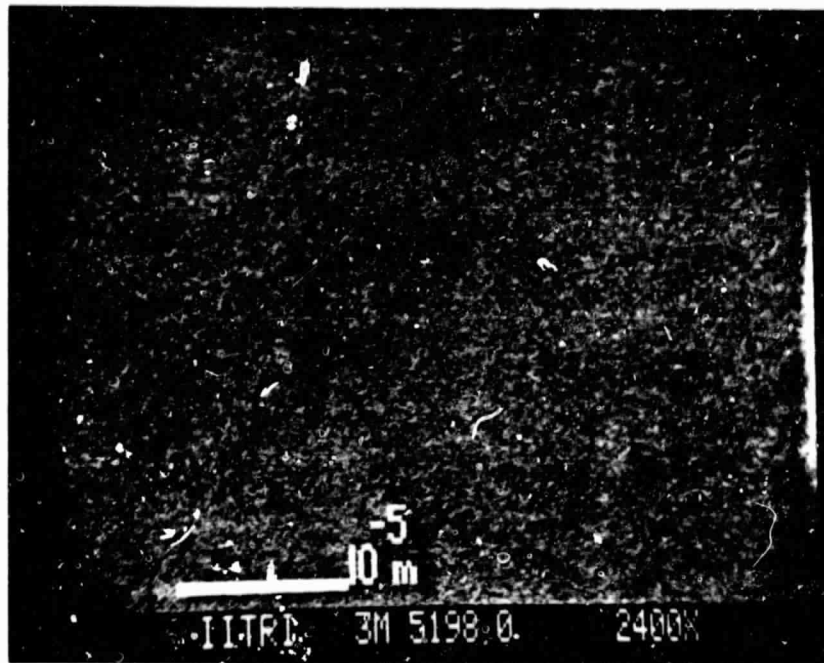
Figure 2.9.5a:  3M 5198 Oxide Surface, 0 Degrees, 2400x
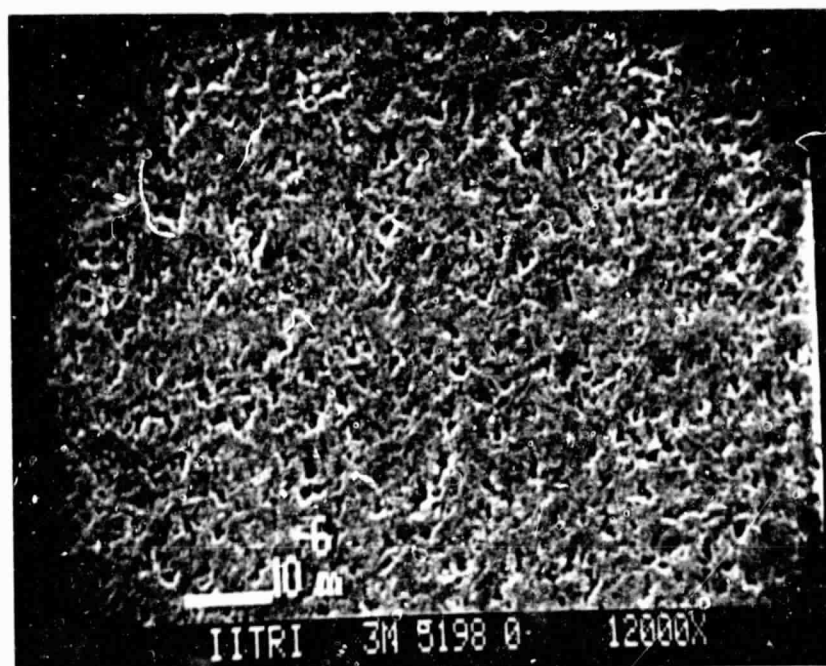


Figure 2.9.5b:  3M 5198 Oxide Surface, 0 Degrees, 12000x

Figure 2.9.5c:  3M 5198 Oxide Surface, 45 Degrees, 2400x
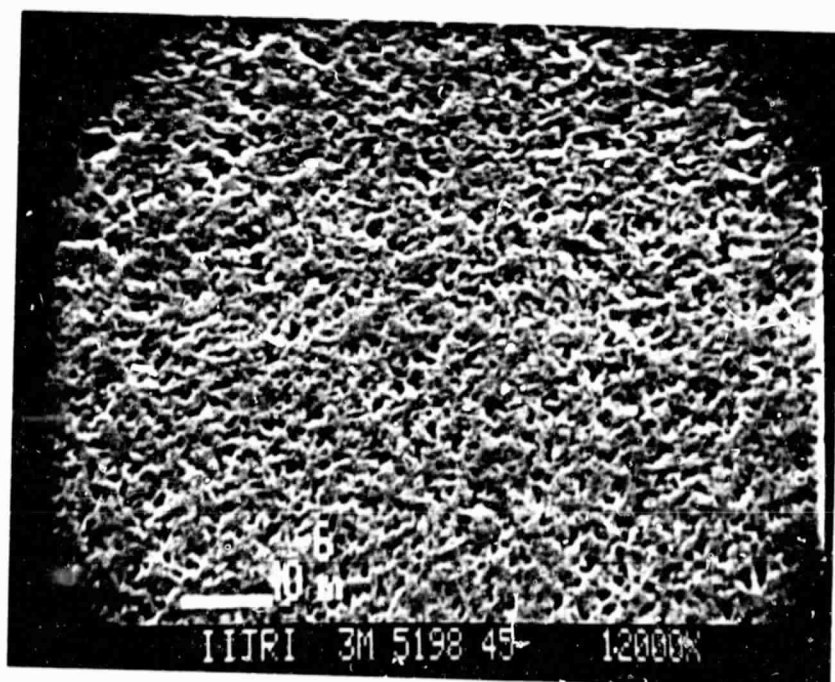


Figure 2.9.5d:  3M 5198 Oxide Surface, 45 Degrees, 12000x

63

## 2.10 Oxide Surface Cleanliness

Debris on a tape oxide surface can lift the tape away from the head and may constitute a major source of crop-outs. The following test compared two of the subject tape types, Ampex 721 and 3M 5198, in an attempt to correlate the cleanliness of their oxide surfaces with the higher drop-out rate associated with Ampex 721 (Section 4.4).

### 2.10.1 Procedure

Virgin 3950 ft x 1/4 inch samples of Ampex 721 (lot 11Q024182) and 3M 5198 (lot 41575-1-01-26) were mounted on the transport of a Kybe Corp Model CT-100 Tape Tester. The tester was modified by replacing conventional tape guides with crowned guide rollers, eliminating the oxide surface scraper blade, and stopping the cleaning tissue drive mechanism so that the entire length of the test tape would contact the same spot on the cleaning tissue during a given test run. After each forward end to end pass of the tape samples, the tissue cartridges were removed, the tissues were advanced a few inches and marked to indicate the run number, the tapes were rewound, and the tissue cartridges were reinstalled for the next run. The amount of debris on the tissues were observed subjectively and tissues from the different tape types were compared.

### 2.10.2 Results

The white cleaning tissues contrast well with loose oxide, but any light colored debris present on the oxide surfaces was not likely to be identified during the test.

Four test runs were conducted on the Ampex 721 sample. Two test runs were conducted on the 3M 5198 sample before testing was halted due to the guidance problem described below that may have affected the results of the second run.

**IIT RESEARCH INSTITUTE**

The heaviest accumulation of debris occured where the edges of the tapes pass across the cleaning tissue. Debris accumulation at the edges after the first Ampex 721 run was heavy enough that some loose particles fell off the tissue and were lost. Debris accumulation at the edges after the first 3M 5198 run was estimated at less than 1/10 of the amount from the first Ampex 721 run. Subsequent Ampex 721 runs also produced heavy edge debris but no loose accumulations, and the amount of debris produced during each run appeared to stabilize following the initial run. In contrast, the 3M 5198 sample produced more edge debris on the second run than on the first run. This result may be due to inadequate guidance and/or a defective reel flange that caused light scraping of the 3M 5198 sample against the reel flange during the first rewind and the second test run.

Much less debris accumulated away from the edges of the tape samples, but the effects of repeated test runs away from the tape edges were similar to the results at the tape edges. The Ampex 721 sample produced more debris than the 3M 5198 sample during the first run. The Ampex 721 sample produced a relatively constant amount of debris during subsequent runs that exceeded the debris produced by 3M 5198 during its first run. More debris accumulated on the second 3M 5198 run, but it was associated with the guidance problem.

All of the accumulated debris from both tape types was uniformly dark in color and was associated with loose oxide or back coating material.

### 2.10.3 Conclusions

Virgin Ampex 721 has more loose dark surface debris than virgin 3M 5198. Ampex 721 may continue to produce debris following cleaning, but this effect cannot be compared with the 3M 5198 results.

The test procedure could be modified to detect light colored debris by staining the tissue dark prior to a test run. The sample length employed for this test series may be excessive. Use of 1000 foot samples is under consideration for any future testing.

## 3. MAGNETIC PROPERTIES

This section includes the results from three series of M-H measurements on the subject tape types and parameters derived from the measurements. The first test series includes measurements of longitudinal properties at $20^\circ$C and 20% relative humidity including measurements of four or more samples on three of the tape types. The second test series shows the relationship between temperature and the coercivity and residual induction of single longitudinal tape samples. Finally, the magnetic properties of single transverse samples and orientation ratios of the tapes are reported.

An accurate calibration method or standard has not yet been obtained for the remanence (M) axis of the M-H curve plotter. Comparison of the current results with various manufacturer's specifications suggests that the reported results are only 0.7 times other manufacturer's specifications. Saturation induction and residual induction are directly dependent on the maximum applied field, and this effect is under investigation as the source of the M axis calibration inaccuracy. Discrepancies in the M axis calibration will only affect the values of saturation induction Ms and residual induction $M_r$ which can easily be corrected in future reports when a more accurate calibration is obtained. The squareness and orientation ratios, and the switching field distributions (SFD) can be calculated with arbitrary M-axis scales and do not depend on the absolute accuracy of the calibration.

The SFDs of data obtained for the March 1982 report were calculated from measurements with the H axis expanded five times. During the current reporting period, the M-H curve plotter was modified to produce the dM/dH-H curve which permits direct measurement of the SFD.

## 3.1 Theory of B-H Measurements

According to classical electromagnetic theory, a changing magnetic flux $\phi_B$ induces an electromotive force:

$$\mathcal{E} = -\frac{d\phi B}{dt} \tag{3.1}$$

If the flux density B is constant over a given area A then the flux equals the flux density multiplied by the area:

$$\phi_B = B \cdot A \tag{3.2}$$

Substitution of 3.2 into 3.1 and integration shows that the flux density is equal to the integral of the induced EMF divided by the area:

$$B = -\frac{1}{A} \int \mathcal{E} \, dt \tag{3.3}$$

Equation 3.3 is valid for a magnetic field in a vacuum and is a close approximation when weak magnetic materials such as air, glass, mylar or wood are present. When a ferromagnetic material is present, an external field aligns magnetic domains in the material, and the resultant flux density can be described by:

$$B = \mu o \, H + J \tag{3.4}$$

where $\mu o$ is the permeability of free space and is equal to $1 \frac{gauss}{oersted}$ in the CGS system of units, H is the applied magnetizing field, and J is the magnetization induced in the ferromagnetic material by the applied field H. Equation 3.4 is often written:

$$B = \mu o \, (H + M)$$

where $M = J/\mu o$. Since the magnitude of $\mu o$ is unity in the CGS system, we can ignore dimensions and write:

$$B = H + M$$

68

For technical reasons discussed below, the flux density in the sample produced directly by H cannot be measured directly. Only the induced magnetization M(or J) is measured.

Figure 3.1.1 is a simplified schematic of the IITRI M-H Curve Plotter. The 120 volt 60 hz input power is coupled through isolation transformer T1 and circuit breaker CB1 to the H field control variable autotransformer T2 and the H field range autotransformer T3 to produce a drive voltage across the excitation solenoid L which produces a uniform magnetic field at the H and M pickup coils. The H range switch S1 selects one of two taps on T3 and one of two resistors R1 or R2 in series with the H meter which are connected across the excitation solenoid to indicate the fraction of the selected H range produced by the solenoid. The value of a bank of capacitors C1 places the excitation circuit near resonance to reduce the input current required by the curve plotter.

The voltage across the excitation solenoid is also applied to calibration network including R 15, R 16, and the sample size precision voltage divider. When S3 is in the calibrate position, known in phase sinusoidal voltages developed by the networks are applied to the inputs of the H and M amplifiers to allow adjustment of the oscilloscope input sensitivities. The sample size voltage divider provides an M calibration voltage which is proportional to the sample cross sectional area so that the vertical sensitivity of the oscilloscope can be adjusted in inverse proportion to the sample area as required by the 1/A term of equation 3.3.

The H cal and B cal variable resistors R 15 and R 16 are internal controls which set the output voltages of the calibration networks equal

Figure 3.1.1: Simplified
Schematic of IITRI
M-H Curve Plotter

to the output voltages of the H and M integrators. A standard sample is required for the adjustment of R 16. The peak magnetizing field Hm can be calculated from the solenoid geometry and current or measured by a calibrated magnetometer with an axial probe inserted into the sample holder of the curve plotter. R 15 is adjusted for equal horizontal trace size in the measure and calibrate modes.

Two pickup coils H and M are located in the uniform magnetic field region within the solenoid. The M pickup coils encircles the sample tube so that the voltage induced in M is caused by both the applied field over the cross sectional area of M and the induced magnetization of the sample over the cross sectional area of the sample. Since the M coil area is much greater than the sample area, it is necessary to apply a voltage in series with the M coil to cancel the voltage induced by the applied field. To accomplish this, a sinusoidal voltage is induced in the balance pickup coil B located at one end of the solenoid. This voltage is applied across bridge R9, R10, R11, and C2, and the bridge output is connected in series with the M pickup coil. R10 controls the in-phase amplitude of the balance voltage while R11 sets the phase of the balance voltage equal to the voltage induced in M by the field. Together, these controls are adjusted with the sample holder empty to cancel the voltage induced in M by the field, and the voltage induced by the sample magnetization is applied through switch S2 to the M amplifier. With switch S2 in the M position this voltage is integrated by R5, R6, C6, C7, and C8 before application to the amplifier. With S2 in the dM position the voltage is attenuated by R7 and R8 and is applied to the amplifier without integration.

The H pickup coil is wound around the M pickup coil so that its area is so large with respect to a sample area that the voltage induced in H by the sample magnetization is insignificant with respect to the voltage induced by the field and the voltage can be integrated by R3, R4, C3, C4, and C5 before application to the H amplifier.

The M and H outputs of the M-H curve plotter are connected to the vertical and horizontal inputs respectively of an oscilloscope. The horizontal H axis sensitivity of the oscilloscope can be adjusted for a convenient H axis scale factor. In the calibrate mode, the signal applied to the vertical axis of the oscilloscope is equal to 0.5 gauss/oersted of the applied field setting, which permits the adjustment of the vertical M axis sensitivity for a convenient scale factor. Oscilloscope calibration is detailed in Section 3.4.

Three parameters can be measured directly from oscilloscope photo-graphs of magnetic hysteresis loops. The values are calculated by mul-tiplying photograph measurements by scale factors. The saturation induction $M_s$ is represented by the distance between the value of M at $H = H_m$ and the H axis. The residual induction $M_r$ or remanence is the value of M at $H = 0$, which is the induction in the sample with no applied field following saturation of the sample. $M_r$ is represented by the distance between the M axis intercept and the origin. The coercivity Hc or coercive force is the value of H at $M = 0$, which is the applied field required to reduce the remanence to zero following saturation of the sample. Hc is represented by the distance between the H axis in-tercept and the origin. These parameters are illustrated in Figure 3.2.

## 3.2  Definition and Calculation of Derived Parameters

The saturation induction $M_s$, residual induction or remanence $M_r$, and coercivity Hc defined in Section 3.1 are measured directly from M-H curves produced by the M-H curve plotter. The squareness ratio is defined as the residual induction divided by the saturation induction, or squareness $= M_r/M_s$. When the magnetic particles are oriented during tape manufacturing processes, the values of $M_s$, $M_r$, and $H_c$ depend on the orientation of the tape with respect to the H field applied by the M-H curve plotter. The orientation ratio O.R. is defined as the longitudinal remanence divided by the transverse remanence of a given tape, or O.R. $= M_{rL}/M_{rT}$. Squareness and orientation are dimensionless ratios which generally have higher values for tape with greater particle orientation (transverse samples of tape with greater orientation have lower squareness values). Squareness is always less than 1 while orientation ratio is equal to 1 for unoriented particles and greater than 1 for longitudinally oriented particles.

The parameter symbolized by S* can be measured from a magnetic hysteresis loop by constructing a line tangent to the curve at H = Hc (M=0), measuring the horizontal distance A between the vertical axis and that line at the level of $M_r$, and dividing the resultant value by Hc, as indicated in Figure 3.2.1.

The switching field distribution SFD is defined as the width of the dM/dH-H curve in oersteds at the half amplitude level of the curve. The dM/dH curve can be produced electronically by defeating the integration of the voltage induced in the M pickup coil by the sample, or it can be plotted from slope measurements of the M-H curve. Figures 3.6.1 and 3.6.6 include dM/dH-H curves produced electronically with arbitrary vertical
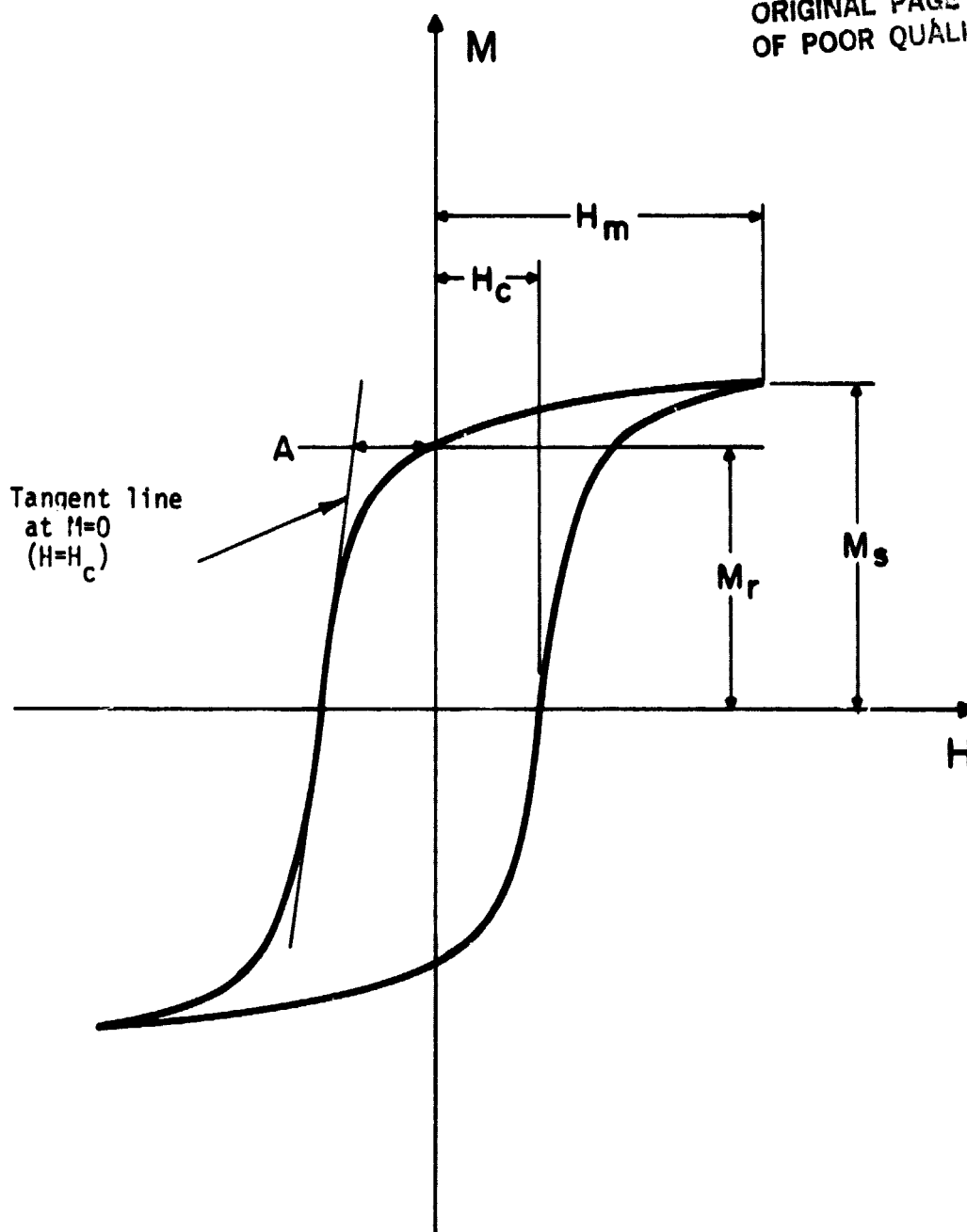
Figure 3.2.1: Typical M-H Hysteresis Loop Illustrating
Definition of $H_m$, $H_c$, $M_s$, $M_r$, and $S^* = A/H_c$

scales. The half amplitude level of the dM/dH-H curve is measured from the horizontal axis and is half the distance between the horizontal axis and the maximum positive or negative value on the curve. Figure 3.10 is a dM/dH-H curve plotted over a range of H which shows the width of the curve at the half amplitude level. The curve approaches zero at Hm, so the half amplitude level can be calculated by dividing the maximum value by 2. The normalized switching field distribution is equal to SFD divided by $H_c$.

The parameters SFD/Hc and S* are associated with the slope of the M-H loop at or around M=0 and are less than 1.0 for longitudinal samples. They are related to the number of magnetic particles which will switch their orientation for a change in the applied field around the value of $H_c$. In general, lower values of SFD/Hc and higher values of S* are associated with shorter transition zones and higher digital output for magnetic media. However, coercivity and residual induction can have a much greater effect on HDDR output than switching parameters.

### 3.3 Sample Preparation

Determine the oxide coating thickness of the tape to be tested. With a micrometer, measure the thickness of sixteen layers of tape obtained adjacent to the tape sample for M-H measurements. Divide this measurement by 16 to obtain the total thickness of one tape layer. Now remove the oxide coating from the mylar base. Place the thickness tape sample oxide up on a clean smooth surface and rub off the oxide with cotton swabs or Kim Wipes saturated with a solvent such as methyl-ethyl-ketone. Remeasure the thickness of sixteen base layers with the oxide

coating removed, divide the measurement by sixteen, and subtract the mylar thickness from the total thickness to determine the oxide coating thickness. Express the oxide coating thickness in mils (1 mil = 0.001 inches). The micrometer must be accurately zeroed and must not apply so much pressure that the tape sample deforms and causes measurement errors. Micrometers with slip mechanisms produce low and repeatable measurement pressure. The micrometer measurements should be read to the nearest 0.1 mil, and a median value of several measurements which do not vary by more than $\pm 0.2$ mil can be employed for the thickness calculations.

Determine the sample width. For longitudinal M-H measurements, tape widths of 250 mils, 500 mils, and 1000 mils may be assumed for 1/4 inch, 1/2 inch and 1 inch wide samples respectively. For transverse measurements, tape samples should be cut to suitable lengths with an accuracy of $\pm 1\%$.

Calculate the cross sectional area of the tape samples in square mils. For longitudinal measurements:

Total area = width x thickness x number of layers

For transverse measurements:

Total area = length x thickness.

For either type of measurement, the sample size must be large enough to provide an adequate signal-to-noise ratio, but it must be small enough to fit within and allow ventilation of a sample tube, and to prevent saturation of the M-H curve plotter amplifiers by large induced voltages. Total areas between 400 $mil^2$ and 2000 $mil^2$ are suitable for electronic considerations, but areas toward the low end of that range are suggested for sample holder considerations. For oxide dimensions of 250 mils x 0.2 mils, ten layers will fit within the glass tube sample holders recommended below.

The sample holder of the IITRI M-H curve plotter accepts sample tubes up to 5/16 inch in diameter. Standard 7mm glass tubing may be cut to 16 inch lengths. Fire polishing of the cut ends should be minimized to prevent narrowing of the ends which may interfere with sample insertion into the tubing.

Insert a minimum sample length of six inches into the sample holder. This minimum allows for excess tape and positioning variability within the sample holder of the M-H curve plotter.

For longitudinal measurements, the number of tapes employed in the total area calculation should be cut to lengths greater than six inches and aligned. End alignment can be achieved by trimming. Then the aligned tapes can be folded longitudinally and inserted into a sample tube. Make the final fold while inserting the sample. A sharp crease is not required for the final fold. The sample must not be twisted or kinked within the sample tube. If a twist or kink develops, it can often be removed by withdrawing the sample slightly. After at least six inches of sample have been inserted, any tape extending from the end of the sample tube can be trimmed. The ends of the sample tube should remain unrestricted.

For transverse measurements, tape should be cut to the length employed in the total area calculation. A minimum of six, twelve, or twenty-four accurately cut lengths are required for 1 inch, 1/2 inch, and 1/4 inch tapes respectively to insure adequate sample length. Each cut length must be rolled and/or folded transversly and inserted sequentially into the sample tube. The first cut and rolled tape

section should be pushed six inches into the sample tube with a rigid instrument, and each subsequent section should be pushed into the sample tube so that it just touches the preceeding section. With the number of lengths recommended above, the total sample length should be within 1% of six inches. A longer sample length indicates gaps between tape sections while a shorter sample length indicates deformation of the tape edges produced by pushing the sections too hard against each other.

A sample code and cross-sectional area should be marked on pressure sensitive paper applied to the empty end of the sample tube.

### 3.4 M-H Curve Plotter Operation and Curve Measurements

An oscilioscope with x-y display capabilities, continuously variable sensitivity controls, DC coupled inputs, and a camera is required. A horizontal sensitivity between 0.2 volts/cm and 0.5 volts/cm is required. A 500 mil$^2$ sample size requires a vertical sensitivity around 20 mV/cm. A wide bandwidth is not required due to the low excitation frequency. The 500 KHz bandwidth and control features of a Tektronix Type 503 oscilloscope are suitable.

Connect the M output of the curve plotter to the vertical or Y input of the oscilioscope. Connect the H output of the curve plotter to the horizontal input of the oscilloscope.

Make sure that the field ($H_m$) control is fully counterclockwise, and select the field range before applying power to the curve plotter. The 2000 oersted range is suitable for high coercivity samples such as cobalt doped $\gamma$-$Fe_2O_3$ tape. Warning: the field solenoid is not designed for continuous operation at high field strengths. Do not

IIT RESEARCH INSTITUTE

78

operate the solenoid at 2000 oersteds for more than one minute at a time or at a duty cycle greater than 10%. The phase and quadrature adjustments must be repeated as the solenoid heats the pickup coils.

Turn on the blower, the amplifiers, the field circuit breaker, and the oscilloscope. Allow at least ten minutes warm up. Leave the field control fully counterclockwise except during short periods when the field is required for calibration or measurements. Do not switch the field range selector or the field circuit breaker unless the field control is turned fully counterclockwise. This procedure will prevent the induction of high voltage transients due to sudden interruption of the field current.

Set the M-dM switch to the M position. Set the H gain switch to the Hx1 position. Remove any sample present in the sample holder. Set the mode switch to the "measure" position and adjust the field control for full scale deflection of the "H" meter. Adjust the in phase balance and quadrature balance controls for a horizontal trace on the oscilloscope. The in phase control affects the tilt of the trace and the quadrature control prevents the elliptical loop appearance of the trace. Note that these controls can be adjusted more accurately by increasing the vertical sensitivity of the oscilloscope. They do not affect the trace when the plotter is in the "calibrate" mode, but their setting should be checked whenever operation of the field solenoid is likely to change the temperature of the pickup coils. The blower directs air over the pickup coils to minimize these temperature changes.

Set the calibration voltage divider to $0.0001/\text{mil}^2$ of the sample cross-sectional area. With the field control counterclockwise (H=0) and the M-H curve plotter in the "calibrate" mode, center the trace on

79

the oscilloscope with the vertical and horizontal position controls. Adjust the field control for full scale deflection on the "H" meter. At this point, a diagonal trace will appear on the oscilloscope. The signal amplitude applied to the horizontal H input of the oscilloscope represents twice the applied peak field, and the signal amplitude applied to the vertical B input of the oscilloscope represents 0.5 gauss/oersted of applied field. For example, if Hm is 2000 oersteds (4000 oe peak-to-peak), the M signal represents 1000 gauss (2000 gauss peak-to-peak). Adjust the oscilloscope vertical and horizontal sensitivity controls for convenient trace width and height. To calculate the scale factors, divide the peak-to-peak H and M values by the width and height of the diagonal trace respectively. For example, if the oscilloscope sensitivities are adjusted for a diagonal six divisions high by eight divisions wide and Hm = 2000 oersteds, the scale factors will be 4000 oersteds ÷ 8 divisions = 500 oe/div and 2000 gauss ÷ 6 divisions = 333 gauss/division. The oscilloscope calibration must be repeated each time the sample cross-sectional area is changed.

With the field control fully counterclockwise and the sample holder empty, set the M-H curve plotter to the "measure" position. Center the oscilloscope trace and adjust the field control for full scale deflection of the "H" meter. Check the phase and quadrature adjustment. Insert the sample tube in the sample holder and insure adequate sample length and uniformity by observing the hysteresis loop on the oscilloscope while positioning the sample. The trace should remain stable for a variation of at least one inch in sample position, and the sample should be placed near the center of the position

range which produces a stable trace. Photograph the M-H hysteresis loop. If SFD measurements are required, set the H gain control to the H x 5 position, center one of the H axis intercepts, and photograph the expanded portion of the curve to enable accurate slope calculations, or set the M-dM switch to the dM position, adjust the vertical gain and position controls of the oscilloscope for a convenient dM/dH-H curve amplitude, and photograph the curve.

When measuring Hc and $M_r$ on the photographs, measure the intercept to intercept distances, multiply by the scale factor, and divide by 2. This reduces parallax error. $M_s$ can also be measured "peak to peak" and divided by two. When measuring the SFD from the dM/dH-H curve, measure the width of the curve at the half amplitude level and multiply the width by the horizontal scale factor. Do not divide the result by two.

Figure 3.3 is a calibration record of the M-H curve plotter. The "standard" Ampex Type 721 sample with a published $M_r$ value of 1000 gauss ± 10% was inserted into the plotter, and the oscilloscope sensitivity controls were adjusted for $M_r = \pm 3$ divisions and $H_m = \pm 4$ divisions which produce scale factors of 333 gauss/division along the vertical axis and 500 oersteds/division along the horizontal axis. Then the calibration voltage divider was set for the sample size, the plotter was switched to the calibrate mode, and the internal calibration controls H cal and B cal were adjusted without changing the oscilloscope sensitivity controls to produce the 8 division wide by 6 division high diagonal calibration trace. Now the apparatus can be recalibrated for
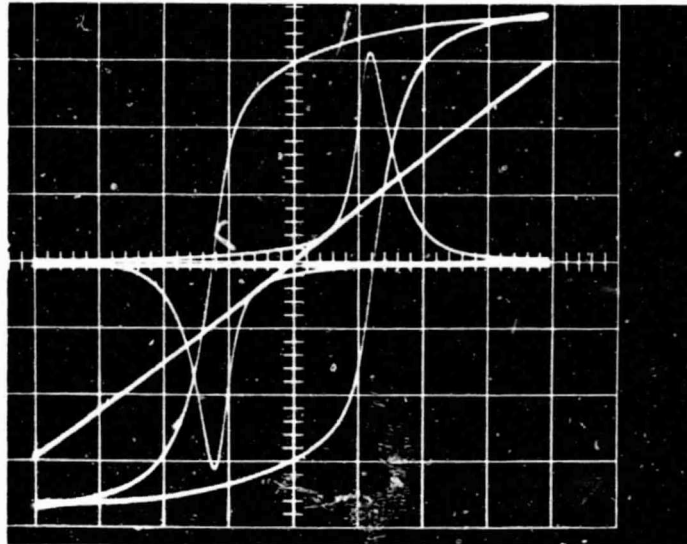
Figure 3.4.1: M axis calibration record with Ampex Type 721 and manufacturers
specification of $M_r$ = 1000 gauss as the "standard".

Horizontal scale is 500 oersteds/division.

Vertical scale is 333 gauss/division for M-H curve and diagonal
calibration trace. Vertical scale for dM/dH-H curve (pulse
waveforms in first and third quadrants) is arbitrary since only
the width at the half amplitude level is required to determine
the SFD. Horizontal trace just below horizontal axis indicates
correct adjustment of balance controls with no sample in the
curve plotter.

IIT RESEARCH INSTITUTE

82

different sample sizes and scale factors by resetting the calibration voltage divider to the sample size and readjusting the oscilloscope sensitivity controls for the desired diagonal calibration trace size without changing the internal calibration controls.

A horizontal trace on Figure 3.4.1 just below the horizontal axis is the no sample signal with proper adjustment of the balance phase and quadrature controls. The positive and negative pulse wave forms in the first and third quadrants are the $dM/dH$-H curve with an arbitrary vertical scale which can be calibrated by graphically measuring the maximum slopes of the M-H curve. Figure 3.4.1 also indicates that the camera has slight parallax errors which are apparent from the asymetric horizontal centering and an apparent M-intercept to M-intercept distance of 5.95 divisions rather than the 6.00 division distance which was intended for the calibration procedure.

### 3.5 Sample Selection and Test Methods

Samples were obtained from randomly selected reels. However, the lots and the locations on the reels from which samples were obtained were selected for availability and economy. Therefore, the multiple sample measurements may not fairly reflect variations which are likely to be encountered with a given tape type. Preparation and measurements of additional samples will continue as time and tape availability permit.

All prepared samples were conditioned at $70 \pm 5°F$ and $20 \pm 10\%$ RH for at least 16 hours prior to any testing. The small samples and their glass sample tubes were maintained  r at least 16 hours

at test temperatures below 20°C and for at least 3 hours at temperatures above 20°C. Sample temperature was maintained in the sample holder by blowing air through the sample tubes and by limiting the time between insertion of the sample and photographing the M-H curves to less than one minute. One end of the sample tubes was always occluded during transfer of the sample tubes to the sample holder which requires exposure of the sample tubes to ambient room conditions for approximately 10 seconds. No condensation was observed in the sample tubes following their transfers.

All longitudinal samples were initially tested at 20° or 21°C during the previous or current reporting periods, then selected samples were tested at 0°C, -18°C, 40°C, and 60°C respectively. One Ampex 466 sample and the Fuji Beridox sample were remeasured at 20°C following temperature tests. Transverse and longitudinal Fuji H621 samples obtained during the current reporting period were measured at 20°C alone.

### 3.6  Results

Figures 3.6.1 through 3.6.5 are typical M-H curves for longitudinal samples of Ampex Types 466, 721 and 797, Fuji Type H621 and 3M Type 5198 respectively. Each photograph corresponds to the indicated line of Table 3.6.1, which presents results of longitudinal measurements on multiple samples along with calculated mean values and standard deviations of each parameter where warranted by a sufficient number of samples.

The "oxide thickness" column of Table 3.6.1 lists the thicknesses calculated from measurements on sixteen layers of tape. Section 2.3
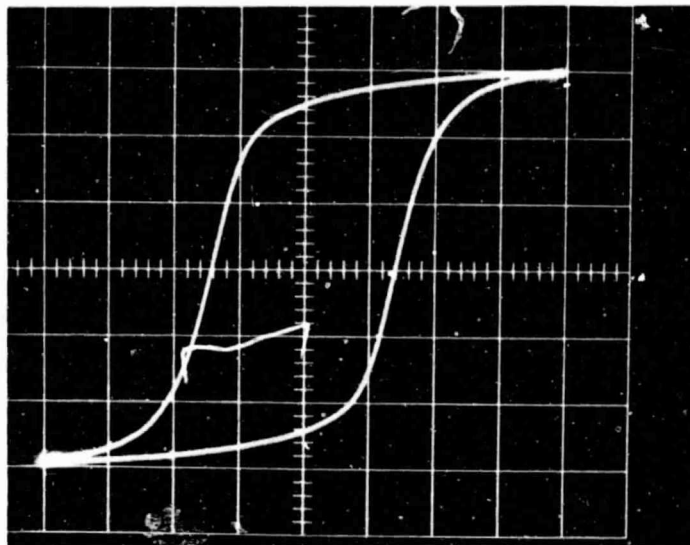
Figure 3.6.1:  M-H curve of Ampex Type 466

Horizontal scale is 500 oersteds/division.
Vertical scale is 333 gauss/division.  Results of
measurements are on fourth line of Table 3.1.
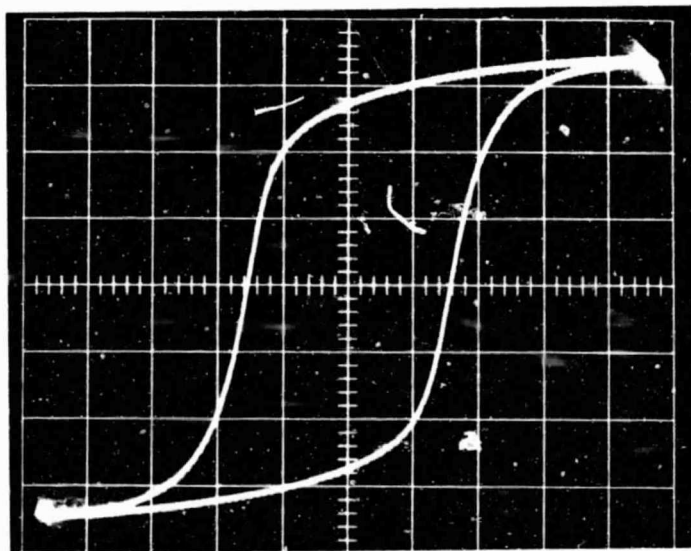


Figure 3.6.2:  M-H curve of Ampex Type 721

Horizontal scale is 400 oersteds/division.
Vertical scale is 333 gauss/division.  The round
CRT of the oscilloscope cut off the curve at Hm
and Ms.  This sample was obtained 1800 ft. into a
reel and had a measured oxide thickness of 0.200 mils.

IIT RESEARCH INSTITUTE
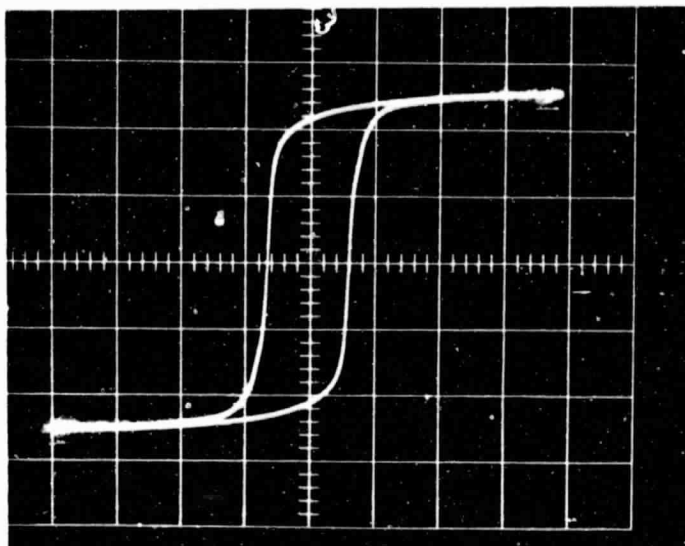
Figure 3.6.3: M-H curve of Ampex Type 797

Horizontal scale is 500 oersteds/division.
Vertical scale is 333 gauss/division. This is the
Lot A-2 sample.
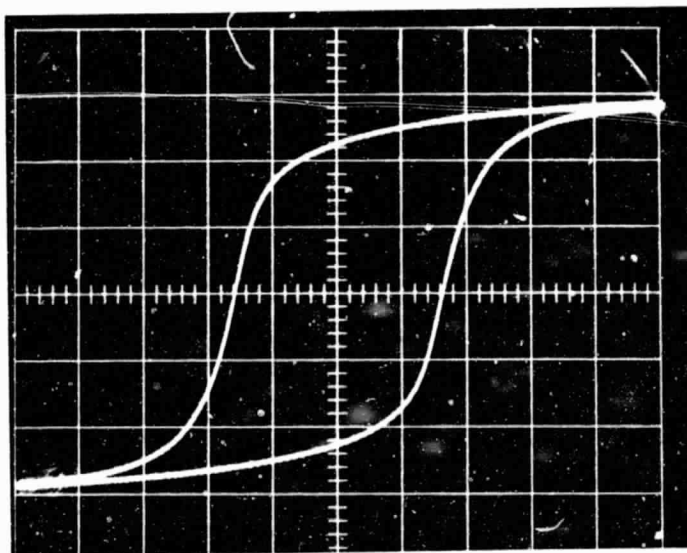


Figure 3.6.4: M-H curve of 3M Type 5198

Horizontal scale is 400 oersteds/division.
Vertical scale is 333 gauss/division. The sample
was obtained 1800 ft. into reel 58.

IIT RESEARCH INSTITUTE
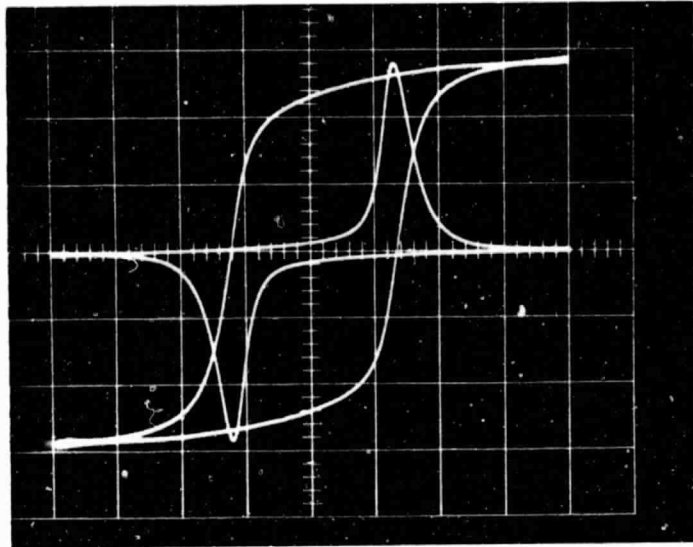
Figure 3.6.5: M-H curve of Fuji H621 with dM/dH-H curve.

Horizontal scale is 500 oersteds/division.

Vertical scale is 500 oersteds/division.
Vertical scale of dM/dH-H curve is arbitrary.
The half amplitude level of dM/dH-H curve is
1.4 divisions above or below the horizontal axis,
and the width of the dM/dH-H curve at that level
is 0.55 divisions x 500 oe/div = 275 oersteds.
The sample is from lot 079903.

IIT RESEARCH INSTITUTE

Table 3.6.1:  Longitudinal Magnetic Properties at 20°C, 20% RH, Multiple Samples

| Tape Manufacturer and Type | Lot or Reel | Location on Reel (± 100 feet) | Oxide Thickness (mils) | Saturation Induction $M_s$ (gauss) | Residual Induction $M_r$ (gauss) | Coercivity Hc (oersteds) | Squareness Ratio $M_r/M_s$ | Switching Field Distribution (oersteds) | Normalized Switching Field Distribution SFD/Hc | S* |
|---|---|---|---|---|---|---|---|---|---|---|
| Ampex 466 | 516604I921 | 100 | 0.20 | 985 | 810 | 663 | 0.822 | 380 | 0.54 | 0.66 |
| | 516644I921 | 1800 | 0.20625 | 1019 | 835 | 675 | 0.819 | 380 | 0.56 | 0.65 |
| | 173I1J | 400 | 0.225 | 1002 | 835 | 713 | 0.833 | 500 | 0.70 | 0.63 |
| | 173I1J | 100 | 0.23125 | 977 | 818 | 700 | 0.837 | 500 | 0.71 | 0.63 |
| | 173I1J,116604201 | 100 | 0.20625 | 994 | 818 | 675 | 0.823 | 400 | 0.59 | 0.68 |
| | 173I1J,112408082 | 100 | 0.225 | 969 | 813 | 700 | 0.844 | 490 | 0.70 | 0.63 |
| | 173I1J,112408081 | 100 | 0.2125 | 1069 | 865 | 700 | 0.828 | 480 | 0.69 | 0.63 |
| Mean | | | 0.215 | 1002 | 831 | 689 | 0.829 | 440 | 0.64 | 0.64 |
| S.D. | | | 0.011 | 31 | 24 | 17 | 0.008 | 60 | 0.07 | 0.02 |
| Ampex 721 | 110024182 | 100 | 0.20625 | 1161 | 927 | 638 | 0.798 | 325* | 0.51 | 0.68 |
| | 110024182 | 100 | 0.19 | 1236 | 985 | 640 | 0.797 | 310 | 0.48 | 0.71 |
| | 110024182 | 1800 | 0.200 | 1152 | 918 | 620 | 0.797 | 300 | 0.48 | 0.70 |
| Mean | | | 0.199 | 1183 | 943 | 633 | 0.797 | 312 | 0.49 | 0.70 |
| S.D. | | | 0.007 | 38 | 30 | 9 | 0.0 | 10 | 0.01 | 0.01 |
| Ampex 797 (all reel identifications include 76142) | 164465222-47,A-1 | 100 | 0.1813 | 1002 | 860 | 325 | 0.858 | 75* | 0.23 | 0.84 |
| | 164465221-4,A-1 | 100 | 0.156 | 1052 | 885 | 313 | 0.841 | 90 | 0.29 | 0.84 |
| | 164465221-4,A-1 | 1800 | 0.180 | 868 | 735 | 320 | 0.847 | 70 | 0.22 | 0.87 |
| | 164465241-15,A-1 | 100 | 0.175 | 960 | 802 | 313 | 0.835 | 80 | 0.26 | 0.88 |
| | 264465291-16,A-2 | 2000 | 0.2125 | 843 | 718 | 325 | 0.852 | 70 | 0.22 | 0.80 |
| Mean | | | 0.181 | 945 | 800 | 319 | 0.847 | 77 | 0.24 | 0.85 |
| S.D. | | | 0.018 | 79 | 66 | 5 | 0.008 | 7 | 0.03 | 0.03 |
| 3M5198 | 41575-1-01-58 | 100 | 0.20 | 910 | 718 | 640 | 0.789 | 340 | 0.53 | 0.57 |
| | 41575-1-01-58 | 1800 | 0.190 | 952 | 752 | 640 | 0.790 | 330 | 0.52 | 0.69 |
| | 41575-1-01-16 | 100 | 0.1875 | 988 | 781 | 650 | 0.790 | 370 | 0.57 | 0.65 |
| | 41575-1-01-16 | 1800 | 0.1875 | 975 | 781 | 650 | 0.801 | 390 | 0.60 | 0.67 |
| Mean | | | 0.191 | 956 | 758 | 645 | 0.793 | 360 | 0.56 | 0.67 |
| S.D. | | | 0.005 | 30 | 26 | 5 | 0.005 | 20 | 0.03 | 0.01 |
| Fuji H621 | 079903 | 100 | 0.231 | 952 | 785 | 638 | 0.825 | 275* | 0.43 | 0.71 |
| | 079952 | 190 | 0.225 | 994 | 818 | 638 | 0.823 | 275* | 0.43 | 0.73 |

*SFD measured from electronically produced dN/dH-H curve.  All other SFDs measured from curves constructed by measuring dN/dH on M-H curves.
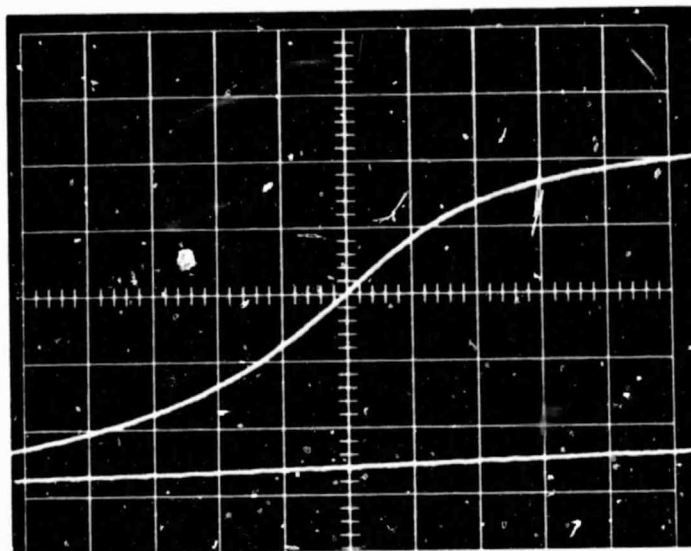
Figure 3.6.6:   M-H curve of 3M Type 5198 sample of Figure 3.6.4 with H-axis
expanded five times to produce a horizontal scale of 80
oersteds/division.  Horizontal trace position was adjusted
to center M = 0 on photograph which corresponds to $H_c$ = 640
oersteds.  Points on the dM/dH-H curve of Figure 3.9$^c$ were
calculated from measurements of this M-H curve.  The sample
was obtained 1800 ft. into reel 58.

| Coordinate Measured From Figure 3.6.6 | | Values Calculated From M-H Coordinates | |
|---|---|---|---|
| H | M | $\Delta M/\Delta H$ | H (average) |
| -320 | 610 | --- | --- |
| -400 | 550 | 0.75 | -360 |
| -440 | 510 | 1.00 | -420 |
| -480 | 447 | 1.575 | -460 |
| -520 | 377 | 1.75 | -500 |
| -560 | 283 | 2.35 | -540 |
| -600 | 157 | 3.15 | -580 |
| -640 | 10 | 3.675 | -620 |
| -680 | -133 | 3.575 | -660 |
| -720 | -257 | 3.10 | -700 |
| -760 | -367 | 2.75 | -740 |
| -800 | -457 | 2.25 | -780 |
| -840 | -533 | 1.90 | -820 |
| -880 | -587 | 1.35 | -860 |
| -960 | -690 | 1.29 | -920 |

ORIGINAL PAGE IS OF POOR QUALITY

SFD = 330 oersteds

Normalized SFD = $\dfrac{SFD}{H_c}$

$= \dfrac{330}{640}$

$= 0.52$
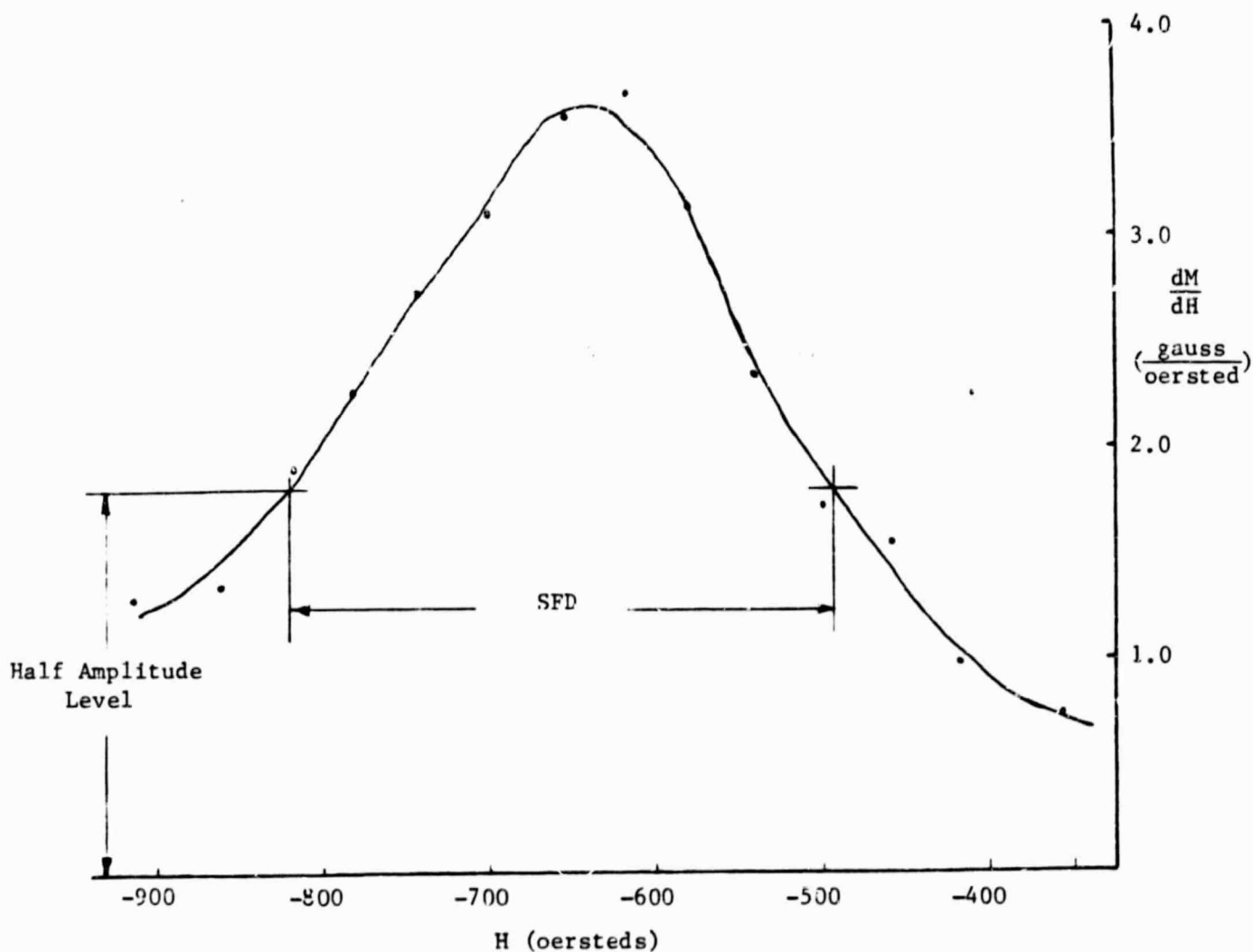


Figure 3.6.7: Values of $\Delta M/\Delta H$ and H (average) calculated from coordinates on M-H curve of Figure 3.8 for 3M Type 5198. For each successive set of points measured on Figure 3.6.6 $\Delta M/\Delta H = (M_n - M_{n-1})/(H_n - H_{n-1})$, and H(average) = $(H_n + H_{n-1})/2$.

90

indicates an accuracy of $\pm$ 0.01 mil ($\pm$10 $\mu$inch) for the thickness
and constitutes a major source of error in the induction measurements.
The thickness measurements errors have no effect on coercivity measure-
ments or squareness which is a dimensionless ratio of two induction
values obtained from the same sample.

The magnetic parameters in the fifth through eleventh columns of
Table 3.1.1 are defined and described in preceding sections. Remember
that the reported induction values $M_s$ and $M_r$ are probably lower than
the actual values by a factor of 0.7 due to the calibration method.
Also, the trend toward higher induction values from samples with
thinner measured oxide thickness may be noted. This indicates that
the relatively large variation in the induction values for a given
tape type is due to thickness measurement error rather than sample
to sample variation. In contrast the squareness ratio $M_r/M_s$ which
does not depend on calibration or thickness measurement errors ex-
hibits relatively small variation within a given tape type. The SFDs
measured from dM/dH-H curve photographs agree well with those mea-
sured from curves plotted by calculating $\Delta M/\Delta H$ from M-H curves, and
the former method is probably more accurate in addition to being much
easier. The precision of the (SFD/Hc) and S* parameters is inherently
lower than that of other parameters. Figures 3.9 and 3.10 are an
example of the previous SFD calculation method, while Figures 3.3 and
3.8 allow direct measurement of SFD.

The results in Table 3.1.1 show that the induction values $M_r$ and
$M_s$ of all five tape types are roughly comparable, as are the coer-

civities, the SFDs, and the S*s of the four cobalt doped tape types. Ampex 797 stands alone with high squareness ratio and S*, and low SFD.

Table 3.2.1 presents measurements of coercivity Hc and residual induction $M_r$ of the subject tapes measured over the range of $-18^{\circ}C$ to $60^{\circ}C$. The relative humidity was 20% for all temperatures greater than $0^{\circ}C$. The coercivity results are plotted three different ways on Figures 3.6.8, 3.6.9a, and 3.6.9b. Coercivities of two earlier cobalt dope tape types over the range of $-10^{\circ}C$ to $+40^{\circ}C$ have been added to these figures to demonstrate technological improvements in the temperature stability of cobalt doped tapes. Figure 3.6.8 plots the absolute values of coercivity while Figures 3.6.9a and 3.6.9b plot the coercivity normalized to the maximum value and to the value at $25^{\circ}C$ respectively. The normalized coercivities of both 3M types 455 and 971 are approximated by the heavy lines of Figures 3.6.9a and 3.6.9b. Coercivity temperature coefficients of Table 3.2.1 were calculated by linear regression analysis which also indicates high correlation coefficients for all of the cobalt dope tape types.

Table 3.6.3 presents the results of M-H measurements on single transversely oriented tape samples along with orientation ratios calculated for the subject tape types. The longitudinal residual induction $M_{rL}$ values employed for the orientation ratio calculations are measurements from tape samples obtained immediately adjacent to the transverse samples.

Table 3.6.2: Effect of Temperature on Longitudinal Magnetic Properties

| Tape Manufacturer and Type (lot) | Residual Induction Hr (gauss) | | | | | Coercivity Hc (oersteds) | | | | | Coercivity Temperature Coefficient (oe/°C) |
|---|---|---|---|---|---|---|---|---|---|---|---|
| | -18°C | 0°C | 21°C | 40°C | 60°C | -18°C | 0°C | 21°C | 40°C | 60°C | |
| Ampex 466 (5166041921) | 844 | 825 | 838 | 802 | 785 | 788 | 725 | 663 | 625 | 588 | -2.6 |
| Ampex 721 (110024182) | 952 | 944 | 918 | 902 | 902 | 7)0 | 663 | 620 | 613 | 575 | -1.5 |
| Ampex 797 (76142; 164485221-4, Lot A-1) | 731 | 725 | 735 | 718 | 693 | 313 | 325 | 320 | 313 | 300 | -0.2 |
| Fuji Beridox (PFD 018) | 893 | 885 | 888 | 852 | 835 | 713 | 675 | 650 | 613 | 600 | -1.5 |
| 3M5198 (41575-1-01-58) | 781 | 788 | 752 | 763 | 738 | 688 | 675 | 640 | 625 | 600 | -1.2 |

**Legend:**
- □ Ampex 466
- △ Ampex 721
- ○ Ampex 97
- ✕ Fuji Beridox
- ■ 3M 5198
- ▲ 3M 455
- ● 3M 971

Coercivity (oersteds)

ORIGINAL PAGE IS OF POOR QUALITY
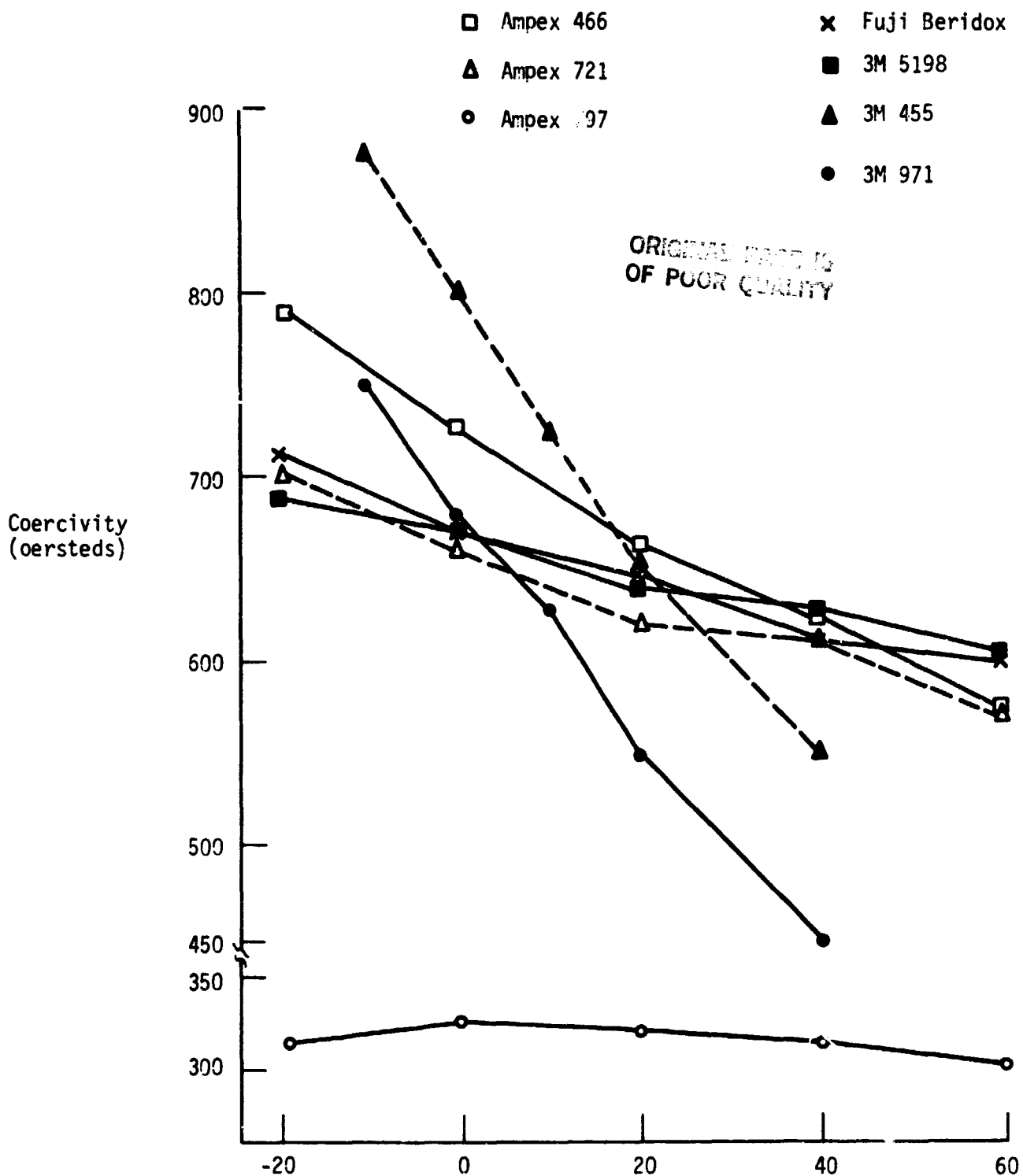
Figure 3.6.8: Effect of temperature on coercivity (Hc).
Note break in coercivity scale.

□ Ampex 466  ✕ Fuji Beridox

△ Ampex 721  ■ 3M 5198

○ Ampex 797
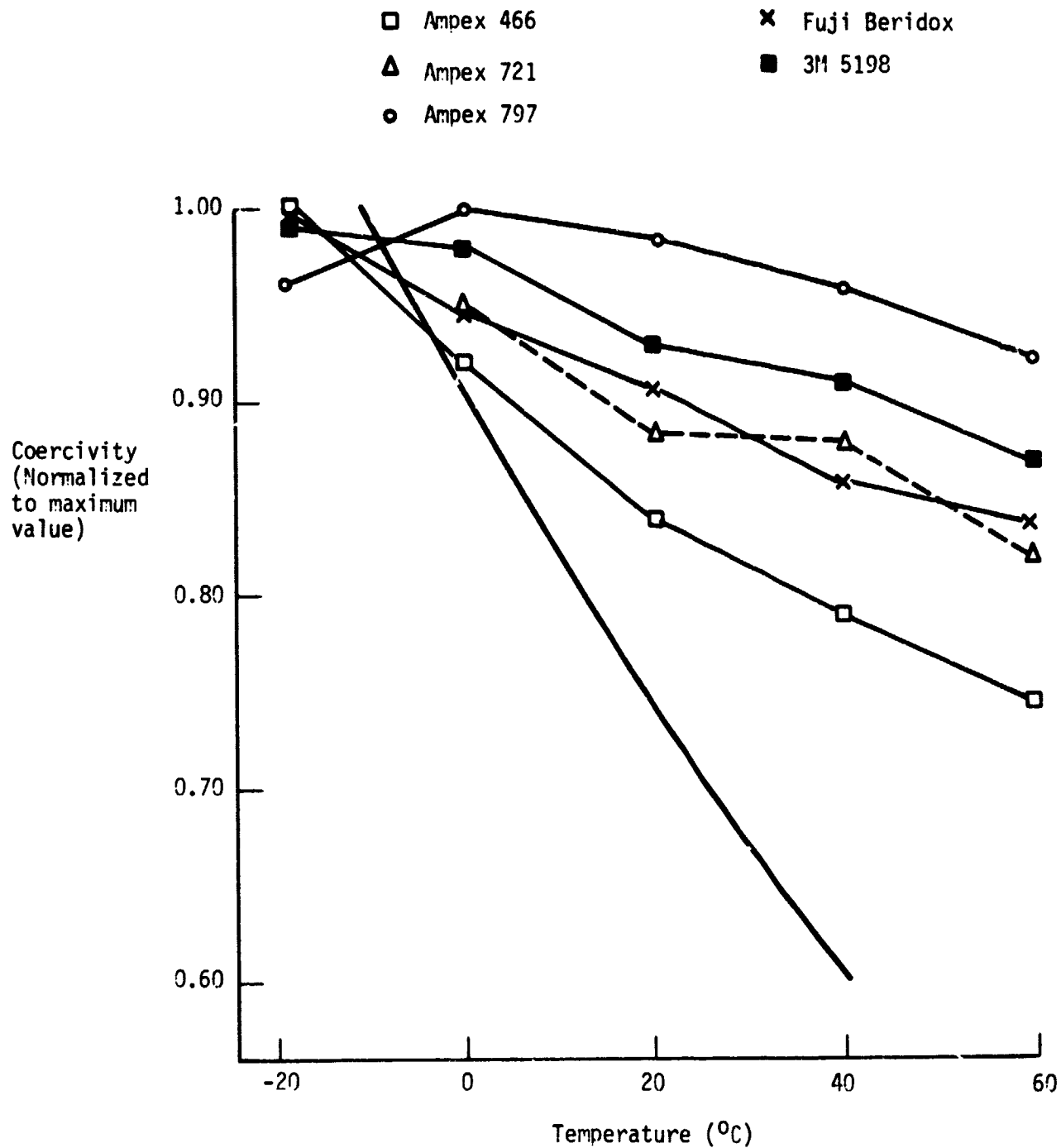


Figure 3.6.9a: Effect of temperature on coercivity (Hc).
Heavy line is typical for 3M types 455 and
971 measured over a range of -10°C to +40°C.
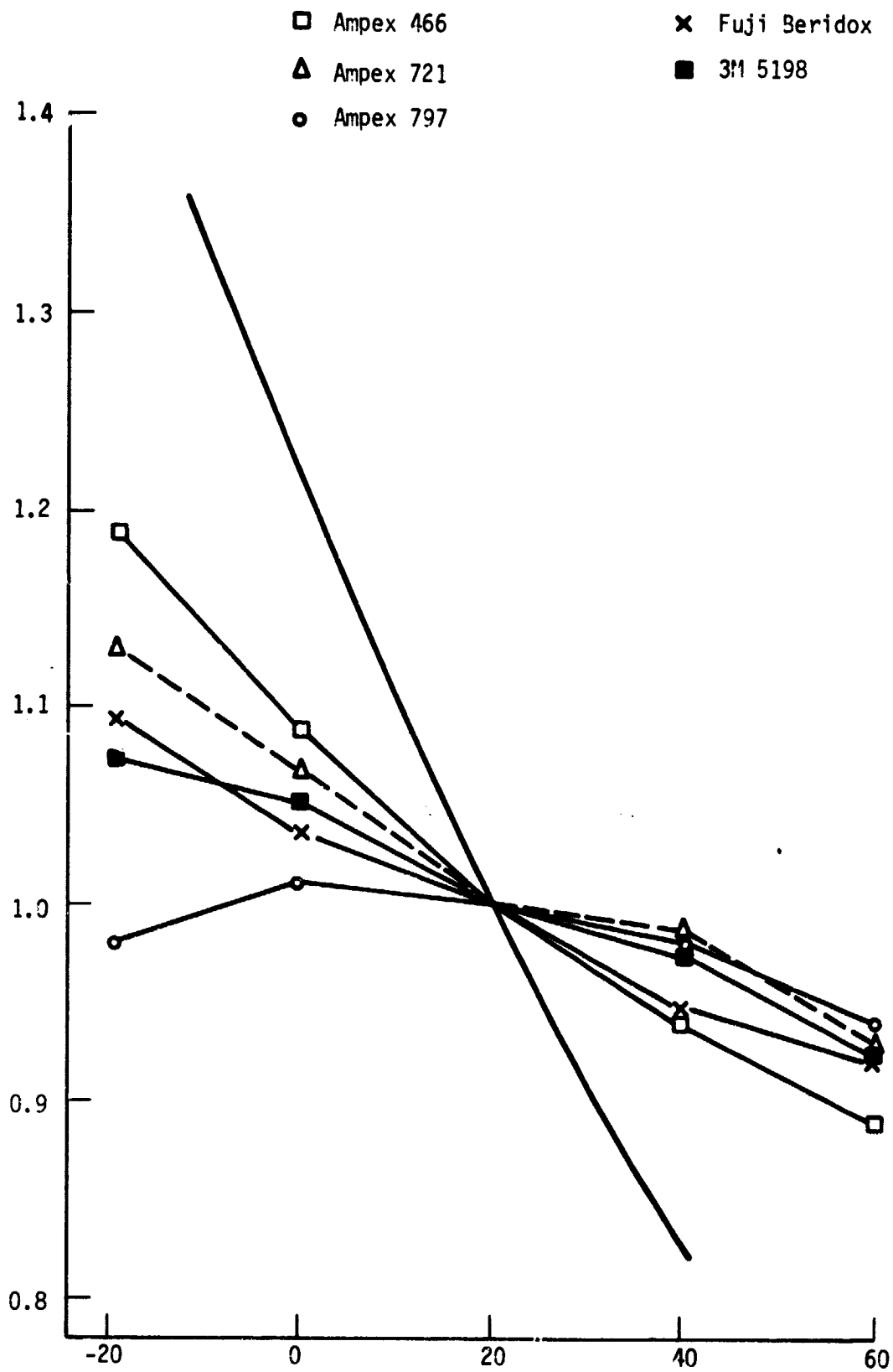
Figure 3.6.9b: Effect of temperature on coercivity (Hc).
Heavy line is typical for 3M types 455 and 971.

96

Table 3.6.3: Transverse Magnetic Properties and Orientation Ratios

| Test<br>Tape Manufacturer and Type (Lot) | Saturation Induction $M_{sT}$ (gauss) | Residual Induction $M_{rT}$ (gauss) | Coercivity $H_{cT}$ (oersteds) | Squareness Ratio $M_{rT}/M_{sT}$ | Orientation Ratio * $M_{rL}/M_{rT}$ |
|---|---|---|---|---|---|
| Ampex 466<br>(516041921) | 969 | 501 | 500 | 0.517 | 1.52 |
| Ampex 721<br>(110024182) | 1102 | 576 | 520 | 0.523 | 1.59 |
| Ampex 797<br>(76142,164485221-4; Lot A-1) | 810 | 267 | 210 | 0.330 | 2.75 |
| Fuji Beridox<br>(PFD 018) | 1002 | 509 | 520 | 0.508 | 1.67 |
| 3M 5198<br>(41575-1-01-58) | 935 | 443 | 500 | 0.474 | 1.70 |

$M_{rL}$ is the longitudinal residual induction of samples obtained from reels immediately adjacent to the transverse samples.

## 3.7 Conclusions

The magnetic measurements conducted to date are probably adequate to characterize virgin samples of the subject tape types and to detect gross variations in future production of the tapes as long as the probable error in the induction calibration is taken into account. Additional tests are recommended following wear and environmental conditioning of the tapes, but it may be possible to eliminate some of the candidate tape types before further testing is conducted.

Taken with the results of Section 4.1, coercivity Hc appears to have the strongest correlation with digital output of all of the magnetic parameters, and the high coercivity tapes will probably be essential for a system that employs wavelengths of less than 100 micro-inches during the record process.

Temperature has little effect on the coercivity of undoped Ampex 797. All of the cobalt doped tapes show some increase in coercivity with decreasing temperatures. Roughly equivalent changes were measured for Ampex 721, Fuji Beridox and 3M 5198, while the coercivity of Ampex 466 changes somewhat more with temperature. Linear regression analysis indicates coercivity temperature coefficients of -2.6 oe/$^\circ$C for 3M 5198, in sharp contrast to coercivity temperature coefficients around 6 oe/$^\circ$C for earlier cobalt doped tape types. The residual inductions Mr of the tapes appear to drop by 5% to 7% over the -18$^\circ$C to 60$^\circ$C temperature range. The detrimental effect of low thermal stability offsets the benifical effect of high coercivity achieved in Ampex type 466.

The transverse magnetic properties of Ampex 466, Ampex 721, Fuji

Beridox, and 3M 5198 are similar. The differences between the transverse properties of those tapes and Ampex 797 are consistent with the high longitudinal squareness ratio of Ampex 797. The longitudinal orientation of the magnetic particles is much greater in Ampex 797 than in the other tapes. The orientation differences are barely discernable by visual examination of scanning electron micrographs of the tape surfaces.

IIT RESEARCH INSTITUTE

99

# 4. ELECTRICAL PROPERTIES

This section characterizes the electrical properties of the subject tape types. The tests compare tape performance with respect to record currents required to achieve maximum outputs at different wavelengths, the magnitude of these maximum outputs, and the output magnitude in response to a constant record current, the resistivities of the tape coatings, and the distribution and size of oxide defects that cause momentary reductions in signal output or "drop-outs." The results of these tests permit predictions of a HDDR system performance with specified coding, signal-to-noise ratio tolerance, and minimum distance between flux reversals.

## 4.1 Record Current Without Bias

This test measures and compares the record current at selected wavelengths required to achieve the maximum attainable reproduce signal level. A square wave current source is applied to the record head, and the current is increased and measured while the reproduce level is monitored to detect its maximum level. A frequency range is selected which allows application of adequately square current waveforms to the record head by the available test equipment, and then the tape transport speed is selected so that the record frequency range corresponds to the range of wavelengths under consideration for a specific application.

### 4.1.1 Procedure

A square wave output voltage from a Krohn-Hite Model 5300 Function Generator was applied to inputs of an Instruments for Industry Model 5100 Wideband Amplifier and a Heathkit Model 1B-1100 Frequency Counter. The output level of the function generator was set to just below the specified maximum input level of the wideband amplifier.

The output of the wideband amplifier was connected to the Honeywell 1" record head in series with a 3 ohm resistor and a 2 ampere fuse. That resistor and the 50 ohm output impedance of the amplifier make the amplifier output appear as a current source to the very low impedance record head. The phase response of the amplifier produces nominal distortion of the applied square wave over the range of 100 KHz to 1.0 MHz, and a tape transport speed of 30 ips was selected to achieve record wavelengths in the range of 30 microinches to 300 microinches. Intermediate wavelengths of 150 microinches and 60 microinches were selected for record current measurements.

The current through the record head was monitored and measured with a Tektronix Type P6019 Current Probe connected to channel 2 of a Tektronix Type 454 Oscilloscope and to a Hewlett-Packard Model 3403C True RMS Voltmeter operating in the auto ranging AC mode.

```
┌─────────────┐          ┌─────────────┐
│ Krohn       │   ___     │ Instruments │        ┌─── 180ohm
│ 5300        │──│  │_│──→│ for         │────────┤     2w
│ Function    │          │ Industry 5100│        └───
│ Generator   │          │ Wideband     │
└─────────────┘          │ Amplifier    │
       │                 └─────────────┘
       ↓
┌─────────────┐
│ Heath Kit   │
│ 1B-1100     │←
│ Frequency   │
│ Counter     │
└─────────────┘
```

┌──────────────────┐                    2amp     ┌──────────────┐
│ Honeywell 96HD   │                             │              │
│ Reproduce        │←─⊐            5ohm          │              │
│ Preamplifier     │              6w             │              │
│ Track 39         │                             │              │
└──────────────────┘                             └──────────────┘
        │
        ↓
┌──────────────────┐                            ┌──────────────┐
│ Honeywell        │                            │ Tektronix    │
│ Direct Reproduce │                            │ P6019        │
│ Amplifier        │                            │ Current Probe│
│ T.P. 1 and 2     │                            │              │
└──────────────────┘                            └──────────────┘
        │                                               │
        │          ┌──────────────────┐                │
        └─────────→│ Tektronix 454    │←───────────────┘
                   │ Oscilloscope     │
                   │ Ch. 1     Ch. 2  │
                   └──────────────────┘
        │                                               │
        ↓                                               ↓
┌──────────────────┐                            ┌──────────────┐
│ HP 3400 A        │                            │ HP 3403      │
│ True RMS         │                            │ True RMS     │
│ Voltmeter        │                            │ Voltmeter    │
└──────────────────┘                            └──────────────┘
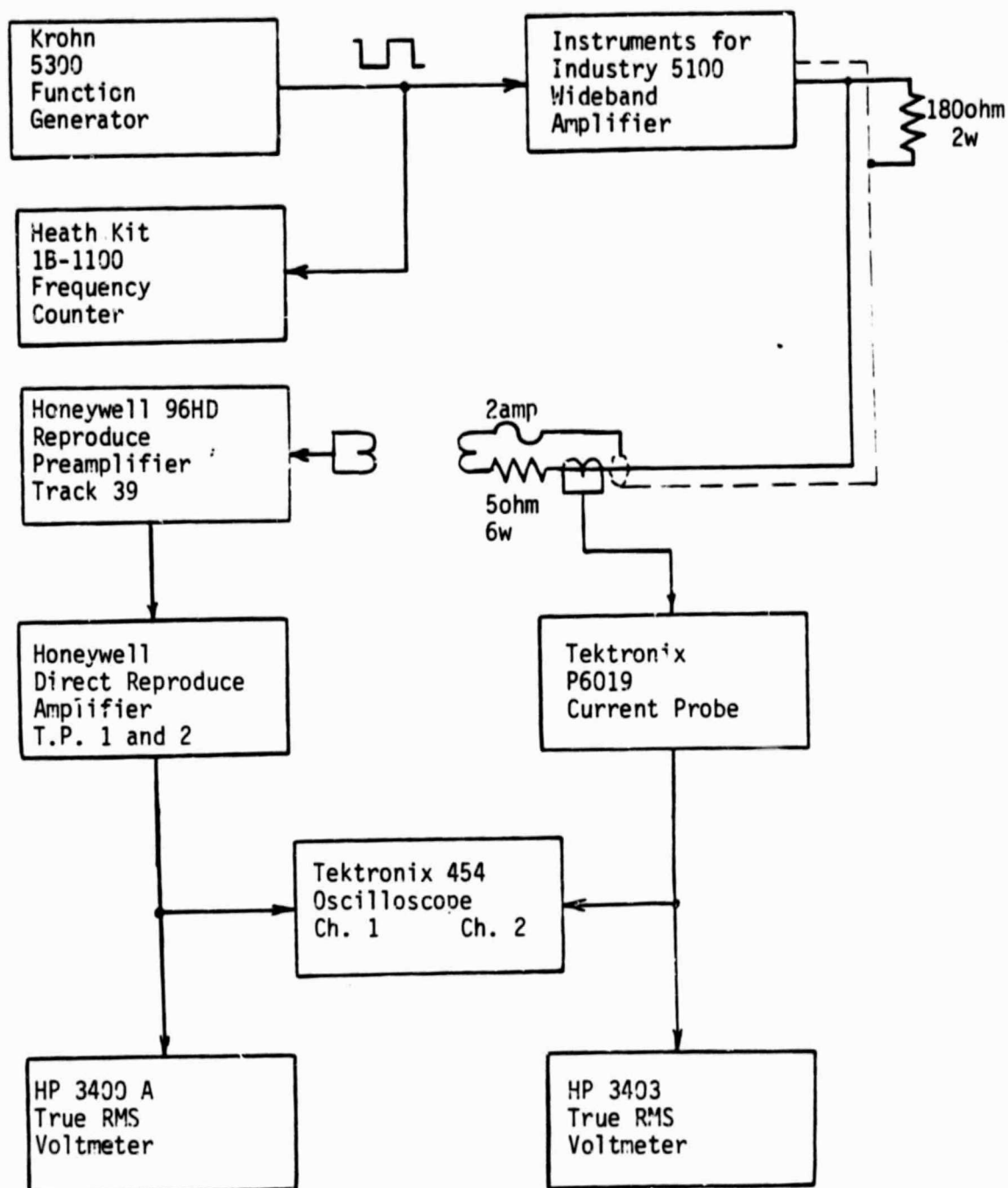
Figure 4.1.1: Test Equipment for Record
Current and Wavelength Response Tests

**IIT RESEARCH INSTITUTE**

The record head and a Honeywell 42 track, 1 inch (17 mil) Reproduce Head are mounted on a Honeywell Model 96HD Tape Recorder. Signals recorded on the test tapes were reproduced through track 39 of the reproduce head and preamplifier, and the 4 MHz Direct Reproduce Amplifier supplied with the tape recorder. The reproduced signal was measured and monitored at test points 1 and 2 of the direct reproduce amplifier which are located before the equalizer circuits of the direct reproduce amplifier. The reproduced output was monitored on channel 1 of the oscilloscope, and the output level was measured with a Hewlett-Packard Model 3400A True RMS Voltmeter.

For each test tape and record wavelength, the output level control of the record amplifier was increased until the maximum output level was observed, and the record current that produced the observed maximum output was measured. Recording continues at the maximum output level for at least 20 seconds after noting the footage counter reading at which maximum output is achieved. Then the record current is turned off, the tape is rewound to the noted footage counter reading, and the maximum output level is measured while reproducing the recorded signal with no record current. This procedure eliminates "feed through" from the record head to the reproduce head during the output level measurement. Although feed through increases as the record current increases and some feed through is present during the maximum output level observation, the output level always decreases for shorter wavelengths ($\lambda \leq 150$ micro-inches) and record currents slightly above the level that produces the maximum output before the feed through interferes with the maximum output level observation. For 300 microinch wavelengths, the output level approaches a plateau as the record current is increased, and the record current that produces the maximum output level is difficult to measure accurately.

A broadband noise measurement was also conducted on each tape with no record current and no recorded signal. Most of this noise is generated or picked up within the reproduce electronics and is not a function of the test tapes.

### 4.1.2 Results

Table 4.1 presents the measured record currents that produced the maximum output level and the measured maximum output levels for each wavelength obtained from virgin samples of each tape type. Figure 4.1.2 presents the same data in graphical form. From this figure, it can be seen that the performances of all four cobalt-doped tape types are substantially equivalent and differ significantly from the undoped $Fe_2O_3$ Ampex Type 797, which has lower record currents and much lower output levels at shorter wavelengths than the other tape types. For all tape types the record current drops with decreasing wavelengths. For the cobalt-doped types, the maximum output level is relatively constant for 300 microinch and 150 microinch wavelengths. The maximum output level drops with decreasing wavelengths for all of the cobalt-doped tape types at wavelengths shorter than 150 microinches and for Ampex 797 at all wavelengths.

The signal-to-noise ratio of the reproduce system is greater than 20 dB for cobalt-doped tapes and wavelengths greater than or equal to 60 microinches (one flux reversal every 30 microinches). The S/N ratio is below 20 dB for 30 microinch wavelengths but might be improved with a band pass filter. Most of the noise is present at the preamplifier outputs which will be used for drop-out detection and measurements.

### 4.1.3 Conclusions

A cobalt-doped tape type appears necessary for high density digital recording achieved by the ability to record wavelengths shorter than 150 microinches. The roughly equivalent performance of the four tested cobalt tape types indicates that the selection of a particular type for an HDDR application can be based on other parameters such as drop-outs, durability, and abrasivity.

### 4.2 Wavelength Response

This test measures the reproduce level from the direct reproduce amplifier for each tape at selected wavelengths with a constant record current. The record current which produced the maximum output level with a 30 microinch wavelength for a given tape type was employed for that tape type.

Table 4.1.1: Record Current for Maximum Output and Wavelength Response with Constant Record Current

| Test — Tape Type (Lot) | Wavelength (microinches) | Record Current | | | Wavelength Response | | | |
|---|---|---|---|---|---|---|---|---|
| | | Record Current that Produces Maximum Output Level (mA rms) | Maximum Output Level Normalized to Level of 300 microinch Wavelength (dB) | Absolute Output Level (mV rms) | Constant Record Current for All Wavelengths (mA rms) | Wavelength (microinches) | Output Level Normalized to Level of 300 microinch wavelength (dB) | Absolute Output Level (mV rms) |
| Ampex 466 (516604 1921) | 300 | 920 | 0.0 | 97.0 | 191 | 300 | 0.0 | 57.0 |
| | 150 | 608 | -0.8 | 89.0 | | 150 | +0.5 | 60.0 |
| | 60 | 270 | -9.4 | 33.0 | | 60 | -5.5 | 30.0 |
| | 30 | 191 | -24.7 | 5.7 | | 30 | -24.5 | 5.7 |
| | noise | 0 | -37.8 | 1.25 | | 196 | +1.0 | 62.0 |
| Ampex 721 (7 593 276J11) | 300 | 942 | 0.0 | 83.0 | 213 | 300 | 0.0 | 55.0 |
| | 150 | 616 | -0.8 | 76.0 | | 150 | -0.4 | 53.0 |
| | 60 | 255 | -9.7 | 27.2 | | 60 | -8.2 | 21.6 |
| | 30 | 213 | -27.8 | 3.4 | | 30 | -24.5 | 3.3 |
| | noise | 0 | -36.4 | 1.25 | | 204 | +0.1 | 56.0 |
| Ampex 797 (76142, 164485222-33, Lot A-1) | 300 | 322 | 0.0 | 95.0 | 116 | 300 | 0.0 | 48.0 |
| | 150 | 220 | -4.1 | 59.0 | | 150 | -1.5 | 41.0 |
| | 60 | 140 | -18.8 | 11.0 | | 60 | -13.4 | 10.5 |
| | 30 | 116 | -36.3 | 1.45 | | 30 | -30.7 | 1.4 |
| | noise | 0 | -37.8 | 1.22 | | 273 | 0.0 | 48.0 |
| Fuji H621 (079903) | 300 | 856 | 0.0 | 97.0 | 195 | 300 | 0.0 | 61.0 |
| | 150 | 514 | -0.9 | 87.0 | | 150 | +0.2 | 62.0 |
| | 60 | 235 | -9.6 | 32.0 | | 60 | -6.3 | 29.5 |
| | 30 | 195 | -25.5 | 5.1 | | 30 | -21.6 | 5.1 |
| | noise | 0 | -37.6 | 1.25 | | 197 | +0.3 | 64.0 |
| 3M 5198 (41752 09 010 42) | 300 | 588 | 0.0 | 89.0 | 207 | 300 | 0.0 | 62.0 |
| | 150 | 472 | -1.1 | 79.0 | | 150 | -0.2 | 61.0 |
| | 60 | 226 | -10.6 | 26.2 | | 60 | -7.7 | 25.7 |
| | 30 | 207 | -26.6 | 4.2 | | 30 | -21.7 | 4.2 |
| | noise | 0 | -37.3 | 1.23 | | 216 | +0.3 | 64.0 |
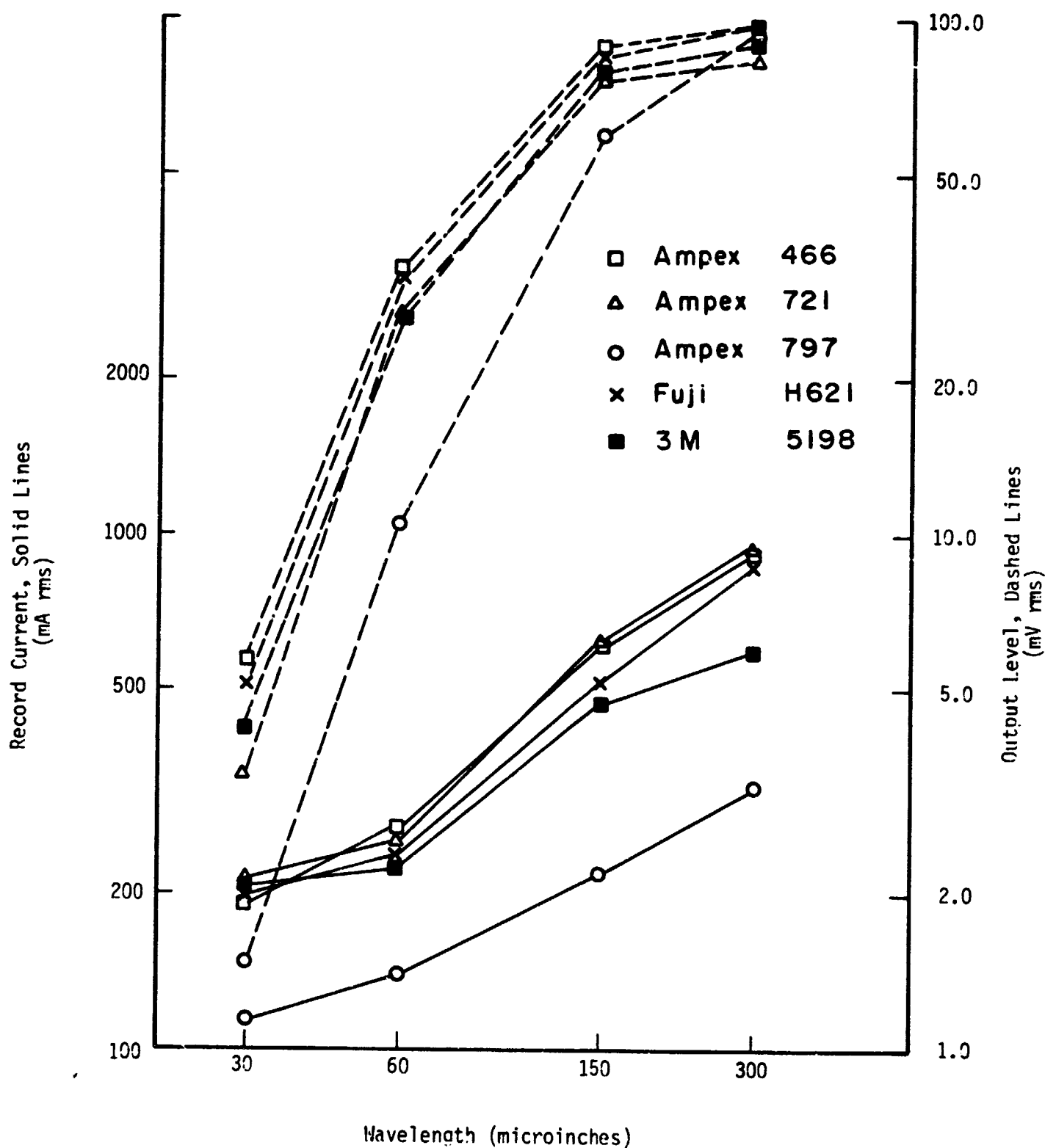
Figure 4.1.2: Record Current for Maximum Output Level

### 4.2.1 Procedure

The test equipment, tape speed, and wavelengths were identical to those employed for the record current test in Section 4.1.1. For each wavelength, the record current was adjusted by varying the output level control of the wideband amplifier until the indicated record current was obtained. Then the reproduce voltage in dB was measured. For each tape, the reproduce voltages were normalized to a reference level of 0.0 dB corresponding to the output level at the 300 microinch wavelength.

### 4.2.2 Results

Table 4.1.1 presents the normalized and absolute output levels produced by the constant record currents that produce the maximum output level at the shortest wavelength. Figure 4.2.1 presents the same data in graphical form. From this figure, it can be seen that the performances of all four cobalt-doped tape types are substantially equivalent and differ significantly from the undoped $Fe_2O_3$ Ampex Type 797. The outputs are generally level at wavelengths from 300 microinches to 150 microinches, drop by about 7 dB between 150 microinches and 60 microinches for cobalt doped tapes, and drop by about 13 dB between 150 microinches and 60 microinches for Ampex 797. The output level of all of the tape types drops rapidly at shorter wavelengths.

### 4.2.3 Conclusions

If the HDDR system is designed for saturation recording with a minimum wavelength of 60 microinches (greater than or equal to 30 microinches between flux reversals for an NRZ format), the output level for a sequence of flux reversals spaced 30 microinches appart
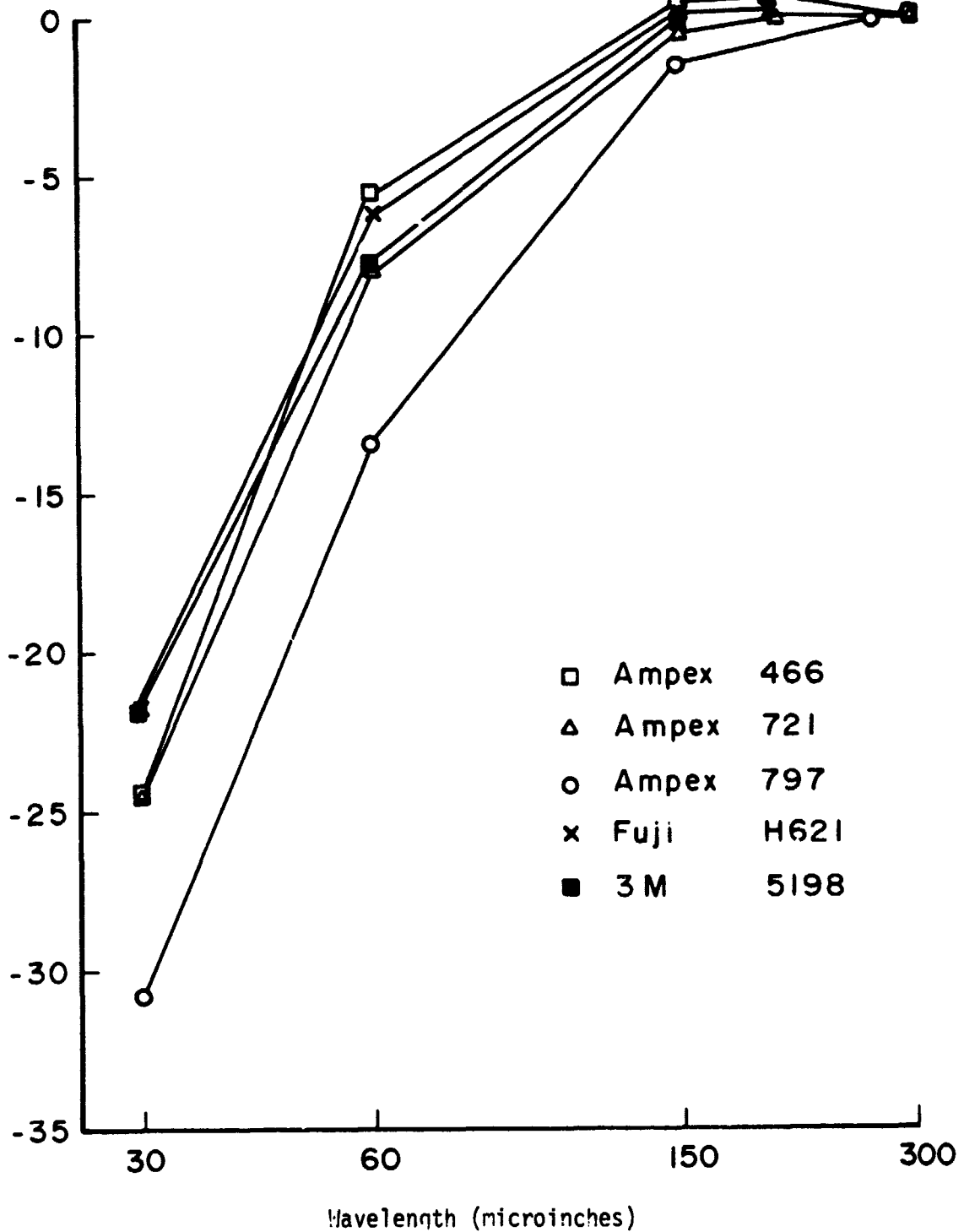
Figure 4.2.1: Wavelength Response with Constant Record Current

will be lower than the output level produced by a sequence of bits which produces more widely spaced flux reversals. Therefore, a code with a narrow bandwidth or read/write equalization may be necessary to maintain a good signal to noise ratio if the minimum distance between flux reversals is to be 30 microinches.

More meaningful wavelength response test conditions might be achieved with a constant record current that produces the maximum output level at the minimum wavelength intended for the system rather than the 30 microinch wavelength arbitrarily selected for this test series. An additional wavelength response test series should be conducted for each wavelength and code proposed by the system designers, with test conditions adopted to simulate the proposed system specifications.

### 4.3 Coating Resistivity

The surface resistance on the coatings of the tape is related to the amount of carbon or graphite added to the overall binder composition. Carbon is generally added to the binder in order to increase conductivity, thereby reducing possible buildup of static charges when operated in a dry atmosphere. However, the addition of excessive carbon may have a weakening effect on the integrity of the binder system. In other studies, carbon has been observed as a constituent of excessive debris accumulation.

#### 4.3.1 Procedure

The coating resistivity of the magnetic oxides and the back coatings of the tape samples were measured with a Hewlett-Packard Model 4329A High Resistance Meter. The test fixture permits five measurements on each sample. The reported oxide results are for 500 VDC test potentials.

#### 4.3.2 Discussion

The coating resistivity test procedure generally followed methods specified in Volume III, Appendix B, paragraph 3-61(b) of IRIG 106-80 and the Electronic Industries Association "Recommended Test Method -- Magnetic Tape Electrical Resistance Coating," RS-342 (ANSI C83.36-1968), which differ mainly in the applied test potential: 500 VDC required in the IRIG Standard and 100 VDC preferred in the EIA Standard. The relationship between resistance and test voltage is probably nonlinear with lower resistance occurring as the test potential is increased. Since low coating resistivity is desirable to prevent the buildup of static electricity, a phenomenon associated with high voltage, the higher test potential appears to be the most rational choice for future

tests. However, the higher power dissipation in the tape samples which results from a high test potential may increase two technical problems in an objective, unbiased evaluation of coating resistivity. First, the test electrodes are secured at each end, and the contact resistance between the tape samples and the electrodes may be less at the tape edges than at the center. Melting of the mylar base at the sample tape edge was evident following some of the tests. On the other hand, the contact force between the electrodes and the samples did not have a large effect on the measured resistivities. Therefore, this first problem can be reduced by applying nominal torque to the screws that secure the electrodes. We found that "finger tight" screws were adequate. The standards do not specify electrode forces.

The second problem which may be associated with power dissipation in tape samples is the tendency for the resistance to increase during the application of the test potential, especially with high resistance tape samples. All of the reported measurements were completed within the 2 minute limit specified by the EIA Standard, and the resistance values appeared to stabilize within that time period. The resistance change is very rapid upon initial application of the test potential and the initial resistance could not be resolved with the slowly responding test equipment. The increasing resistance could result from moisture loss while power is dissipated by the test samples. Despite the increasing resistance and rapid sequential testing of each sample, first at 100 VDC and then at 500 VDC, lower resistivities were obtained with the higher test potential.

One final procedure problem which was not answered in the standards is the possibility of contact between the tape backing and the electrodes if the back-to-back strips are not perfectly aligned on the electrodes. Therefore, some early test results were rejected, and all later tests were conducted with a wide uncoated mylar strip between the two sample strips.

### 4.3.3 Results and Conclusions

The test results are listed in Table 4.3.1. The Ampex Type 797 coating resistivity is well below the $2x10^8$ ohm/square and $1x10^8$ ohm/square limits specified by IRIG 118-79 and EIA RS-342 respectively. The oxide coating resistivities of Ampex Type 721 and Ampex Type 466 were equal to or greater than one hundred times those limits. The oxide resistivity of 3M 5198 was an order of magnitude greater than the limits. The oxide resistivity of Fuji Type H621 is slightly greater than the standard limits. Comparisons of oxide coating resistivities with record current and wavelength response tests indicates that the high resistivities may be related to the high frequency capabilities of the tapes. The resistivities of the back coating of all samples tapes were checked and found to be less than the range of the HP 4329A meter.

## Table 4.3.1: Coating Resistivity

| Tape Type (Lot) | Oxide Electrical Resistance ($\Omega$/square) | | Back Coating Electrical Resistance ($\Omega$/square) |
|---|---|---|---|
| | Mean | S.D. | |
| Ampex 466 (57GJ11, 51660 41911) | $3.6 \times 10^{10}$ | $6.6 \times 10^9$ | less than $10^6$ |
| Ampex 721 (7 593 276GJ11, 21x104061-13) | $1.7 \times 10^{10}$ | $2.3 \times 10^9$ | less than $10^6$ |
| Ampex 797 (*) | $3.6 \times 10^6$ | $4.9 \times 10^5$ | less than $10^6$ |
| Fuji H621 (079903) | $2.4 \times 10^8$ | $1.3 \times 10^7$ | less than $10^6$ |
| 3M 5198 (51575-1-01-58) | $1.8 \times 10^9$ | $1.1 \times 10^8$ | less than $10^6$ |

* Unknown Lot

## 4.4 Drop-outs with 18 Mil Track Width

Square wave currents from a 500 kHz source were applied to the single track record head. The record current and reproduce head azimuth were adjusted to produce maximum reproduce output levels. A 500 kHz record frequency was selected to achieve the best record current waveform, and the tapes were recorded at 30 ips to achieve 60 microinch wavelengths (one wavelength is equivalent to two flux reversals).

Virgin tapes were selected, and data was obtained during the initial record pass and/or during no more than three subsequent passes. One exception was the Fuji H621 sample which had been used previously for record current and wavelength response tests.

Preliminary data were obtained with a prototype drop-out detector, a 500 kHz oscillator, and two electronic counters, one to register total drop-outs and one to register total duration of dropouts in units of wavelengths. Counts were recorded after every 100 feet of tape, and the sequential readings were subtracted to determine drop-outs/100 feet and errors/$1x10^6$ wavelengths (100 feet x 12 inch/ft. x 1 wavelength/$60x10^{-6}$ inches $= 2x10^7$ wavelengths). The average number of errors/drop-out were calculated for each 100 ft. tape segment. Average values of each parameter were also calculated over the entire 1600 ft sample lengths.

The prototype drop-out detector receives the signal from one preamplifier of the Honeywell Model 96HD Recorder, amplifies the signal and provides automatic gain control with a very long time constant in comparison to the longest detected drop-outs, rectifies and filters the gain controlled output, and compares the filtered output to

a switch selectable reference voltage corresponding to the specified threshold level below the normal gain controlled output level. In these preliminary trials, the comparator output was filtered to remove "glitches" at the leading edge of drop-outs just below the threshold level, and the filtered comparator output was applied to the electronic counter that registered drop-outs. The filtered comparator output was also employed to enable the 500 kHz oscillator signal to the second electronic counter that registered errors. Thus an error is defined as one wavelength (two flux reversals) which produce an output signal below the threshold level, and a drop-out is defined as a series of consecutive errors.

The threshold levels were calibrated by applying a square wave modulated sinusoidal waveform to the drop-out detector input and varying the degree of modulation while observing the input signal and the comparator output on an oscilloscope. The accuracy of the calibration method approached $\pm 1$ dB for the 6 dB and 12 dB thresholds, but some distortion of the modulated input signal reduced the accuracy to around $\pm 2$ dB during the 20 dB threshold calibration. During the calibration, it was noted that the drop-out detection signal did not enable the error signal until after the first wavelength of a drop-out had passed. This source of error did not appear to be significant with respect to the typical length of drop-outs detected on the sample tapes. It was also noted that the filtered drop-out detector signal occasionally failed to trigger the drop-out counter or triggered it twice for what appeared to be a single drop-out. These two sources of error tend to cancel each other, but their overall effect on the data was not quantified. Digital filtering of the detected reproduce signal of the tape and the addition of a one-shot pulse generator to the comparator

output which are planned in the final implementation should eliminate all sources of count errors.

The errors/$10^6$ wavelengths parameter should be equivalent to Bit Error Rates (BER) for randomized NRZ recordings with an equal number of 1's and 0's.

### 4.4.1  Preliminary Results

Prior to the collection of data, the total errors registered was observed for sequential passes of the same track, threshold level, and sample tape segment to check for repeatability.  Subsequent error registrations were within 10% of each other with a definite trend toward a reduction in the number of errors with an increasing number of passes of a given sample.  The results of the final verification trial are presented in tabular and histogram form for the 20 dB results from the center track of a 1 inch Ampex 721 sample (Lot 51x014231=12).  During the second pass, an extra drop-out was detected in the second 100 foot tape segment (500 ft to 600 ft), separate drop-outs in the fourth and fifth segments of the first pass were both recorded as occuring in the fifth segment, the drop-outs detected in the sixth segment of the first pass were not detected, and the total number of drop-outs detected was only 73% of the number registered for the second pass.  Despite these discrepencies, histograms of the results show that the total number of errors registered for this sample is adequately repeatable for tape characterization.

The following series of tables and histograms presents data which compare results from different tape types in 1 inch and ¼ inch widths

Table 4.4.1

DURATION AND DISTRIBUTION OF 20 dB DROP-OUTS ON CENTER TRACK OF 1/4" x 1600' TAPES

Location on Reel (x 100 ft.)

| Tape Type (lot) | Parameter | 4-5 | 5-6 | 6-7 | 7-8 | 8-9 | 9-10 | 10-11 | 11-12 | 12-13 | 13-14 | 14-15 | 15-16 | 16-17 | 17-18 | 18-19 | 19-20 | Mean Values |
|---|---|---|---|---|---|---|---|---|---|---|---|---|---|---|---|---|---|---|
| Ampex 466 (1124C7092) | Errors/$10^6$ Wavelengths | 4.40 | 8.95 | 0 | 0 | 6.10 | 0 | 0 | 0 | 0 | 3.20 | 0 | 0 | 0 | 0 | 1.25 | 0 | 1.5 |
| | Errors/drop-out | 88 | 60 | - | - | 122 | - | - | - | - | 32 | - | - | - | - | 25 | - | 60 |
| | Drop-outs/100 ft. | 1 | 3 | 0 | 0 | 1 | 0 | 0 | 0 | 0 | 2 | 0 | 0 | 0 | 0 | 1 | 0 | 0.5 |
| Ampex 466 (112048092) | Errors/$10^5$ Wavelengths | 6.10 | 0 | 0 | 1.15 | 0 | 2.75 | 4.05 | 3.40 | 2.55 | 5.00 | 6.15 | 4.40 | 0 | 4.60 | 17.25 | 0 | 3.6 |
| | Errors/drop-out | 1 | - | - | 23 | - | 55 | 81 | 68 | 51 | 100 | 123 | 88 | - | 46 | 86 | - | 82 |
| | Drop-outs/100 ft. | 122 | 0 | 0 | 1 | 0 | 1 | 1 | 1 | 1 | 1 | 1 | 1 | 0 | 2 | 4 | 0 | 0.9 |
| Ampex 721 (110Q24182) | Errors $10^6$ Wavelengths | 60.85 | 19.95 | 43.90 | 34.00 | 27.35 | 19.50 | 13.10 | 52.20 | 9.85 | 13.65 | 38.50 | 26.50 | 14.20 | 24.00 | 14.70 | 43.45 | 28.5 |
| | Errors/drop-out | 174 | 133 | 55 | 97 | 109 | 98 | 66 | 116 | 56 | 273 | 96 | 106 | 95 | 160 | 294 | 109 | 118 |
| | Drop-outs/100 ft. | 7 | 3 | 6 | 7 | 5 | 4 | 4 | 9 | 3 | 1 | 8 | 5 | 3 | 3 | 1 | 8 | 4.8 |
| 3M 5198 (41575-1-01-21) (add 1700' to location) | Errors/$10^6$ Wavelengths | 8.45 | 10.95 | 0 | 0 | 7.35 | 0 | 0 | 16.45 | 0 | 0 | 0 | 5.10 | 19.15 | 0 | 0 | 17.6 | 5.33 |
| | Errors/drop-out | 169 | 110 | - | - | 147 | - | - | 329 | - | - | - | 102 | 127 | - | - | 70 | 122 |
| | Drop-outs/100 ft. | 1 | 2 | 0 | 0 | 1 | 0 | 0 | 1 | 0 | 0 | 0 | 1 | 3 | 0 | 0 | 5 | 0.9 |

Wavelength = 60 microinches ≡ 2 flux reversals

An error is defined as two consecutive flux reversals which produce an output signal smaller than the threshold level (20 dB)

A drop-out is a series of consecutive errors

Data obtained with 18 mil track width

Figure 4.4.1: Duration and Distribution of 20 dB
Drop-outs on Center Track of 1/4" x 1600' Tapes

Ampex 466 (112407092)
   8 drop-outs
   Average 60 errors/drop-out
   1.5 errors/$10^6$ wavelengths

Ampex 466 (112048092)
   14 drop-outs
   Average 82 errors/drop-out
   3.6 errors/$10^6$ wavelengths
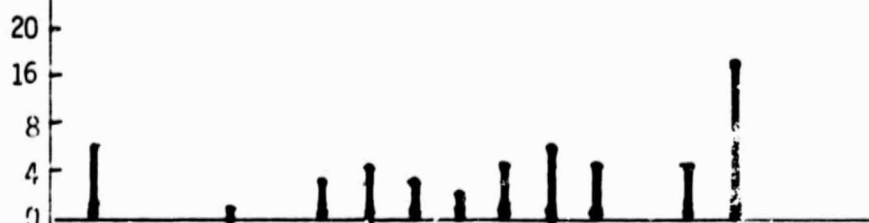
Ampex 721 (11Q024182)
   77 drop-outs
   Average 118 errors/drop-out
   28.5 errors/$10^6$ wavelengths

3M 5198 (41575-1-01-21)
   (add 1700' to location)
   14 drop-outs
   Average 122 errors/drop-out
   5.3 errors/$10^6$ wavelengths

Errors/$10^6$ Wavelengths
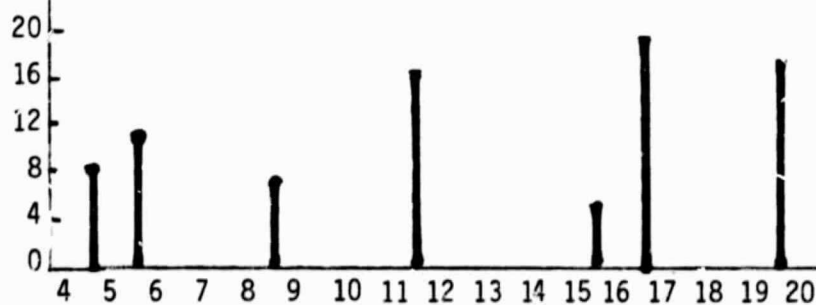
Location on Reel
(Feet x 100)

IIT RESEARCH INSTITUTE

118

Table 4.4.2

Duration and Distribution of 20 db Drop-outs
on Center Track of 1"x1600' Tapes

| Tape Type (lot) | Parameter | Location on Reel (x100 ft) | | | | | | | | | | | | | | | | Mean Values |
|---|---|---|---|---|---|---|---|---|---|---|---|---|---|---|---|---|---|---|
| | | 4-5 | 5-6 | 6-7 | 7-8 | 8-9 | 9-10 | 10-11 | 11-12 | 12-13 | 13-14 | 14-15 | 15-16 | 16-17 | 17-18 | 18-19 | 19-20 | |
| Ampex 721 (510094252) | Errors/10⁶ Wavelengths | 0 | 0 | 0 | 0 | 11.1 | 0 | 0 | 0 | 0 | 26.4 | 0 | 6.5 | 0 | 0 | 0 | 0 | 2.75 |
| | Errors/Drop-out | - | - | - | - | 111 | - | - | - | - | 528 | - | 130 | - | - | - | - | 220 |
| | Drop-outs/100 ft | 0 | 0 | 0 | 0 | 2 | 0 | 0 | 0 | 0 | 1 | 0 | 1 | 0 | 0 | 0 | 0 | 0.25 |
| Ampex 721 (51x014231=12) First Pass | Errors/10⁶ Wavelengths | 0 | 0 | 0 | 13.85 | 13.05 | 16.95 | 0 | 0 | 0 | 0 | 0 | 58.05 | 27.85 | 0 | 0 | 14.85 | 8.98 |
| | Errors/Drop-out | - | - | - | 277 | 261 | 210 | - | - | - | - | - | 387 | 186 | - | - | 149 | 239 |
| | Drop-outs/100 ft | 0 | 0 | 0 | 1 | 1 | 2 | 0 | 0 | 0 | 0 | 0 | 3 | 3 | 0 | 0 | 2 | 0.75 |
| Ampex 721 (51x014231-12) Second Pass | Errors/10⁶ Wavelengths | 0 | 3.90 | 0 | 0 | 26.25 | 0 | 0 | 0 | 0 | 0 | 0 | 45.05 | 26.6 | 0 | 0 | 14.80 | 7.29 |
| | Errors/Drop-out | - | 78 | - | - | 263 | - | - | - | - | - | - | 450 | 266 | - | - | 296 | 292 |
| | Drop-outs/100 ft | 0 | 1 | 0 | 0 | 2 | 0 | 0 | 0 | 0 | 0 | 0 | 2 | 2 | 0 | 0 | 1 | 0.50 |
| 3M 5198 (43056 17 010 24) | Errors/10⁶ Wavelengths | 0 | 0 | 0 | 0 | 0 | 0 | 0 | 0 | 0 | 0 | 0 | 0 | 0 | 0 | 0 | 9.65 | 0.60 |
| | Errors/Drop-out | - | - | - | - | - | - | - | - | - | - | - | - | - | - | - | 193 | 193 |
| | Drop-outs/100 ft | 0 | 0 | 0 | 0 | 0 | 0 | 0 | 0 | 0 | 0 | 0 | 0 | 0 | 0 | 0 | 1 | 0.06 |
| Fuji H 621* (0799031) | Errors/10⁶ Wavelengths | 0 | 0 | 0 | 0 | 0 | 0 | 0 | 299 | 0 | 0 | 0 | 0 | 0 | 0 | 0 | 0 | 18.7 |
| | Errors/Drop-out | - | - | - | - | - | - | - | 239 | - | - | - | - | - | - | - | - | 239 |
| | Drop-outs/100 ft | 0 | 0 | 0 | 0 | 0 | 0 | 0 | 25 | 0 | 0 | 0 | 0 | 0 | 0 | 0 | 0 | 0.25 |

Wavelength = 60 microinches ≡ 2 flux reversals
An error is defined as two consecutive flux reversals which produce
an output signal smaller than the threshold level
A drop-out is a series of consecutive errors

* Sample previously used for record current and wavelength response tests

Data obtained with 18 mil track width

119

Figure 4.4.2: Duration and Distribution of 20 dB
Drop-outs on Center Track of 1" x 1600' Tapes

Ampex 721
(510094252)
4 drop-outs
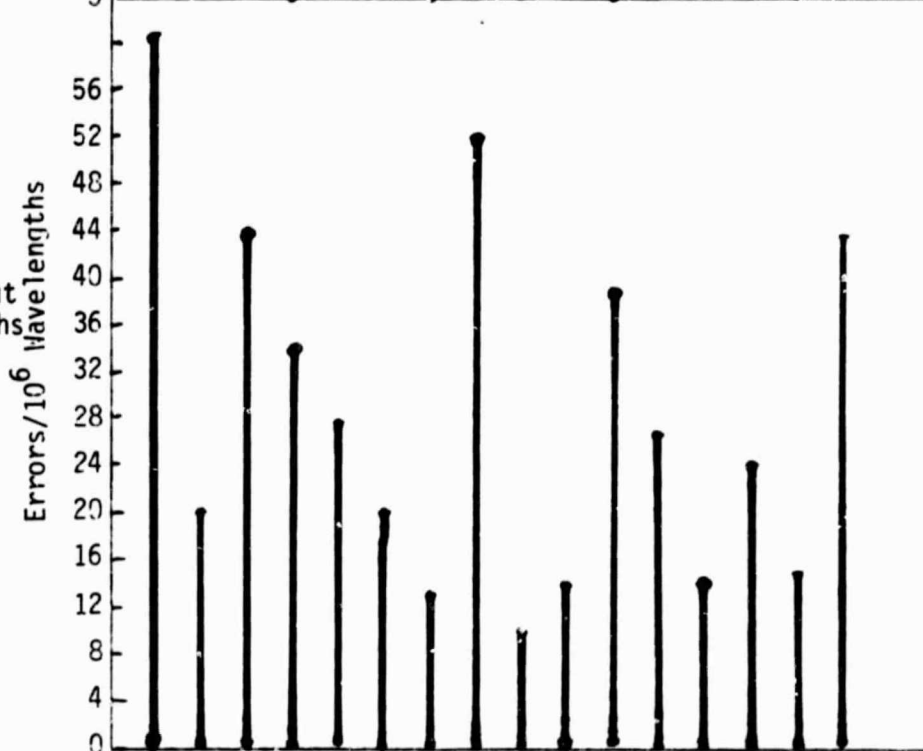Average 220 errors/drop-out
2.8 errors/$10^6$ wavelengths

ORIGINAL PAGE IS
OF POOR QUALITY

Ampex 721
(51x014231=12)
First Pass
12 drop-outs
Average 239 errors/drop-out
9.0 errors/$10^6$ wavelengths

Ampex 721
(51x014231=12)
Second Pass
8 drop-outs
Average 292 errors/drop-out
7.3 errors/$10^6$ wavelengths

3M 5198
(43056 17 010 24)
1 drop-out
Average 193 errors/drop-outs
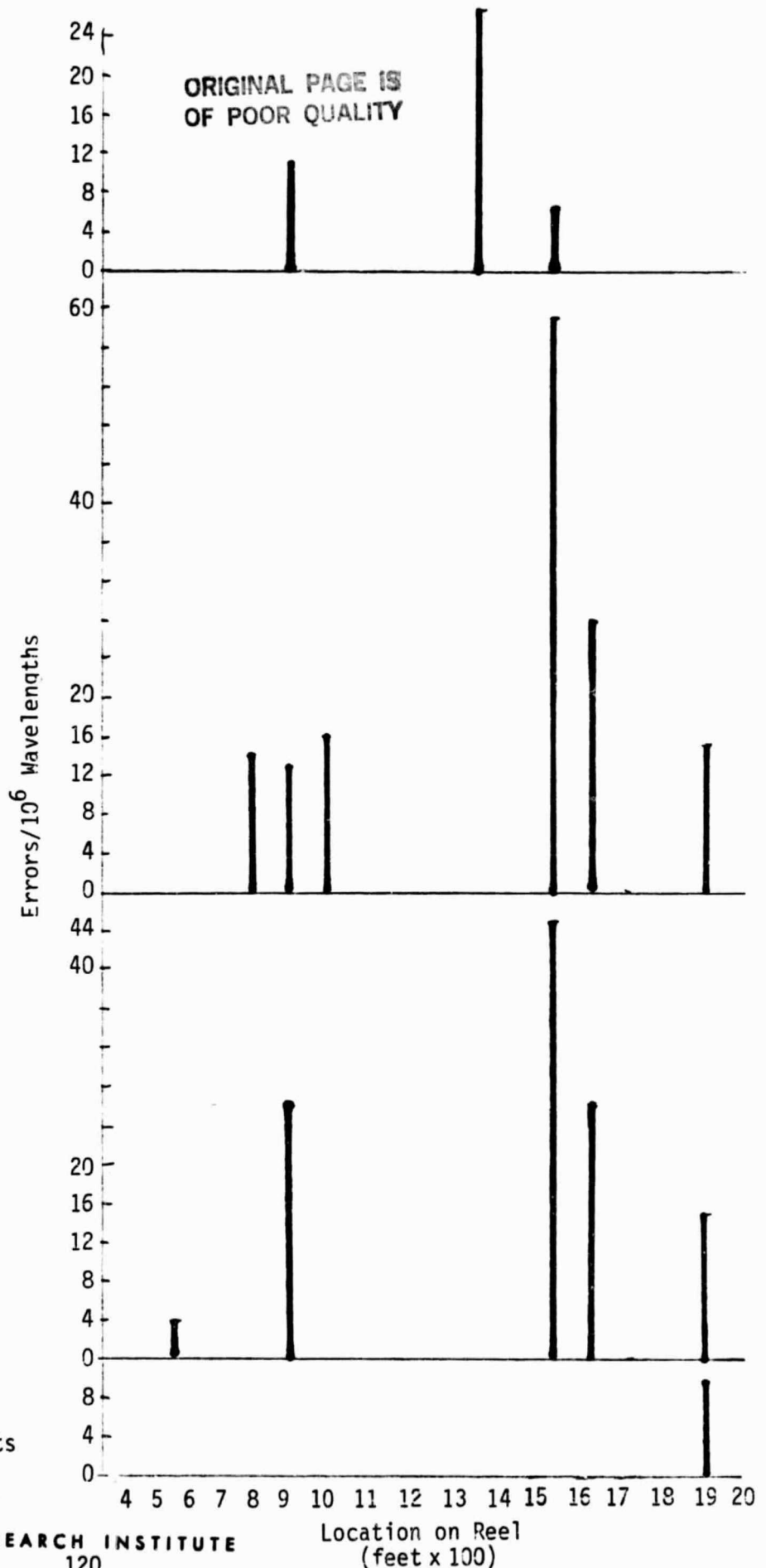0.6 errors/ $10^6$ wavelengths

Errors/$10^6$ Wavelengths

Location on Reel
(feet x 100)

Table 4.4.3

Duration and Distribution of 12 dB Drop-outs on Center Track of 1"x1600' Tapes

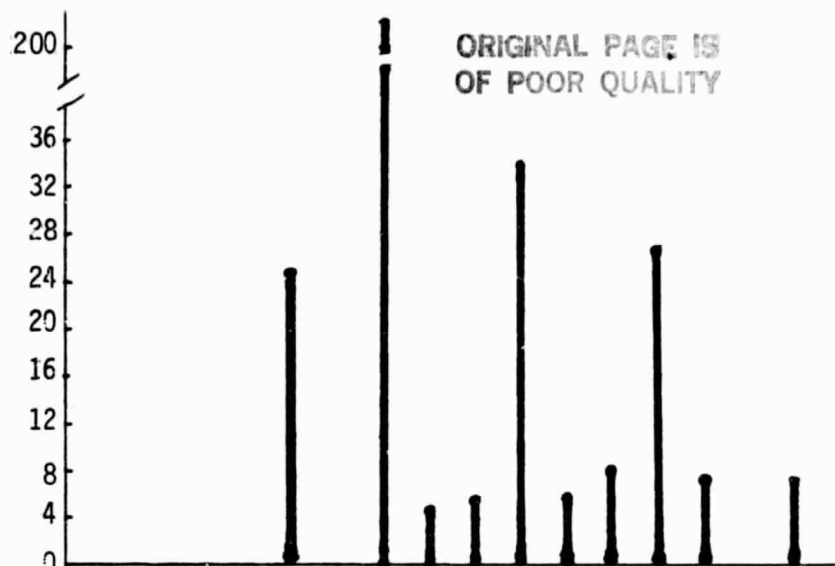| Tape Type (lot) | Parameter | Location on Reel (x100ft) | | | | | | | | | | | | | | | | Mean Values |
|---|---|---|---|---|---|---|---|---|---|---|---|---|---|---|---|---|---|---|
| | | 4-5 | 5-6 | 6-7 | 7-8 | 8-9 | 9-10 | 10-11 | 11-12 | 12-13 | 13-14 | 14-15 | 15-16 | 16-17 | 17-18 | 18-19 | 19-20 | |
| Ampex 721 (510094252) | Errors/10^6 wavelengths | 0 | 0 | 0 | 0 | 24.6 | 0 | 202 | 4.75 | 5.45 | 33.45 | 6.10 | 7.80 | 26.9 | 6.85 | 0 | 7.10 | 20.34 |
| | Errors/drop-out | – | – | – | – | 164 | – | 4048 | 95 | 109 | 334 | 122 | 156 | 179 | 137 | – | 142 | 434 |
| | Drop-outs/100 ft | 0 | 0 | 0 | 0 | 3 | 0 | 1 | 1 | 1 | 2 | 1 | 1 | 3 | 1 | 0 | 1 | 0.94 |
| Ampex 721 (51x014231=12) | Errors/10^6 Wavelengths | 0 | 12.95 | 5.50 | 48.9 | 0 | 27.05 | 8.35 | 7.45 | 4.50 | 8.25 | 0 | 68.6 | 36.05 | 7.20 | 8.60 | 17.15 | 16.28 |
| | Errors/drop-out | – | 259 | 110 | 326 | 0 | 271 | 83.5 | 149 | 90 | 83 | – | 172 | 361 | 144 | 172 | 343 | 180 |
| | Drop-outs/100 ft | 0 | 1 | 1 | 3 | 2 | 3 | 2 | 1 | 1 | 2 | 0 | 8 | 2 | 1 | 1 | 1 | 1.81 |
| 3M 5198 (43056 17 010 24) | Errors/10^6 Wavelengths | 9.40 | 21.50 | 11.80 | 6.40 | 13.05 | 4.65 | 26.45 | 8.80 | 0 | 15.35 | 11.35 | 5.70 | 4.65 | 0 | 0 | 17.15 | 9.77 |
| | Errors/drop-out | 94 | 143 | 118 | 64 | 131 | 93 | 176 | 176 | – | 154 | 114 | 114 | 93 | – | – | 172 | 130 |
| | Drop-outs/100 ft | 2 | 3 | 2 | 2 | 2 | 1 | 3 | 1 | 0 | 2 | 2 | 1 | 1 | 0 | 0 | 2 | 1.5 |
| Fuji H 621* (079903) | Errors/10^6 Wavelengths | 0 | 0 | 0 | 0 | 0 | 0 | 1.70 | 649 | 0 | 3.85 | 0 | 0 | 0 | 0 | 3.00 | 0 | 41.10 |
| | Errors/drop-out | – | – | – | – | – | – | 34 | 185 | – | 77 | – | – | – | – | 60 | – | 180 |
| | Drop-outs/100 ft | 0 | 0 | 0 | 0 | 0 | 0 | 1 | 70 | 0 | 1 | 0 | 0 | 0 | 0 | 1 | 0 | 4.6 |

Wavelength = 60 microinches = 2 flux reversals
An error is defined as two consecutive flux reversals which produce an output signal smaller than the threshold level
A Drop-out is a series of consecutive errors

*Previously used for record current and wavelength response tests
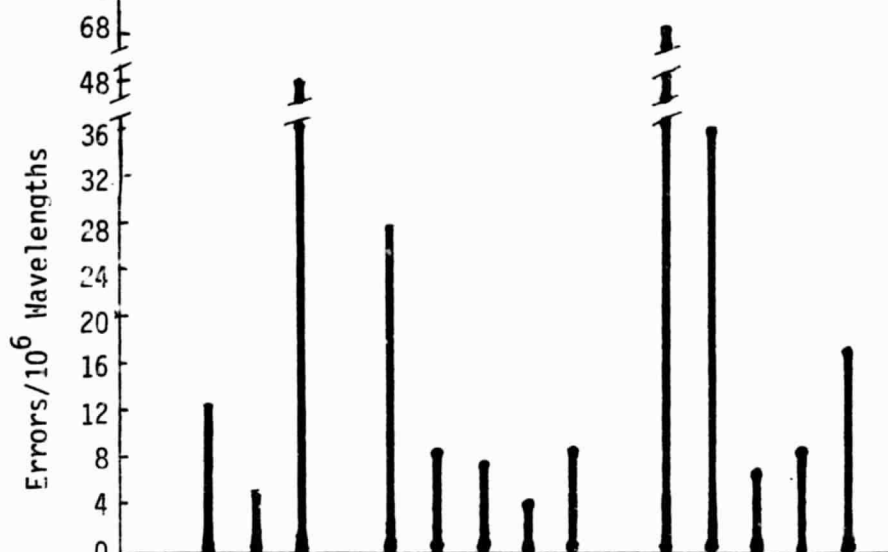Data obtained with 18 mil track width

Figure 4.4.3: Duration and Distribution of 12 dB
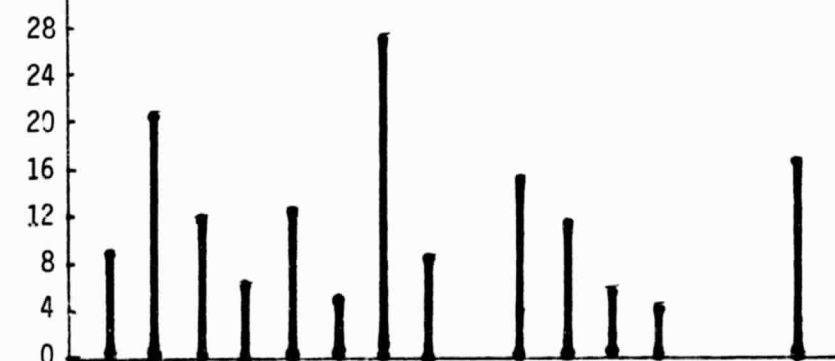Drop-outs on Center Track of 1" x 1600' Tapes

Ampex 721
   (510094252)
   15 Drop-outs
   Average 434 errors/drop-out
   20.3 errors/10^6 wavelengths

Ampex 721
   (51x014231=12)
   29 Drop-outs
   Average 180 errors/drop-out
   16.3 errors/10^6 wavelengths

3M 5198
   (43056 17 01024)
   24 Drop-outs
   Average 130 errors/drop-out
   9.8 errors/10^6 wavelengths

Fuji H621
   (079903)(Sample previously
   used for record current and
   wavelength response tests)
   73 Drop-outs
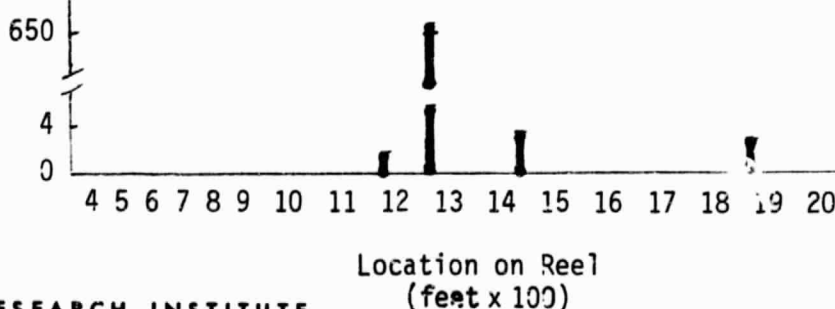   Average 180 errors/drop-out
   41.1 errors/10^6 wavelengths

ORIGINAL PAGE IS
OF POOR QUALITY

Errors/10^6 Wavelengths

Location on Reel
(feet x 100)

Table 4.4.4

Comparison of Drop-out Distribution and Duration on Center
Track and Track 0.25 Inch From Edge of 1"x1600' Tapes

| Tape Type (lot) and Threshold | Track | Parameter | Location on Reel (x100 ft) | | | | | | | | | | | | | | | | Mean Values |
|---|---|---|---|---|---|---|---|---|---|---|---|---|---|---|---|---|---|---|---|
| | | | 4-5 | 5-6 | 6-7 | 7-8 | 8-9 | 9-10 | 10-11 | 11-12 | 12-13 | 13-14 | 14-15 | 15-16 | 16-17 | 17-18 | 18-19 | 19-20 | |
| Ampex 721 (510094252) 20 dB | Center(21) | Errors/10⁶ Wavelengths | 0 | 0 | 0 | 0 | 11.1 | 0 | 0 | 0 | 0 | 26.4 | 0 | 6.5 | 0 | 0 | 0 | 0 | 2.75 |
| | | Errors/Drop-out | — | — | — | — | 111 | — | — | — | — | 528 | — | 130 | — | — | — | — | 220 |
| | | Dropouts/100 ft | 0 | 0 | 0 | 0 | 2 | 0 | 0 | 0 | 0 | 1 | 0 | 1 | 0 | 0 | 0 | 0 | 0.25 |
| | Side(33) | Errors/10⁶ Wavelengths | 0 | 0 | 457.40 | 0 | 0 | 0 | 17.80 | 21.70 | 13.55 | 0 | 0 | 0 | 0 | 0 | 0 | 0 | 31.90 |
| | | Errors/Drop-out | — | — | 4574 | — | — | — | 178 | 434 | 271 | — | — | — | — | — | — | — | 1701 |
| | | Drop-outs/100 ft | 0 | 0 | 2 | 0 | 0 | 0 | 2 | 1 | 1 | 0 | 0 | 0 | 0 | 0 | 0 | 0 | 0.38 |
| 3M 5198 (43056 17 010 24) 12 dB | Center(21) | Errors/10⁶ Wavelengths | 9.40 | 21.50 | 11.80 | 6.40 | 13.05 | 4.65 | 26.45 | 8.80 | 0.00 | 15.35 | 11.35 | 5.70 | 4.65 | 0.00 | 0.00 | 17.15 | 9.77 |
| | Side(33) | Errors/10⁶ Wavelengths | 12.70 | 10.05 | 13.00 | 25.85 | 5.40 | 36.80 | 15.30 | 12.30 | 0.09 | 13.50 | 8.00 | 4.55 | 33.30 | 34.10 | 0.00 | 16.25 | 15.19 |

Wavelength = 60 microinches ≡ 2 flux reversals
An error is defined as two consecutive flux reversals which
    produce an output signal smaller than the threshold level
A drop-out is a series of consecutive errors

Data obtained with 18 mil track width

Figure 4.4.4: Comparison of Drop-out Distribution and Duration on Center Track and Track 0.25 Inch from Edge of 1" x 1600' Tapes

ORIGINAL PAGE IS OF POOR QUALITY

Ampex 721
(510094252)
20 dB
Center Track(21)
4 drop outs
average 2.75 errors
$\overline{10^6 \text{ wavelengths}}$
0.25 dropouts/100ft

Ampex 721
(510094252)
20 dB
Side Track (33)
6 drop outs
average 31.9 errors
$\overline{10^6 \text{ wavelengths}}$
0.38 dropouts/100ft

3M 5198
(43056 17 010 24)
12 dB
Center Track(21)
average 9.77 errors
$\overline{10^6 \text{ wavelengths}}$

3M 5198
(43056 17 010 24)
12 dB
Side Track (33)
average 15.19 errors
$\overline{10^6 \text{ wavelengths}}$

Errors/10^6 Wavelengths

Location on Reel
(x100 ft)

IIT RESEARCH INSTITUTE

124
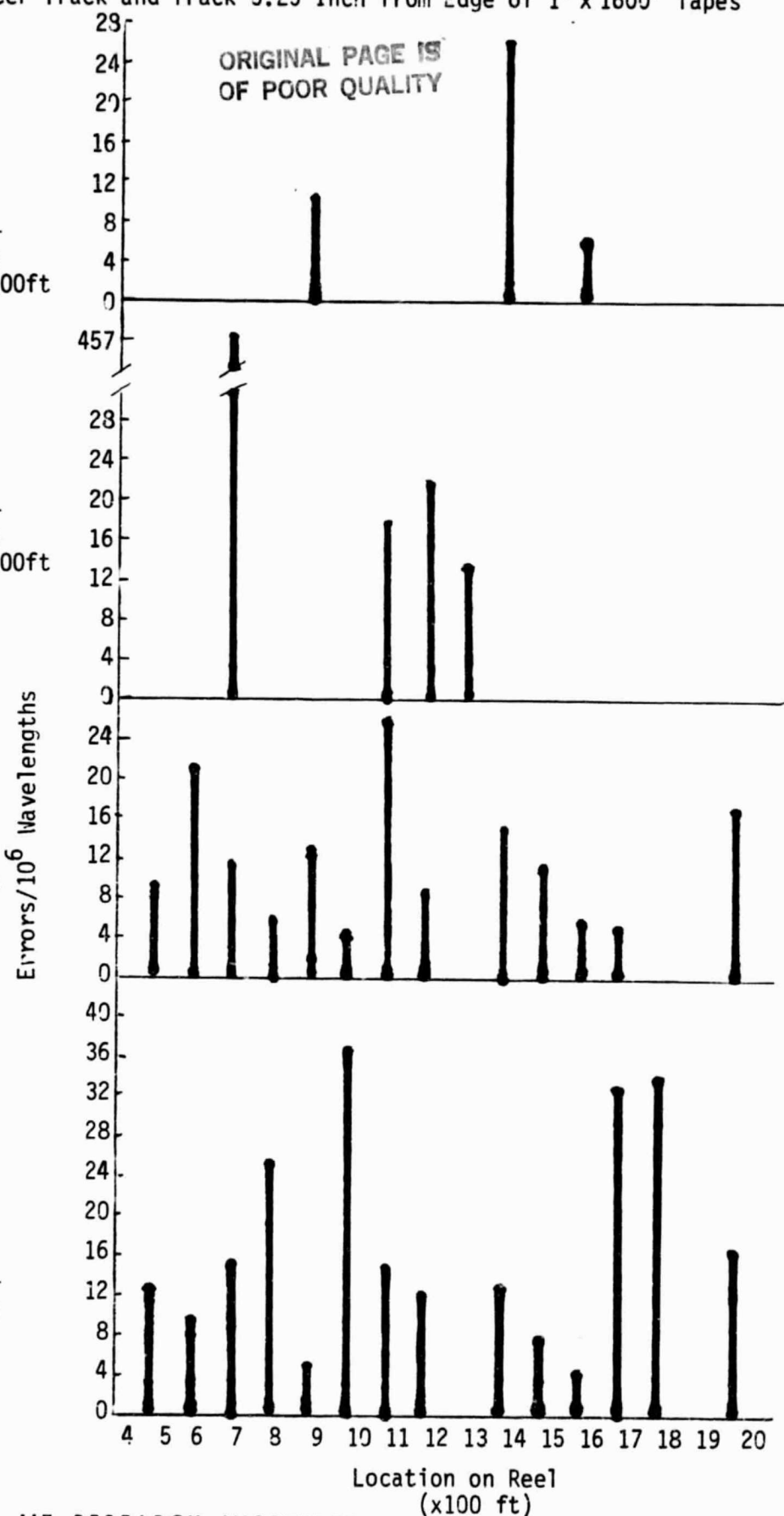
with specified threshold levels and from specified track locations. The last set compares results from a center track and a side track about 0.25 inch from the edge of the 1 inch tape samples.

### 4.4.2 Conclusions

The center track of the 1 inch 3M 5198 sample at the 20 dB level was the only sample which produced an error rate below the $1/10^6$ rate considered acceptable by IITRI. Large variations in error rate can be expected from these tapes, especially when checking a short segment of tape with a system that can recover data from drop-outs less severe than the 20 dB level because long segments of tape may have no drop-outs but the length of a single-drop out is likely to generate many errors.

For center tracks of ¼ inch tape and data recovery above the 20 dB level, the lowest BERs can be expected from Ampex 466 and 3M 5198, while much higher BERs can be expected from Ampex 721.

The limited results from center and side tracks was not considered conclusive, but a trend toward higher error rates on side tracks is suggested by the data.

The number of drop-outs detected on 1 inch samples of 3M 5198 and Fuji H621 at the 20 dB level is so small that the mean values for those trials should not be considered statistically valid. Contaimination of the Fuji H621 sample during previous use is possible. White debris was observed on that sample in the severe drop-out segment (1100 ft. to 1200 ft) which can be recovered for analysis.

## 4.5 Dropouts with 7.3 mil Track Width

A second series of preliminary dropout measurements have been conducted on Fuji H621 and 3M 5198 samples with a 20 dB dropout threshold and a 7.3 mil track width. This narrow track video head was designed for high frequencies, and it was necessary to increase the tape speed to 60 IPS in order to maintain a signal to noise ratio greater than 20 dB. Tapes were also recorded at 60 IPS with a 1.0 MHz record signal to maintain the 60 microinch wavelength. The record current at this higher frequency is slightly less square than the 500 kHz square wave record current of the 18 mil track width preliminary measurements.

Dropouts were measured on thirteen tracks near the center of each 1 inch wide tape sample during sequential passes. The distance between track centers was 20.8 mils, the first track was 315±5 mils from the edges of the tape samples, and the last track was 565±5 mils from the edges of the samples. Dropout locations along the length of the samples were calculated to within ±10 feet.

The total errors registered on the error counter were printed once every 2 seconds or every 10 feet of tape, and each change of error registrations between adjacent 10 foot tape segments was considered a single dropout. Oscilloscope monitoring of the comparator input demonstrated that this dropout counting method was accurate for low dropout rates (<1 dropout/100 feet), and that very few of the error registration changes on higher dropout rate samples were caused by more than one dropout per 10 foot tape segment. This dropout counting method was more accurate then the counter method employed with the 18 mil track width measurements.

Other details of the dropout measurement procedure were the same as for the 18 mil track width data. These tapes are available for distribution to the OEMs.

### 4.5.1 Results

Table 4.5.1 lists the error rates for each track and each tape sample, and the dropout rates and average dropout lengths for each tape sample. Wide variations in the error rates and the dropout rates between tracks of a single tape sample and between tape samples of a single type are evident. The average dropout lengths are relatively constant at about 200 errors/dropout or 12 mils/dropout. Note the particularily high dropout rate for track 502 of 3M 5198 reel 24. Most of this high error rate was attributed to dropouts with a characteristic depth profile that was present along most of the length of the track, suggesting a source such as grit on a roller during production. The ends of 3M 5198 reels 9 and 24, and the beginning of 3M 5198 reel 16 were not analyzed due to high error rates and dropout rates on all tracks. These apparently defective sections of tape may not have been totally eliminated within the analyzed lengths indicated in the second column of Table 4.5.1 and results from a smaller section (Figure 4.5.1) suggest that 3M 5198 samples equivalent in length to the 2600 foot and 2700 foot Fuji samples could be obtained with error rates 20% less than the averages for all tracks indicated on Table 4.5.1. One very long multitrack dropout on a Fuji H621 sample was not redetected after degaussing and re-recording the sample.

Table 4.5.1: Error Rates from 20 dB Dropouts on Thirteen 7.3 mil Wide Tracks of Fuji H621 and 3M 5198 Tapes

| Tape Type (lot of reel) | Section of Reel Analyzed (feet) | Error Rate (Errors/$10^6$ wavelengths) Location of Track Center (±5 mils from edge) | | | | | | | | | | | | | | Dropout Rate (Dropouts/100 feet) | Average Dropout Length Errors/(Dropout) |
|---|---|---|---|---|---|---|---|---|---|---|---|---|---|---|---|---|---|
| | | 315 | 336 | 357 | 377 | 398 | 419 | 440 | 461 | 482 | 502 | 523 | 544 | 565 | Average for all Tracks | | |
| Fuji H621* (079552) | 300 to 2900 | 9.1 | 7.3 | 3.7 | 7.8 | 9.7 | 6.2 | 6.8 | 4.1 | 3.5 | 7.1 | 4.6 | 4.2 | 3.7 | 6.0 | 0.52 | 228 |
| Fuji H621 (079903) | 300 to 2900 | 1.2 | 2.8 | 4.3 | 4.7 | 3.4 | 2.1 | 2.0 | 2.2 | 3.? | 2.3 | 3.3 | 3.7 | 2.7 | 2.9 | 0.33 | 177 |
| Fuji H621 (079903) | 300 to 2900 | 1.4 | 1.7 | 2.6 | 3.5 | 4.0 | 1.4 | 0.6 | 1.1 | 0.9 | 2.3 | 2.9 | 2.7 | 2.4 | 2.1 | 0.23 | 186 |
| Fuji H621*** (079903) | 200 to 2900 | 3.9 | 3.3 | 3.9 | 4.2 | 4.2 | 2.5 | 2.4 | 4.9 | 2.9 | 7.9 | 15.3 | 7.2 | 3.2 | 5.1 | 0.35 | 291 |
| Fuji H621 (079903) | 200 to 2900 | 3.3 | 2.7 | 2.8 | 1.6 | 2.2 | 2.3 | 1.2 | 2.9 | 1.8 | 0.9 | 1.7 | 1.8 | 4.1 | 2.2 | 0.22 | 205 |
| 3M 5198 (43056 17 010 9) | 800 to 8400 | 13.6 | 15.9 | 12.8 | 11.6 | 12.7 | 10.9 | 13.7 | 12.3 | 12.0 | 10.9 | 10.1 | 15.6 | 10.4 | 12.5 | 1.46 | 173 |
| 3M 5198 (43056 17 010 16) | 1500 to 8900 | 25.6 | 22.7 | 35.3 | 25.8 | 26.9 | 20.3 | 26.6 | 22.2 | 18.5 | 30.3 | 17.3 | 20.2 | 23.3 | 24.2 | 2.42 | 200 |
| 3M 5198 (43056 17 010 24) | 600 to 8400 | 8.9 | 12.3 | 11.8 | 12.5 | 10.1 | 10.3 | 10.7 | 10.8 | 12.4 | 80.4 | 18.7 | 19.1 | 14.5 | 12.5 | 1.24** | 186** |

* Transport malfunction may have increased errors and dropouts by 3% for tracks 440 through 565

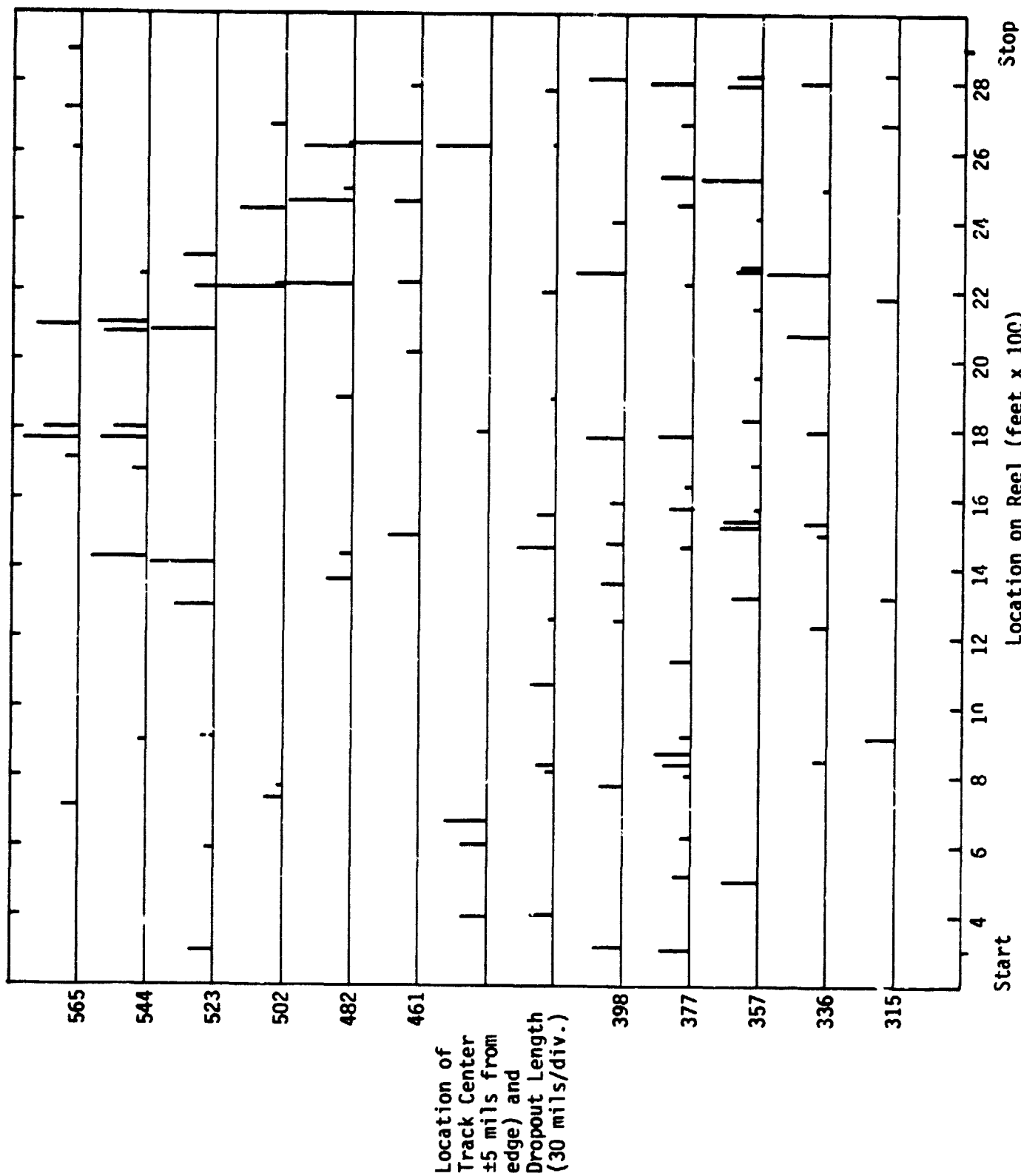** Does not include data from track 502

*** High error rates on tracks 502, 523, and 534 include errors from a single large dropout which was not redetected after degaussing and re-recording sample. Average for all tracks without this dropout were 3.8 errors/$10^6$ wavelengths, 222 errors/dropout, and 0.34 dropouts/100 feet.
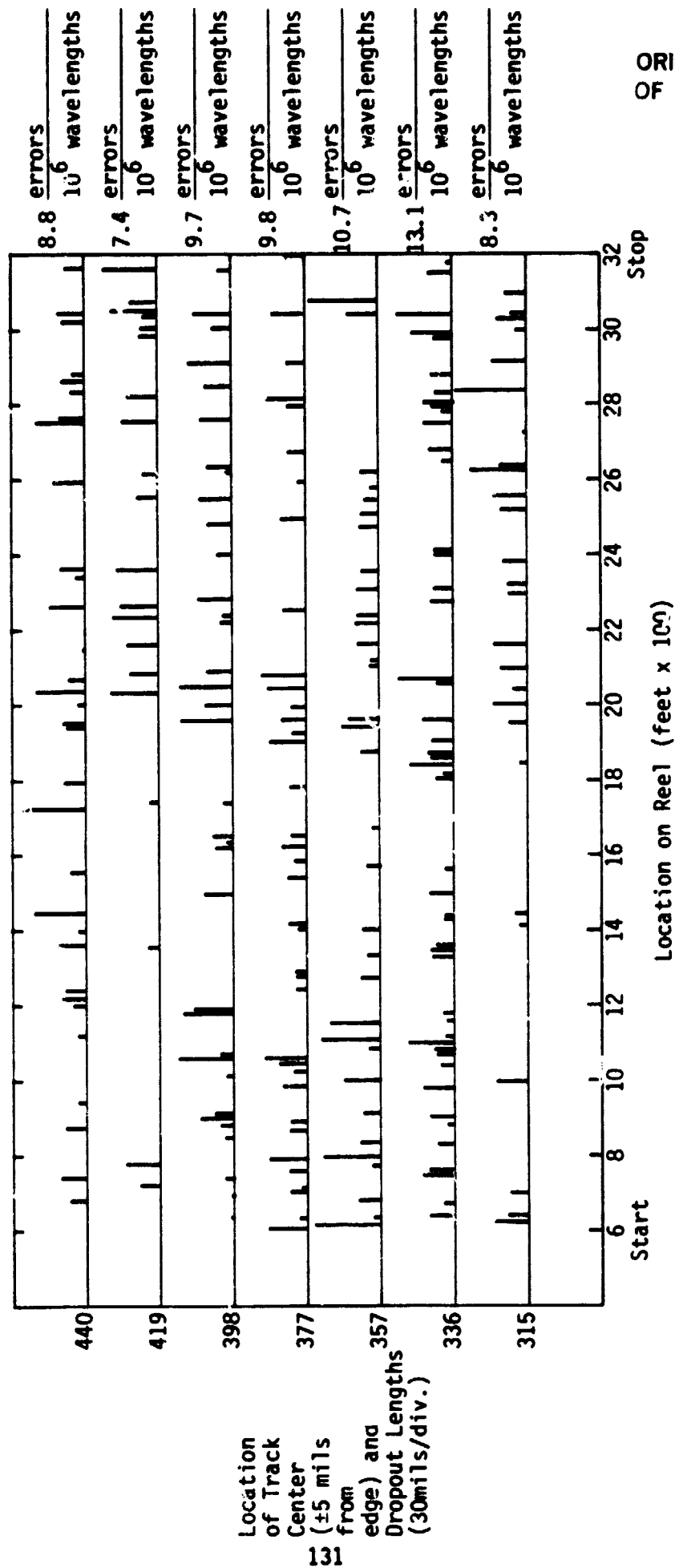
Figures 4.5.1 and 4.5.2 are maps of every dropout detected on the second Fuji H621 sample of the table and on seven 2600 foot tracks of 3M 5198 reel 24 respectively. The horizontal axes of these figures represent distance along the tape, and each of the horizontal lines represent a single track with the track locations in mils from the tape edge to the track center indicated along the vertical axes of the figures. Each dot or vertical bar was considered a single dropout with the location indicated by the track line at its base and its position along the horizontal axis. The height of each bar represents the length of each dropout, with the distance between two adjacent track lines equivalent to a dropout length of 500 errors or 30 mils. The dots represent dropouts less than 3 mils long.

The dropout location distributions on Figures 4.5.1 and 4.5.2 were typical of most of the sampled tracks. The dropouts are isolated, more or less randomly distributed events along the length of each sample. Many of the long dropouts, such as the four events around 2620 feet on the tracks at 419, 440, 461 and 482 mils of Figure 4.5.1 occur on adjacent tracks, indicating that they are the result of single flaws wider than the track spacing. A flaw that affects four tracks with this track spacing is between 60 and 100 mils wide.

The dropouts on Figures 4.5.1 and 4.5.2 were also employed for the frequency of occurrence versus length histograms of Figures 4.5.3 and 4.5.4. Figure 4.5.3 compares the length distributions of the Fuji H621 and 3M 5198 samples. Figure 4.5.3 shows that the relative frequency of occurrence of dropouts longer than the track width

Figure 4.5.1:  Location of 20dB Dropouts on Thirteen 7.3 mil Tracks
of a 2500 foot Fuji H521 Sample.

130

Figure 4.5.2: Location of 20dB dropouts on seven 7.3 mil tracks of a 2600 foot 3M 5198 sample. Average results for this sample are 152 errors/dropout, 9.7 errors/10⁶ wavelengths, and 1.3 dropouts/100 feet.

131
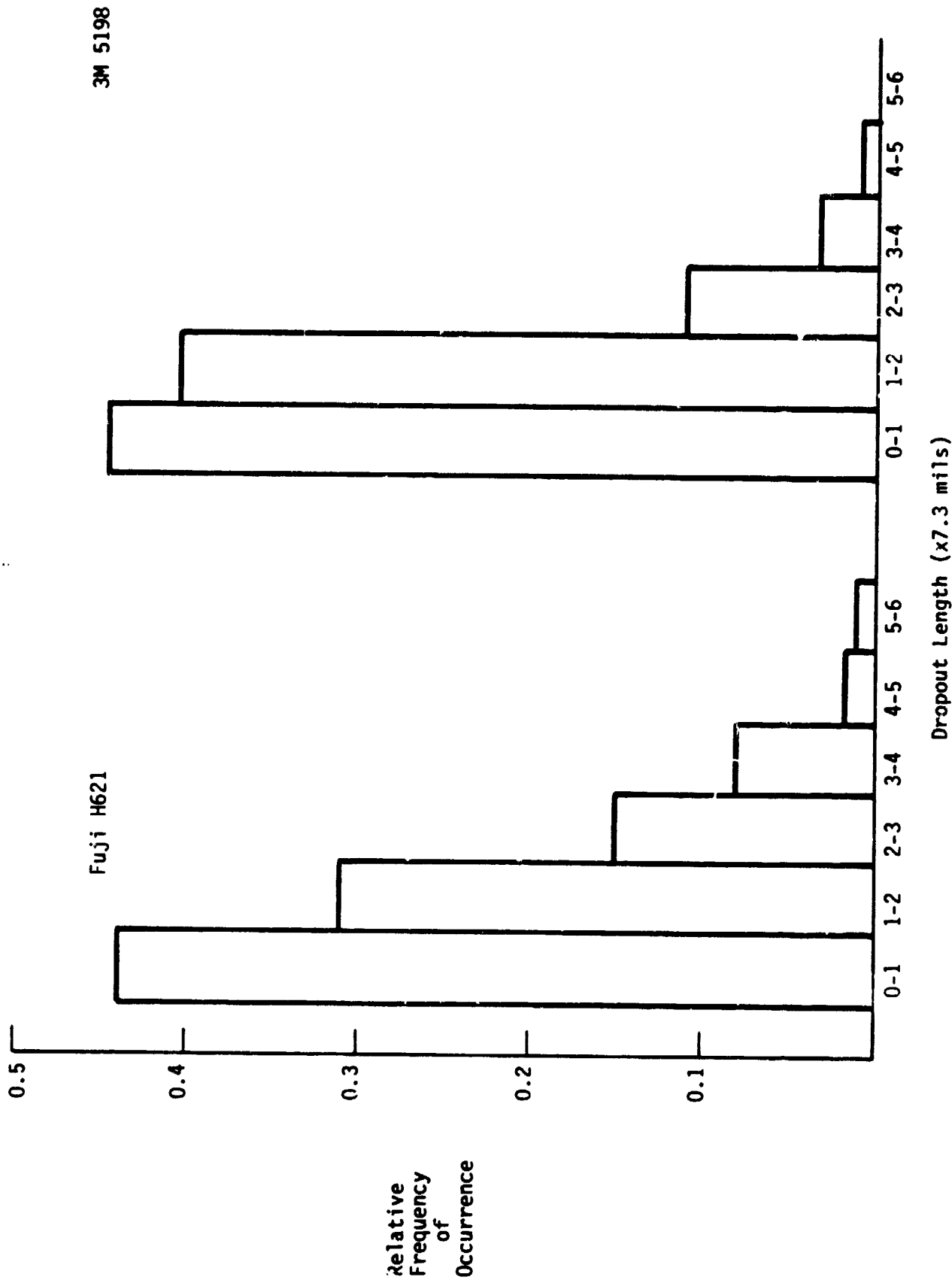
Figure 4.5.3: Dropout Length Frequency of Occurrence on Fuji H621 and 3M 5198 Samples
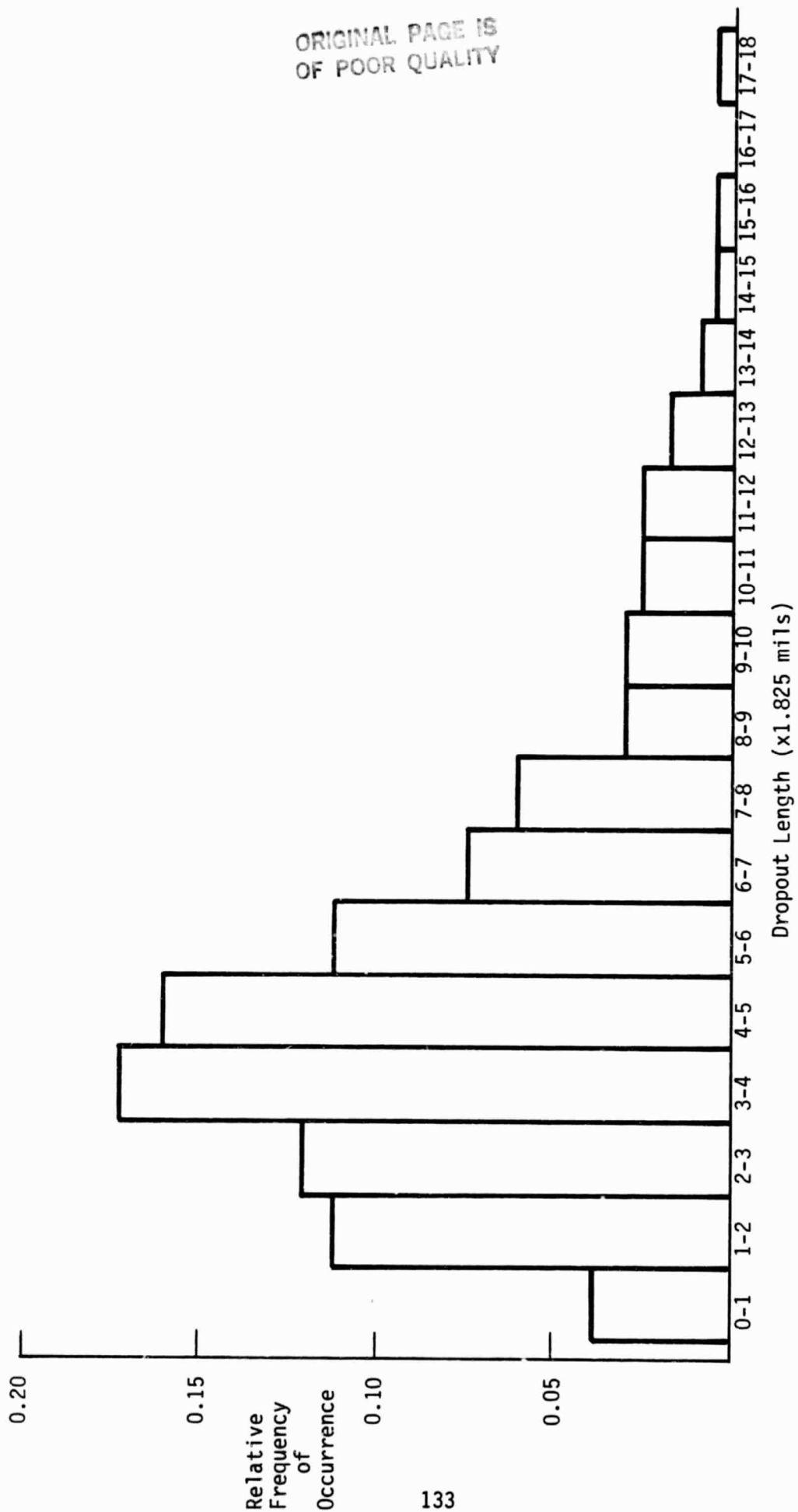
132

Figure 4.5.4: Dropout Length Frequency of Occurrence on 3M 5198 Sample

133

decreases with increasing dropout length. Very long dropouts may occur with greater relative frequencies on Fuji H621 than on 3M 5198. Figure 4.5.4 shows that the dropout length with the maximum frequency of occurrence is close to the track width. The bin width of Figure 4.5.4 is equal to one fourth of the track width and was selected to enhance any increased frequency of occurrences at even multiples of the track width. Increased frequencies at multiples of the track width are not apparent on the histogram.

### 4.5.2 Discussion

The dropout rates and error rates of 3M 5198 are twenty to fourty times greater with a 7.3 mil track width than the results of Table 4.4.2 in the May 1982 progress report obtained with an 18 mil track width. Similar large increases in these parameters for Fuji H621 are masked by a single atypical 100 foot segment from which the 18 mil track width data was obtained. The frequency of occurrence histograms indicate that small oxide flaws are more common than large flaws. A simple dropout model could begin with the assumption that an oxide flaw causes a rate of change of magnetic flux equal to zero over the effective area of the flaw. Then the length of a dropout is determined by the length over which the coincident flaw width to track width ratio exceeds the threshold level to normal reproduce signal level ratio. Flaws with effective widths smaller than 90% of the track width will never produce 20 dB dropouts, and the frequency of occurrence of long dropouts will be low due to the low frequency of occurrence of large flaws. In addition, small flaws that produce only subthreshold signal reductions in the reproduce level with a wide track system may produce individual

dropouts and increased BER with a narrow track system. Narrow tracks and track spacings also increase the number of tracks that can be affected by a single large flaw.

It should be possible to relate the threshold sensitivity of a given head gap width (track width) to the actual length and width of dropouts selected for high stability with repeated measurements. This information will enable selection of proper threshold levels for standard IRIG heads to achieve results that predict the performance of narrow track HDDR systems with specified track widths and immunity from dropout depth.

### 4.5.3 Conclusions

The 7.3 mil track width results show that large variations can be expected from dropout measurements on different tracks, lots or reels of a single tape type, and that large samples must be analyzed for comparison of results between tape types. Based on the results of Table 4.5.1, dropout rates and error rates of virgin 3M 5198 are about four times greater than dropout rates and error rates of Fuji H621 with 7.3 mil track widths.

The dropout location diagrams indicate that tapes cannot be screened to obtain long segments with no dropouts across the width of the tape. Although the number of samples in these preliminary studies are too small to accurately predict tape yields, the results suggest that screening of Fuji H621 or 3M 5198 could reduce the maximum dropout rates and error rates by one half with a yield greater than 50%, and that defective tracks on tape segments can be readily identified.